Ultrafast Organic Lasers And Solid-State Amplifiers

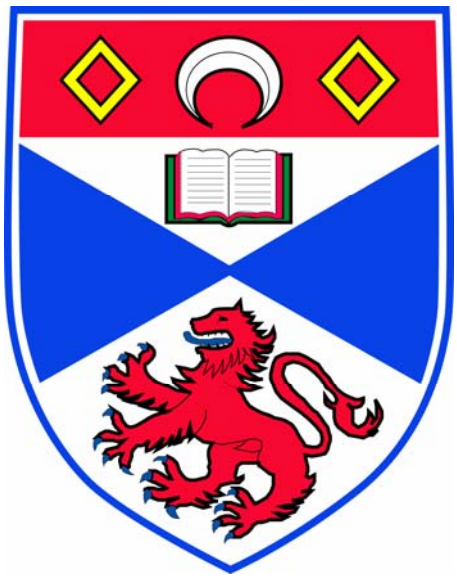

Mark Goossens MSc

A thesis submitted to the School of Physics and Astronomy, at the University of St Andrews, for the degree of Doctor of Philosophy.

The J. F. Allen Physics Research Laboratories
School of Physics and Astronomy
University of St. Andrews
North Haugh
St. Andrews, KY169SS
Scotland

February 2007

Abstract

This thesis presents an investigation of the lasing dynamics and optical amplification devices using conjugated polymers. Spectroscopic studies of conjugated polymers and dendrimers were also performed. Conjugated polymers and dendrimers are materials with great potential as display materials and tuneable lasers due to their broad spectra and high optical gains.

The effect of conjugation is studied in MEH-PPV and an anisotropy measurement of two different cored dendrimers has been shown to verify a theoretical prediction on their depolarisation. Singlet emission from a highly efficient phosphorescent dendrimer is also observed and is the first known report of fluorescence from this class of dendrimers.

Conjugated polymers exhibit optical gain over broad spectral ranges, which have led to much interest in their potential as novel laser gain media. Investigations into lasing from conjugated polymers has been confined mainly to studying the lasing properties and not the temporal dynamics of the laser pulses. In this work an investigation into the lasing dynamics of a 2D-DFB conjugated polymer laser is demonstrated with the first sub-picosecond laser pulses observed for a polymer laser. A novel encapsulated laser fabricated via a soft lithography route was also studied and exhibited laser pulse of 6 ps duration.

The high gain observed over broad spectral ranges also means that these materials are suitable for use as optical amplifiers. Broadband gain in a conjugated polymer solution was demonstrated with a gain of 30 dB accessible across a 60 nm wavelength range. In the solid state the limited thickness of films (~ 100 nm) and the uneven nature of the film edges had limited the ability to study the amplification of a probe signal. The first practical solid state conjugated polymer amplifier has been demonstrated. The device uses grating structures to couple a probe signal into and out of the gain region. The gain dynamics of different length amplifiers were studied and an 18 dB gain was observed in a 300 μm device length using a conjugated polymer blend of RedF and F8BT. Further work on a conjugated polymer MEH-PPV led to a 21dB gain in a 1 mm device.

Declarations

I, Mark Goossens, hereby certify that this thesis, which is approximately thirty four thousand words in length, has been written by me, that it is a record of the work carried out by me and that it has not been submitted in any previous application for a higher degree.

Signature of candidate: Date:

I was admitted as a research student and as a candidate for the degree of Doctor of Philosophy in October 2002; the higher study for which this is a record was carried out at the University of St Andrews between October 2002 and July 2006.

Signature of candidate: Date:

I hereby certify that the candidate has fulfilled the conditions of the Resolution and Regulations appropriate for the degree of Doctor of Philosophy in the University of St Andrews and that the candidate is qualified to submit this thesis in application for that degree.

Signature of supervisor: Date:

Copyright Declaration

In submitting this thesis to the University of St Andrews I understand that I am giving permission for it to be made available for use in accordance with the regulations of the University Library for the time being in force, subject to any copyright vested in the work not being affected thereby. I also understand that the title and abstract will be published, and that a copy of the work may be made and supplied to any bona fide library or research worker, that my thesis will be electronically accessible for personal or research use, and that the library has the right to migrate my thesis into new electronic forms as required to ensure continued access to the thesis. I have obtained any third-party copyright permissions that may be required in order to allow such access and migration.

Signature of candidate: Date:

Acknowledgements

There are many people I would like to thank for their help and support during my PhD. First of all I would like to thank my supervisor, Professor Ifor Samuel for the support and guidance over the years and for giving me the chance to perform interesting and stimulating research. I also need to thank the numerous members of the Organic Semiconductor Centre who have graced us with their presence over the years. There are too many to name all but special thanks go to Justin and John for their help in getting me started and for being great friends. Graham, Phil, Ebinazar, Chris, Andrew and Jean-Charles thanks for the help and support.

Thanks to all of you who shared the PhD experience with me and who I have worked with over the last few years. Dimi for being the wonderful person she is and for being a great friend in and out of the lab, good luck with the rest of the PhD. Andreas, nearly there my Greek friend, thanks for all your help and for showing the rest of us mere mortals how to play basketball. Finally thanks go to Andy who started with me as an undergraduate those many years ago. It's not the same without you mate, far quieter!

Last but certainly not least I must acknowledge the enormous amount of help and advice given to me by Dr Arvydas Ruseckas over the years. I have thoroughly enjoyed the work we have done together and thanks for being a great teacher, even if the subject matter is ultrashort he was always there to help for as long as it took for me to understand.

Outside of the Department I will miss all my friends in New Hall who I have lived with over the years, Laura, Nick, Anjali, Mog,, Lara and many others. Special thanks go to Matt (and his sidekick Alix) as well as Becky for being great friends and fantastic wardens.

There are three miscreants in the department who deserve most of the credit for keeping me sane during the PhD years. Maerkey, Mikey and Steve! Thanks for being great friends and good luck in your new jobs. A huge hug goes to V for being a great friend for so long.

Last but certainly not least are my family. Without the love and support of my mum and dad, Sjanie and Ruud, and my fantastic sisters Sandra and Marleen, I would not have made it this far. Thanks for being there and for who you all are.

Contents

Chapter 1

Introduction

Polymer materials are found all around us in our daily lives, from the materials used to make carrier bag to the synthetic fibres used in our clothing. The chemical family of polymers encompasses such a diverse range of materials that almost any required mechanical property can be provided by a polymer material. It is this diversity of applications and their ease of processing that have led to the use of polymer materials in such diverse applications.

Changes in the chemical structure of the polymer materials allows its mechanical properties to be tuned, a polymer can be flexible such as an overhead transparency or very hard and rigid such as the polycarbonate material CDs are made from. The one property which all conventional polymers exhibit, is their electrical insulation which is why so many electrical cladding tubes are made from polymer materials. However, a class of conducting polymers was first discovered by Heeger, McDiarmid and Shirakawa in the 1970s which gained them the Nobel prize in Chemistry in 2000[1-3]. Their discovery of conducting polymers with the versatility of plastic materials yet with electrical properties has led to many interesting new applications for polymer materials.

In recent years a class of semiconducting polymer have attracted a .great deal of interest The discovery in 1990 of electroluminescence [4] from a conjugated polymer has led to exciting new research and applications of these materials. Potential applications of conjugated polymers have been demonstrated in optoelectronic devices such as photovoltaic cells [5], field effect transistors [6], photodetectors [7] and the key

application of the organic light-emitting diode (OLED) [8-10] which has driven much of the interest in these materials. OLEDs are now commercially manufactured [11] and much of the recent research has been focussed on driving this application to the marketplace. With an increasing demand for colour displays rising, especially with the advances in mobile technology which require small area displays, the OLED display market is predicted to be worth in excess of $500 million [12]. New applications such as televisions based on conjugated polymer technology [13] have recently come to the prototype stage. Massive investment in manufacturing processes and factories is ongoing as these devices based on conjugated polymers have many manufacturing advantages over inorganic devices due to their simpler processing properties [14]. Another potential device application is for an alternative to the inorganic laser diode, optically pumped lasers have been demonstrated and the broad spectra of these conjugated polymers means they can potentially be tuneable over a large spectral range [15] and support ultrafast pulses.

In this thesis the theory of conjugated polymers is introduced in Chapter 2 with discussion of their electronic structure as well as the absorption and emission of light in these materials. Stimulated emission as the mechanism for gain is also discussed along with potential loss mechanisms. A novel class of materials known as conjugated dendrimers is also described.

Chapter 3 introduces the experimental techniques and instruments used in this work. Special emphasis is placed on the femtosecond laser sources and the detection systems, as the aim of this work was to study the properties of these materials in the ultrafast regime. The layouts of experimental setups are also detailed.

In Chapter 4 various optical spectroscopic studies are performed on conjugated polymer and dendrimer materials to probe their behaviour. The effect of breaks in the conjugation on the properties of a well known polymer 2-methoxy-5-(2'-ethylhexyloxy)-

1,4-phenylene vinylene (MEH-PPV) are studied in absorption and emission at cryogenic temperatures. Steady state and time-resolved measurements on conjugated dendrimers are performed to probe their anisotropy properties to test a theoretical model previously proposed. The singlet state emission from a phosphorescent dendrimer is observed via a femtosecond up-conversion technique.

Significant attention has been focussed on conjugated polymers as novel laser gain media [16-19] and they have exhibited high optical gain across a broad wavelength emission range In Chapter 5 a distributed feedback laser based on wavelength scale microstructures [20] is studied. The gain material is the conjugated polymer MEH-PPV. Emphasis is placed on the measurement of the temporal dynamics which are rarely studied [21], the broad emission range of conjugated polymers means that they could be used to sustain an ultrashort pulse and potentially be mode-locked in the future.

The conjugated polymer two-dimensional distributed feedback laser was found to support ultrashort pulse generation of 410 fs pulses. The pulse width was observed to shorten with an increase in excitation energy above the laser threshold. A simple rate equation model was used to describe this behaviour as the growth of amplified spontaneous emission. Further work on a novel encapsulated laser structure created by soft lithography [13] was performed and pulsewidths as short as 6 ps were recorded from this easily fabricated structure. Conjugated polymer laser devices are thus a potential light source for future communications networks which are compatible with the low-cost polymer optical fibre technology (POF) for short-haul networks [22].

The high gain available from conjugated polymers across broad wavelength ranges also indicates their potential use as broadband amplifiers. Solution based optical amplification from a conjugated polymer has so far only been demonstrated once over a broad range [18]. In Chapter 6 a solution amplifier based on the F8BT polymer is reported which exhibits gain over 55 nm with a peak gain of 40 dB. Accessing gain in the

solid-state would be more practical for actual devices based on these materials but the thin nature of spin-coated films have so far precluded any device based on solid state gain. A device architecture is reported utilising grating structures fabricated into a substrate (upon which the polymer is then spin coated) to couple a probe beam into and out of a gain region. This is the first reported solid state conjugated polymer optical amplifier with controlled probe signal propagation into and out of a polymer film. An optimised blend of RedF and F8BT was used as a gain material and a gain of 18 dB in a 300 μm device was observed. Further work on a MEH-PPV amplifier device is reported which exhibited a gain of 21 dB in a 1 mm device.

References for Chapter 1

[1] A. J. Heeger. *Reviews of Modern Physics*, **73**, 681 (2001).

[2] A. G. McDiarmid. *Reviews of Modern Physics*, **73** 701, (2001).

[3] H. Shirakawa. *Reviews of Modern Physics*, **73**, 713 (2001).

[4] J. H. Burroughes, D. D. C. Bradley, A. B. Brown, R. N. Marks, K. Mackay, R. H. Friend, P. L. Burns, and A. B. Holmes. *Nature*, **347**, 539 (1990)

[5] N. S. Sariciftci, *Current Opinion in Solid State & Materials Science* **4**, 373 (1999)

[6] J. H. Burroughes, C. A. Jones, and R. H. Friend , *Nature* **335**, 137 (1988).

[7] G. Yu, J. Wang, J. McElvain, and A. J. Heeger, *Advanced Materials*. **10**, 1431 (1998

[8] C. W. Tang and S. A. VanSlyke, Applied Physics Letters, **51**, 913 (1987).

[9] J. H. Burroughes, D. D. C. Bradley, A. R. Brown, et al., *Nature* **347**, 539 (1990).

[10] R. H. Friend, R. W. Gymer, A. B. Holmes, et al., *Nature* **397**, 121 (1999).

[11] Pioneer, *Introduction of a Monochrome 256x64 OLED Display for car stereos* (1999).

[12] S. Resources, *Long Term Forecast: Organic Light-Emitting Diode Displays* (www.stanfordresources.com, 2000).

[13] www.samsung.com, press release May 2005

[14] J. R. Lawrence, P. Andrew, W. L. Barnes, G. A. Turnbull and I. D. W. Samuel, *Applied Physics Letters*, **81**, 1955 (2002)

[15] D. Moses. *Applied Physics Letters*, **60**, (1992).

[16] F. Hide, M. A. Diaz-Garcia, B. J. Schwartz, M. R. Andersson, Q. Pei, and A. J. Heeger. *Science*, **273**, 1833, (1996).

[17] N. Tessler. *Advanced Materials*, **11**, 363, (1999).

[18] M. D. McGehee and A. J. Heeger. *Advanced Materials*, **12**, 1655,(2000).

[20] GA. Turnbull, P. Andrew, M. J. Jory, W. L. Barnes, and I. D. W. Samuel, *Physical Review B*, **64**, 125122 (2001)

[21] Stagira S, Zavelani-Rossi M, Nisoli M, DeSilvestri S, Lanzani G, Zenc C, Mataloni P, Leising G, *Applied Physics Letters*, **73**, 2860 (1998)

[22] J. R. Lawrence, G. A. Turnbull, I. D.W. Samuel, *Applied Physics Letters* **80**, 3036 (2002).

[23] Y. Koike, T. Ishigure, M. Satoh, and E. Nihei. *Pure and Applied Optics*,**7**, 201, (1998).

Chapter 2

Theory of Organic Semiconductors

2.1 Introduction

The label “semiconductor” has generally only been applied to crystalline inorganic materials, such as Silicon, Indium Gallium Arsenide and Indium Phosphide. The advances in electronic and optoelectronic devices based on inorganic semiconductor technology have allowed us to achieve technological improvements which have transformed our society over the past fifty years. The advent of faster electronics and computers leading to the spread of high speed communication, (whether the internet or mobile phones), together with advances made in display and medical devices have left few lives have unaffected by inorganic semiconductors.

Within inorganic semiconductors covalent bonding between the atoms leads to a periodic arrangement of these atoms in a lattice structure. Due to the crystalline arrangement and the overlapping of electronic orbitals within the lattice the discrete atomic states behave like a band structure with a well defined energy-momentum dispersion relation for both electrons in the conduction band and holes in the valence band. The composition of semiconductors can be controlled with the addition of different elements to produce a compound semiconductor. This control of doping allows a control over the properties of the compound semiconductor. This control has been the strength of inorganic semiconductors in that they can be tuned to the application by introducing dopants during manufacturing.

A novel class of organic semiconductors which have been studied in this thesis are different in that their mechanical properties are similar to plastics. Plastic materials are classically electrical insulators and hence have been used as cladding for electrical wires for many years. Organic semiconductors combine the mechanical properties of plastic materials with the electronic properties of inorganic semiconductors. Different classes of organic semiconductors include conjugated polymers, which are long chained polymers (similar to plastics) and conjugated small molecules.

In order to explain the properties of organic semiconductors the nature of chemical bonds will be briefly discussed.

Organic compounds are based on carbon atoms attached to each other in a chain of varying lengths and geometries with other atoms (or molecules) attached to this carbon backbone. In conjugated molecules carbon atoms are covalently bonded via alternating single and double bonds. A simple demonstration of how carbon atoms form a double bond can be obtained by looking at the electronic structure of Ethene (C_2H_4) shown in Figure 2.1.

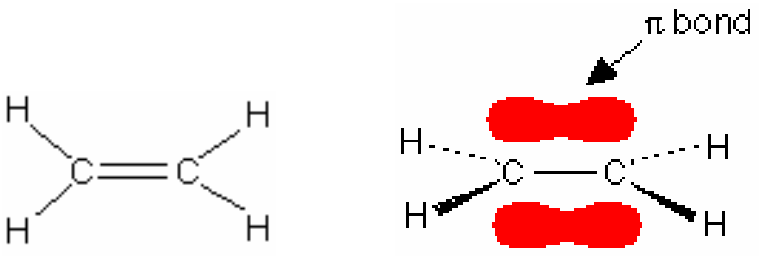

Figure 2-1: Chemical Structure of the Ethene molecule and an illustration of the chemical bonds. The π bond is an overlap of two bonds on attached atoms.

Ethene has two carbon atoms connected by a double bond and four hydrogen atoms, two attached to each carbon atom via single bonds. There are four electrons in the outer shell of a Carbon atom and it has an electronic configuration of $1s^2 2s^2 2p^2$. Ethene is

a specific case the following description of bonding provides a demonstration of this mechanism. The outer two p electron orbitals of Carbon are unpaired and are free to mix with the 2s orbitals to form three equally hybridised orbitals in the sp^2 state leaving the last valence electron in a p orbital. The three hybrid orbitals lie in a plane at 120^0 angles to each other.

These three orbitals and the remaining p orbital then make up the bonding orbitals of the carbon atom and when two carbon atoms attach to each other two sp^2 orbitals overlap to form a single σ bond. The remaining p orbital on each carbon atom then overlap with each other, above and below the plane of the molecule (Figure 2.1) to form a π bond which provides the molecule with a rigid chain as in order for the two carbon atoms to rotate relative to each other the bond has to be broken.

Ethene is a small molecule and for larger conjugated organic molecules the chain is usually made up of alternating single and double bonds, this is described as conjugation. In a conjugated molecule such as a benzene ring (C_6H_6), see Figure 2.2, each Carbon atom has four valence electrons, three of which form the sigma bonds to each other and the hydrogen atoms. The remaining 6 electrons occupy the remaining p orbitals which are perpendicularly aligned to the σ bonds. The p orbitals between neighbouring carbon atoms form several double bonds such that the benzene ring ends up with alternating single and double bonds.

This is a conjugated π system where the weakly bound π -electrons are said to be delocalised as they can no longer be identified with a particular Carbon to Carbon bond as their wavefunction is delocalised over the entire ring. The weakly bound π -electrons are responsible for the semiconductor properties of this class of organic materials as they provide a source of electrons not bound but delocalised such that they can move along the carbon chain and contribute towards conduction and hence semiconducting properties.

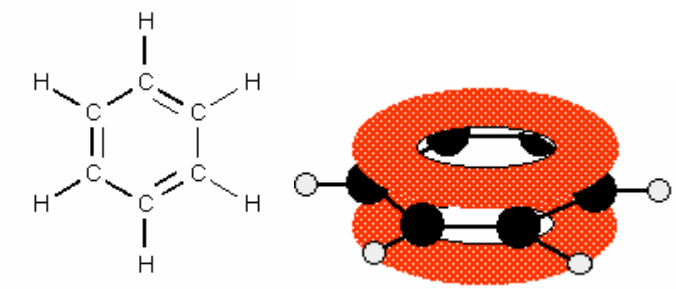

Figure 2.2: The chemical structure of Benzene and an illustration of the delocalisation of the π bonds

All organic semiconductors have some sort of extended conjugated p system. Some organic semiconductors are small molecules where the conjugation is over a relatively short distance but for classical polymers which are made up of repeat units (monomers) the delocalised π system can theoretically extend over the entire chain, a classical polymer like trans-polyacetylene shown in Figure 2.3 illustrates how the conjugation can easily extend over a long polymer chain. This is of course an idealised version as any defects will create a break in the conjugation, but over the entire length of the polymer chain a large percentage is conjugated.

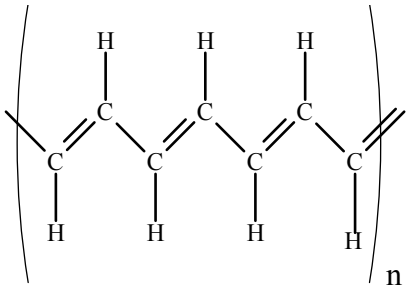

Figure 2-3: Polyacetylene structure with alternating single and double bonds.

2.2 Absorption and emission of light

In organic semiconductors the bonding and anti-bonding orbitals create two pseudo continua of energy levels separated by an energy gap. This allows the material to have a band like electronic structure and the π orbital energy corresponds thus to an optical energy. Optical spectroscopy is thus an invaluable tool to probe the properties of these materials.

The absorption of light in a molecule is governed by the interaction of the electromagnetic radiation field with the material. A photon may be absorbed from the field and an electron excited to a higher energy state, if the energy of the photon corresponds to the energy gap between the ground and excited state of the material. The strength of the interaction can be experimentally determined by measuring the molar absorption or the extinction coefficient ε, as expressed by the Beer-Lambert Law [1] in Equation 2.1. The intensity of light I with frequency v travelling a distance z through a material of concentration c is related to the initial intensity I_0 by.

$$I(z,v) = I_0 10^{-\varepsilon(v)cz} \qquad \text{(Equation 2.1)}$$

The extinction coefficient can be related to the electronic structure of the molecule by examining the electronic energy levels shown in Figure 2.4. In the upper section the molecular potential energy is plotted as a function of molecular coordinates of the molecule, the corresponding lower section shows the classical absorption and emission spectra of a molecule.

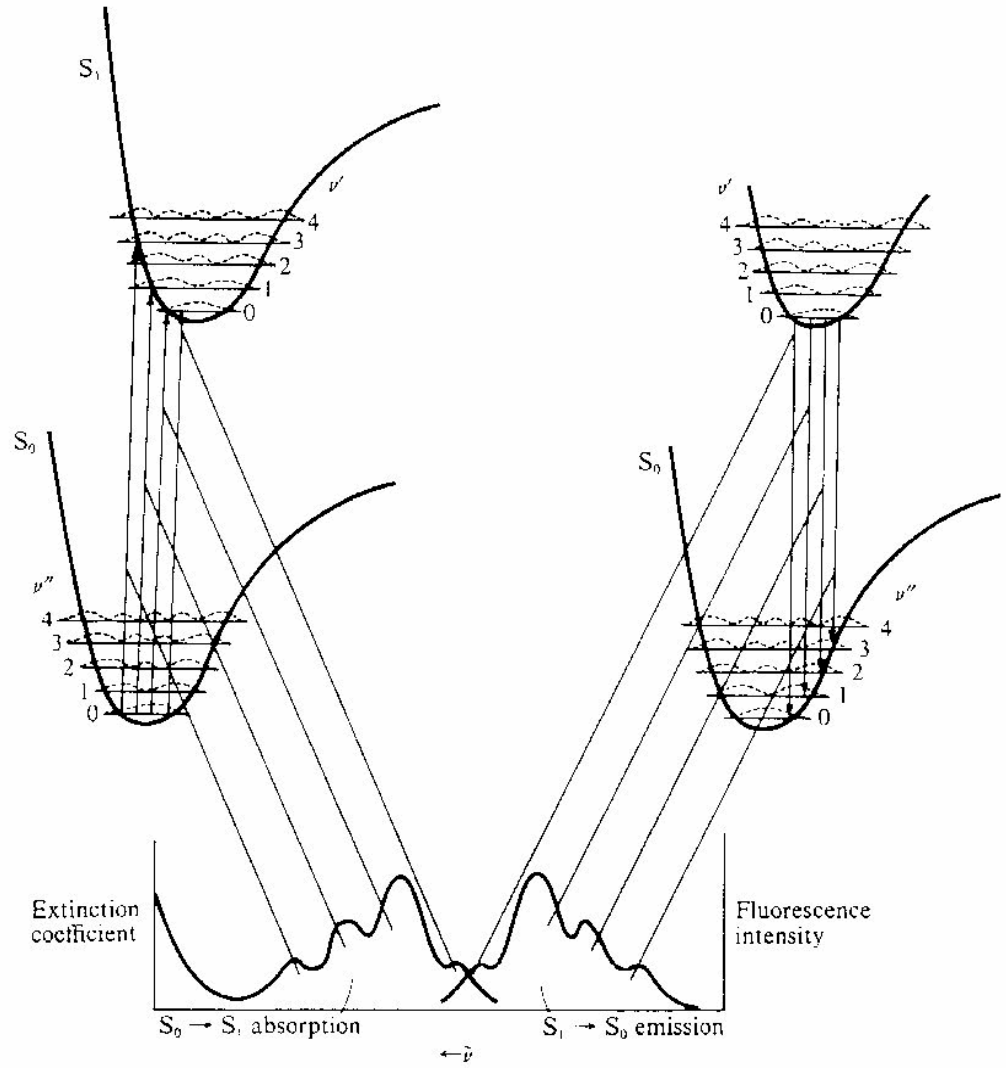

Figure 2-4: Electronic configuration representation of absorption and emission [2]

Absorption is illustrated on the left hand side and the spacing of the energy levels within the potential are greater than K_bT_{room} so that the lowest vibronic level of the ground state (S_0) is populated at room temperature. The ground state and excited state potentials are offset from each other due to the difference between their nuclear configuration coordinates. The ground state to excited state transition is the vertical line with the electronic transition occurring in 10^{-15} seconds and the nuclear rearrangement in

about 10^{-12} seconds as described in the Franck-Condon principle [2,3], which states that any nuclear re-arrangement occurs after electronic transitions have occurred.

As a photon is absorbed an electron is excited from the S_0 ground state into an excited state vibronic level (S_1). The excited state level depends on the energy of the photon absorbed and the probability of excitation into any given level depends on the overlap of the groundstate wavefunction with the excited state wavefunction for that level. This creates an envelope of vibronic bands in the absorption spectrum which is known as the Franck-Condon envelope [3].

After the electron has been excited the charge density within the molecule will change from that in the ground state and in order to minimise its energy the molecule will rearrange to accommodate the new electron density. When the molecule is in solution the solvent environment surrounding the excited molecule may a2so rearrange as a result of these changes. Thus the excited state potential changes shape as is evident on the right hand side of Figure 2.4. This produces a shift between the 0-0 transitions in absorption and fluorescence.

An excited electron will decay to the lowest vibronic level of the excited state non-radiatively and then return to the ground state by a combination of radiative and non-radiative processes (radiative decay is shown as a vertical line in Figure 2.4). When returning to the ground state the electron may decay to any vibronic level (not just the lowest) before internal conversion causes the electron to return to the lowest ground state level. This gives rise to the vibronic progression evident in Figure 2.4. The absorption from the ground state to a level within the excited state manifold is observed as the different structures within the spectra (due to the energy differences between these states 0-0, 0-1, 0-2 etc.). Likewise for emission the relaxation to the ground state manifold (followed by non-radiative transfer to $S_0(0)$) leads to the differences in photon energy released depending on which vibronic level the electron decayed to.

The intensity of the absorption of a given photon is limited by the relative orientations of the polarisation of the electromagnetic field of the photon and the electric dipole moment of the molecule. If these are perpendicular to each other then field and the dipole cannot couple together and thus there is no interaction. If the relative angle between the field and the dipole is θ then the strength of the interaction is proportional to $\cos^2\theta$. Emission will be polarised in the direction of the electric dipole moment of the molecule. Thus if the dipole moment changes between absorption and emission the absorbed and emitted photons will be polarised in different directions.

Alternatively the molecule may not be straight and as the excitation travels along the molecule before it decays the dipole moments where the photon was absorbed and where the new photon is emitted will be different. Therefore the measurement of polarisation changes is a powerful tool to probe energy migration in conjugated organic materials. The difference in polarisation is quantified as the anisotropy of a material and reflects the change in direction of the polarisation between absorption and emission. It can be defined as r

$$r = \frac{I_{\parallel} - I_{\perp}}{I_{\parallel} + 2I_{\perp}} \qquad \text{(Equation 2.2)}$$

where $I_{\parallel}$ is the intensity of the emission when the excitation is polarised parallel to the polarisation of the emission and $I_{\perp}$ is the intensity of the emission when the excitation is polarized perpendicularly to the polarization of the emission. The angle between the two dipoles (φ) is related to the anisotropy by the Perrin equation [4]

$$r = \frac{1}{5}(3\cos^2\varphi - 1) \qquad \text{(Equation 2.3)}$$

The anisotropy is a function of $\cos^2 \varphi$ and the maximum value is when the absorption and emission dipoles are collinear. This leads to a maximum value of anisotropy of r = 0.4.

The absorption and emission of conjugated molecules are usually near mirror images of each other with a small Stokes' Shift between the fluorescence and absorption spectra peaks (shown in Figure 2.4). Figure 2.5 shows the absorption and photoluminescence spectra of a well-known conjugated polymer poly(2-methoxy-5-(2'-ethylhexyloxy)-1,4-phenylene vinylene) also named MEH-PPV.

As can be seen in Figure 2.5 the absorption is much broader than the photoluminescence and both are mainly structureless. There is a large shift between the emission and absorption peaks and this is explained by considering the disordered nature of the polymer chains [5,6]. Conformational disorder means that the polymer chains are twisted and folded leading to breaks in the conjugation and as such the polymer chain

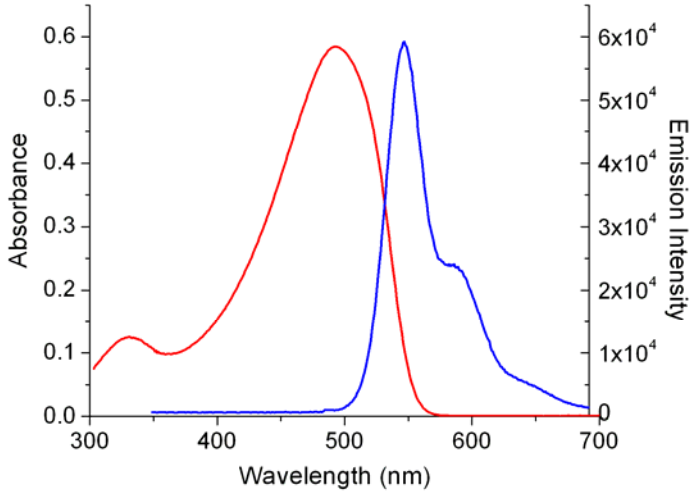

Figure 2-5: Absorption and emission spectra of a common conjugated polymer MEH-PPV

contains many shorter conjugated segments. The inhomogeneously broadened absorption of these shorter segments determines the overall absorption spectra of the polymer [6].

The photoluminescence of the polymer may be expected to be broadened in a similar way but this is obviously not the case as seen in Figure 2-5. The difference in the structure of the photoluminescence may be explained by the intra-chain migration of excitons along the polymer backbone chain or via inter-chain interactions to another chain [6,7,8,9], the three-dimensional nature of these folded chains lead to possible migration to an adjoining segment on the same chain or to another segment on another chain. Upon excitation an exciton is created on one segment and then migrates to segments of longer conjugation length (and lower energy) and when they arrive there they become stuck as they are now in an energy minimum and cannot migrate to adjoining segments of higher energy [10,11].

The trapped excitation then decays radiatively from these lower energy segments and thus the photoluminescence spectrum is predominantly that of the longer segments. Put simply, a broader selection of segments will absorb photons but by the time the fluorescence decay occurs the excitation has migrated to a subsection of segments of lower energy and thus is not broadened as much. Thus also contributes to the difference in the peak positions of emission and absorption.

Despite the emission spectra not being as broad as the absorption spectra, organic semiconductors still exhibit very broad emission spectra in the visible region compared to many inorganic materials. This broad emission range can be useful for applications such as light emitting diodes (LEDS), broadband tuneable lasers and amplifiers and are thus an exciting class of materials for photonic applications

2.3 Stimulated Emission in Conjugated Semiconducting Polymers

In order to achieve lasing action or optical amplification from a conjugated polymer the material must exhibit gain. When optically pumped this means that stimulated emission is responsible for this and the general gain mechanism if briefly introduced her as well as potential loss mechanisms.

2.3.1 The Gain Mechanism

For lasing to occur, the presence of stimulated emission is required. In Section 2.2 luminescence was shown to result from the transition between a singlet excited state (S_1) and the ground state (S_0). These two states have many vibronic sublevels (υ = 0,1,2,3…) as shown in Figure 2.6.

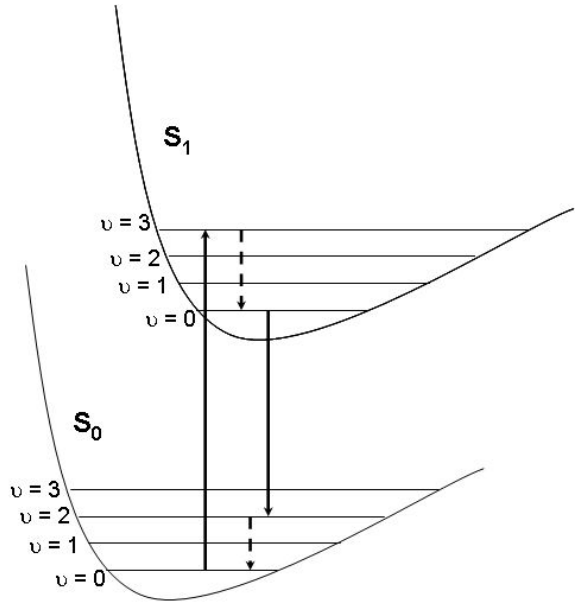

Figure 2.6 - A typical four level laser scheme.

Conjugated polymers exhibit strong stimulated emission for the transition S_1 (υ = 0) to a vibronic level of the ground state S_0 (υ). As shown in Figure 2.6 the process of gain starts when the material is excited from the ground state to a higher vibronic level of the excited state. Fast non-radiative relaxation then takes place from this state to the lowest vibronic level (υ = 0) of the excited state. A radiative optical transition then occurs from this state to a higher vibronic level of the ground state. Again fast non-radiative relaxation to the lowest level of the ground state occurs.

This leads to a classic four level laser system where the population of the excited state is higher than the ground state it relaxes to. Due to the fast non-radiative relaxation in the ground state to its lowest level this means that there is almost always a population inversion as the higher vibronic levels are quickly depleted. This means that when light passes through a gain medium its intensity is amplified according to Equation 2.4,

$$I = I_0 \exp[(g(\lambda) - \alpha)l] \qquad \text{Equation 2.4}$$

where I is the emission intensity after passing through the gain, I_0 is the initial intensity of the emission, λ is the length of the gain interaction region, $g(\lambda)$ is the gain coefficient and α the loss coefficient. In this four level laser system the gain depends on the volume density of excited states N_{exc} and this relationship is defined by:

$$g(\lambda) = N_{exc}\sigma_{SE}(\lambda) \qquad \text{Equation 2.5}$$

The wavelength dependence of the stimulated emission cross-section normally resembles the photoluminescence spectrum of the material.

As can be seen in Equation 2.3 several factors affect the amplification of the intensity entering the gain medium. The most important factor is that gain needs to be larger than the losses in the medium. This net gain is then only used over the interaction length of the gain medium and emission. The final parameter is that the number of excited states limits the size of the gain coefficient.

2.3.2 Potential Loss Mechanisms

The first parameter that will limit the use of a gain medium is if the sum of the losses is higher than the available gain. In order to extract the most gain from the material the losses need to be minimized if possible. Several potential loss mechanisms exist and are outlined below.

Ground state absorption of the emission light by the gain material leads to a loss of signal. This re-absorption is known as self-absorption and occurs if there is an overlap of the emission and absorption spectra of the gain material. In Section 2.2 the emission and absorption spectra of conjugated polymers were shown to be separated due to the nature of the polymer chain. The polymer chain is broken by defects and this leads to a variety of chain lengths all of which can absorb, but due to the favourable energy conditions the excitations transfer to the longer chains, which emit at longer wavelengths. The shift between emission and absorption also means that this may not be a large contributing loss factor but needs to be considered depending on the gain material properties and the wavelength of the signal being amplified. Another loss associated with signal attenuation within the gain material is excited state absorption. This occurs when there is radiative absorption in the excited state to a higher energy state.

Materials such as conjugated polymers are synthesised with typically many thousands of repeat units. Defects such as unwanted elements or breaks/twists in the

chain are thus important to eliminate if possible . As has been discussed earlier there are many such breaks (caused by twisting for instance) in the chain leading to a variety of chain lengths contributing to the spectra but unwanted additional elements in the chain may lead to more problems. If, for example, oxygen is dissolved in the polymer chain it can break the conjugation and produces a carbonyl group on the chain. Such a group attached to the polymer chain is known to be an efficient luminescence quencher [12]. Scattering within the material can also be a contributing factor.

When photo-pumped by high energy lasers, conjugated polymers can also incur losses at high excitation densities. With typical excitation densities of 10^{16} - 10^{20} cm^3 [13] the spacing between these excitations (excitons) is quite short on a polymer chain. There are several mechanisms for interaction between excitons situated near to each other. They can interact by non-radiative recombination, which is known as exciton-exciton annihilation [14] and they could potentially form interchain species if the nearest exciton is on a different chain but in the solid state they can be close together.

The existence of these interchain species has been hotly debated in the past decade due to some conflicting reports. MEH-PPV studied in solution, in neat film and a blend with polystyrene was found to exhibit stimulated emission in the solution and blend but only very weakly in the neat film [15]. The stimulated emission decay dynamics of the blend and the solution were also very similar though those for the neat film and were comparable to aggregated organic molecules. However, photo-oxidation of these films was found to be responsible for the lack of stimulated emission in PPV films [14] and explains many of the earlier conflicts. Later research on MEH-PPV, CN-PPV and PPV [16] using the time correlated single photon counting (TCSPC) technique established that the lifetime of the MEH-PPV neat film was longer than that in solution (similar to CN-PPV) but MEH-PPV does not exhibit the same red-shift and broadening of the emission spectrum as CN-PPV. The emission in CN-PPV was found to be due to emission from an

interchain excitation [17]. Interchain interactions were considered to be present in MEH-PPV but the dominant emission is from an intra-chain excitation compared to CN-PPV.

Further work on the photoluminescence quantum yields (PLQY) of PPV derivatives created a confusing picture as the consistent relationship between PLQY, radiative lifetime and PL decay suggested no interchain interaction [18]. It was not until later, that work on a wider range of derivatives explained this contradiction. They found that the interchain interaction was heavily dependent on the structure of the material studied. Parameters affecting interchain interactions varied from solvent used, concentration of polymer, the temperature as well as the conditions during film deposition [19].

Further transient absorption studies of MEH-PPV films have shown that at higher excitation densities the behaviour observed is due to exciton-exciton annihilation [20].

2.4 The Dendrimer Concept

Conjugated molecules as described in the previous sections have mainly fallen into two categories, small organic molecules [21] or conjugated polymers [22. Small molecules have well defined structures compared to conjugated polymers but also have some disadvantages. They are usually deposited using evaporation techniques, which limits the size of the substrate to be used and for commercial potential this would limit production and increase costs for small molecule devices.

Conjugated polymers are normally dissolved in solution and are then deposited using solution processing techniques. Solution processing allows the organic semiconductor layer to be printed in place (using techniques similar to ink-jet printing for instance). This flexibility is a major advantage for devices with commercial potential as these techniques lend themselves more to mass production. However, even though

conjugated polymers are well studied they are more difficult to synthesise and purify compared to small molecules. During synthesis varying molecular weights of the material are produced at the same time (different length polymer chains, an effect commonly known as polydispersity). This as well as the fact that the processing conditions can lead to varying electronic and optical properties [23,24], means that more work is to be done to produce a material and deposition process which will lend itself to reliable and reproducible mass production.

One other class of materials which has been developed in recent years has been the semiconducting dendrimer. These conjugated dendrimers are specially designed materials which have been developed mainly for use in display applications such as OLEDs. A conjugated dendrimer is made up of three separate sections as shown in Figure 2.7. The dendrimer consists of a core which has several branched conjugated linking groups known as dendrons and at the end of the dendron surface groups are attached.

Each of the three parts plays a role in the properties of the dendrimer. For optoelectronics applications such as OLEDs for instance, the core will be a light emitting unit, the dendrons separate the cores and the surface groups control the solubility in solvents.

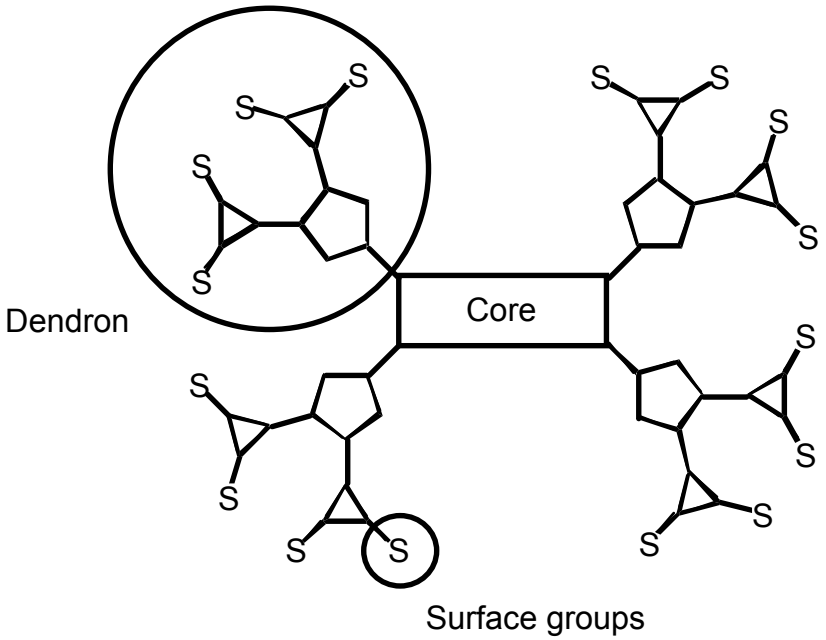

Figure 2-7 - Dendrimer structure, a light emitting core is attached to several conjugated branches and at the ends of the branches surface groups are attached.

The branching of the dendrons leads to a shielding effect which inhibits interactions between excitations and the surrounding environment. The effect of adding dendrons on the optical properties of the dendrimer has been studied [25] using Rose Bengal with an observed reduction in the aggregate emission upon addition of dendrons.

This molecular architecture has led to many new materials for which the electrical, optical and processing properties have been independently tuned [26,27]. The core will control the emission range, the electronic properties are adjusted by tuning the number and type of dendrons and the surface groups can be changed to allow solubility in different solvents enabling simpler processing compared to polymers.

This modular approach to material design has several advantages over semiconducting polymers. Tuning the solubility of a polymer usually leads to changes in its emission properties. Whereas in dendrimers the choice of core is not limited by the structure of the dendrimer many of the fluorophores would not lend themselves to

incorporation as a repeat unit in a conjugated polymer. Most research on dendrimers has been to produce solution-processed OLEDs with these devices being some of the most efficient of its kind [28].

Chapter 2 References

[1] PW Atkins. *Physical Chemistry*, Chapter 16. Oxford University Press, Fifth Edition, (1994)

[2] M Pope and CE Swenberg, *Electronic Processes in Organic Crystals*, Oxford University Press (1982)

[3] JB Birks. *Photophysics of Aromatic Molecules*, Chapter 3, Wiley and Sons (1969)

[4] J. Perrin. *Journal de Physique et le Radium*, **7**, 390, (1926).

[5] H Bassler, C Brand, M Deusen, EO Gobel, R Kertsing, H Kurtz, U Lemmer, RF Mahrt and A Ochse. *Pure and Applied Chemistry*, **67**,377 (1995)

[6] B Mollay, U Lemmer, R kertsing, RF Mahrt, H Kurtz, HF Kauffmann and H Bassler, *Physical Review B*, **50**, 10769 (1994)

[7] MCJM Vissenberg and MJM de Jong, *Physical Review Letters*, **77**, 4820 (1996)

[8] GR Hayes, IDW Samuel and RT Phillips, *Physical Review B*, **52**, R11569 (1995)

[9] MML Grage, T Pullerits, A Ruseckas, M Theander, O Inganas and V Sundstrom. *Chemical Physics Letters*, **339**, 8253 (2000)

[10] H Bassler and B Schweitzer, *Accounts of Chemical Research*, **32**, 173 (1999)

[11] S Heun, RF Mahrt, A Greiner, U Lemmer, H Bassler, DA Halliday, DDC Bradley, PL Burn and AB Holmes. *Journal of Physics: Condensed Matter*, **5**, 247, (1993)

[12] Rothberg LJ, Yan M, Galvin ME, Kwock EW, Miller TM and Papadimitrakopoulus F, *Synthetic Metals*, **80**, 41 (1996

[13] Kranzelbinder G, Leising G, *Reports on Progress in Physics*, **63**, 729, (2000)

[14] Denton GJ, Tessler N, Harrison NT, Friend RH. *Physical Review Letters*, **78**, 733, (1997).

[15] M. Yan, L. J. Rothberg, F. Papadimitrakopoulos, et al. Phys. Rev. Lett. **72**, 1104 (1994).

[16] I. D. W. Samuel, G. Rumbles, R. H. Friend, S. C. Moratti, and A. B. Holmes. *Synthetic Metals*, **84**, 497, (1997).

[17] IDW Samuel, G Rumbles, CJ Collison, B Crystall, SC Moratti, AB Holmes, *Synthetic Metals*, **76**, 15 (1996)

[18] N. C. Greenham, I. D. W. Samuel, G. R. Hayes, R. T. Philips, Y. A. R. R. Kessener, S. C. Moratti, A. B. Holmes, and R. H. Friend. *Chemical Physics Letters*, **241**, 89, (1995).

[19] T. Nguyen, I. B. Martini, J. Liu, and B. J. Schwartz. *Journal of Physical Chemistry B*, **104**, 237, (2000).

[20] D. Vacar, A. Dogariu, and A. J. Heeger. *Advanced Materials*, **510**, 669, (1998).

[21] CW Tang and S. A. Van Slyke, *Applied Physics Letters.* **51**, 913 (1987)

[22] JH Burroughes, DDC Bradley, AR Brown, et al., *Nature* **347**, 539 (1990).

[23] T-Q Nguyen, RC Kwong, ME Thompson and BJ Schwartz, *Applied Physics Letters*, **76**, 2454 (2000)

[24] Y Shi, J Liu, and Y Yang, *Applied Physics* **87**, 4254 (2000)

[25] FGA Jansen, EMM DeBrabander-Vandenberg and EW Meier, *Science*, **266**, 1226 (1994)

[26] JNG Pillow, M Halim, JM Lupton, PL Burn and IDW Samuel, *Macromolecules*, **32**, 5985 (1999)

[27] M Halim, JNG Pillow, IDW Samuel, and PL Burn, *Advanced Materials*, **11**, 371 (1999)

[28] Anthopoulos TD, Markham JP, Namdas EB, Samuel IDW, Lo SC, Burn PL, *Applied Physics Letters* **82**, 4824 (2003)

Chapter 3

Experimental Techniques

3. 1 Introduction

Optical spectroscopic techniques are important tools to investigate the optical characteristics of conjugated polymers and dendrimers. In this chapter the optical spectroscopy techniques and the equipment used in this work will be outlined. First the classical steady state absorption and photoluminescence measurement techniques used during this thesis are introduced. Then the experimental techniques performed at the Femtosecond Laser-Amplifier Facility at the School of Physics and Astronomy will be discussed.

The equipment will be discussed followed by the various experimental layouts available and used during this research. Time-resolved measurements were performed using femtosecond lasers as excitation sources to provide the ultimate time resolution. This short time resolution has enabled measurements of the temporal dynamics of material and device emission into the femtosecond regime.

The use of femtosecond lasers has also meant that with the aid of specialised instruments based on nonlinear optics, the wavelength of the laser output could be converted to a desired wavelength. The operation of the lasers as well as the wavelength conversion is discussed as well as the various detection techniques available in the laboratory.

3. 2 Absorption Measurements

The theory of absorption was explained earlier in Chapter 2 and classically the absorption (A) of a sample is defined in Equation 3.1

$$A = -\log_{10}(T) \qquad \text{(Equation 3.1)}$$

where T is the transmission of the sample. The absorption is related to the molar extinction coefficient ε by Equation 3.2, where c is the concentration and l is the path length of the sample.

$$A = \varepsilon c l \qquad \text{(Equation 3.2)}$$

The absorption measurements in this work were performed using a Varian Cary 300 absorption spectrometer. The spectrometer was configured using a double beam geometry in order to eliminate the effects of the solvent and cuvette. During sample measurements the first measurement involved producing a baseline using a cuvette of solvent in each arm of the spectrometer. This enables the determination of the instrument zero absorption level and thus allows for the compensation of differences in absorption between the optical paths of the two arms. The measurement is repeated using the same cuvette of solvent in the reference arm and the sample to be measured in a cuvette in the sample arm. Using the ratio of the intensities between the two arms the instrument calculates the absorption of the sample and virtually eliminates the background absorption from the solvent. The baseline method works well for eliminating weak solvent and cuvette absorption but in the deep ultraviolet region data measurements are impossible as the solvent and cuvette normally absorb strongly at these wavelengths making measurements impossible.

When performing temperature dependence measurements using a cryostat (Oxford Instruments DN-V liquid nitrogen cooled cryostat) this baseline could not be taken as two cryostats cannot be placed in the instrument simultaneously. This means that a baseline cannot be measured against a similar solvent spectrum. The spectra were recorded relative to an empty reference arm. The contribution of the solvent was accounted for by measuring its absorption on its own (relative to free air) at the same temperatures as for the sample measurements.

3.3 Photoluminescence measurements

Steady state photoluminescence spectroscopy is a powerful tool for probing the excited state of a sample. Measurements were recorded using a Jobin-Yvon Fluoromax 2 spectrometer. The Fluoromax 2 uses a xenon bulb as a continuous excitation source, which using a monochromator can be tuned to the desired excitation wavelength. The emission of the excited sample is collected at 90 degrees to the excitation and discriminated using a second monochromator which scans across the visible spectrum. Finally the signal is detected by a photomultiplier tube operating in single photon counting mode. To avoid self-absorption effects in the spectra the solutions are normally prepared with a peak absorbance of $A < 0.1$

3.4 Steady State Anisotropy

Anisotropy was introduced in Chapter 2.2 and steady state anisotropy is performed in Chapter 4. Steady state anisotropy was performed using the Fluoromax 2 spectrometer. Polarisers were introduced into the instrument in both the excitation and emission arms. The spectra of both vertically and horizontally polarised excitation and emission were measured.

The steady state spectrometer used in this investigation was a single emission channel system in an L-geometry which means only one polarization can be measured at one time and that the emission is collected perpendicular to the excitation signal direction. With this method there is a problem in that the monochromator in the emission channel does not have the same transmission efficiency for vertically and horizontally polarised light. Thus if a sample is illuminated with vertically polarised light, for instance, then if an emission polariser is rotated, the measured intensities change even if the emitted light is unpolarized. Thus the measured intensities are not the desired vertical and horizontal values but are changed by the detection system. The goal is thus to measure the unbiased polarisation intensities.

These unbiased values are denoted by $I_{\parallel}$ for the parallel and $I_{\perp}$ for the perpendicular emission. The actual measured intensities in the emission channel are

denoted by a double subscript referring to the polarisation state of the excitation and emission polarisers, for instance, I_{VH} means this is the signal measured with vertically polarised excitation and horizontally polarised emission. The measured value is thus related to the unbiased value by the sensitivity of the emission channel to the different polarisation states, in this case termed S_V and S_H. Equations 3.1 and 3.2 follow on from this but Equations 3.3 and 3.4 are related only to $I_\perp$. This is because the emission is being detected perpendicular to the direction of the excitation signal. Thus for a sample excited with horizontally polarised excitation the emission signal for both vertical and horizontal can both related to the perpendicular emission $I_\perp$ [1].

$$I_{VV} = S_V I_\parallel \qquad \text{Equation 3.1}$$

$$I_{VH} = S_H I_\perp \qquad \text{Equation 3.2}$$

$$I_{HV} = S_V I_\perp \qquad \text{Equation 3.3}$$

$$I_{HH} = S_H I_\perp \qquad \text{Equation 3.4}$$

The ratio of Equations 3.3 and 3.4 allows us to determine the ratio between the polarisation sensitivities of the detection channel, S_V/S_H which is known as the G factor and allows us to determine the ratio between the unbiased polarisation values $I_\perp / I_\parallel$.

$$\frac{S_V}{S_H} = \frac{I_{HV}}{I_{HH}} = G \qquad \text{Equation 3.5}$$

Using Equations 3.1, 3.2 and 3.5 the degree of polarisation (P_r) of the emission can be determined.

$$P_r = \frac{I_\parallel}{I_\perp} = \frac{S_H I_{VV}}{S_V I_{VH}} = \frac{I_{HH} I_{VV}}{I_{HV} I_{VH}} \qquad \text{Equation 3.6}$$

Rearranging the anisotropy definition in Equation 2.2 we get:

$$r = \frac{P_r - 1}{P_r + 2} \qquad \text{Equation 3.7}$$

The anisotropy is related through Equation 2.3 to the angle between the absorption and emission dipoles φ. This can be rearranged to

$$\varphi = \cos^{-1}\sqrt{\frac{5r+1}{3}} \qquad \text{Equation 3.8}$$

3.5 Solution amplifier setup

In order to study the gain of a material in solution the following experimental layout was used. The experimental layout for the optical amplifier is shown in Figure 3.1, based on a Photonics Technology International GL-302 dye laser system. A nitrogen laser generates 500 ps pulses at 337 nm and is used as a common excitation source for the polymer amplifier and the probe dye laser. This output is split into two ~500 μJ pulses which are then used to transversely pump the cells containing the laser dye and polymer solutions. The amplifier cell was mounted at an angle to avoid feedback between the facets of the cuvette which could lead to lasing. The tunable probe source consisted of a cuvette of laser dye inside a grazing-incidence Littman oscillator. The tuning range of the oscillator depends on the available dyes (which can be excited at 337nm). The output of the tunable oscillator was then focused through the pumped region of the 10mm long amplifier cell and timed to arrive immediately after the excitation of the polymer solution. By traversing a region being optically pumped the probe beam encounters a gain medium which has a significant fraction of the polymer chains in their excited state, and this leads to amplification by stimulated emission.

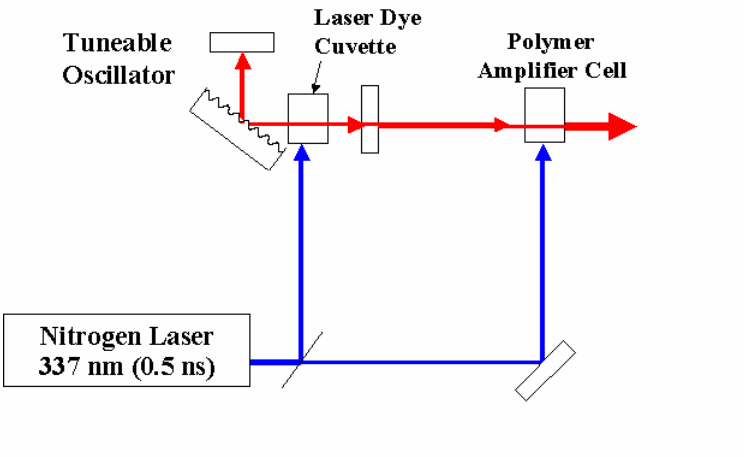

Figure 3.1: Solution optical amplifier experimental configuration.

Optical amplification of the tuneable oscillator output is measured by first attenuating the probe beam and then measuring the gain in the beam (when passed through an excited gain region) using an energy meter or a charge coupled device [CCD] detection system. As the pump and probe beams make only one pass in the cuvette this setup is also known as a travelling wave optical amplifier.

3.6 Femtosecond Laser Amplifier Facility

The femtosecond laser-amplifier facility at the Organic Semiconductor Centre (University of St Andrews) was developed in order to study ultrafast processes in physical samples such as organic or inorganic semiconductors. The facility is based around a femtosecond SpectraPhysics MaiTai pump laser which is a laser oscillator capable of producing 100 fs pulses (tuneable between 750 nm and 850 nm at a repetition rate of 80 MHz). This output can be passed through two regenerative amplifiers to achieve higher pulse energies at different repetition rates. An Optical Parametric Amplifier (OPA) is also available to produce wavelengths from 200 nm to 10 μm at 100 fs pulses.

In order to study ultrafast processes both the excitation sources and detection systems need to be able to operate in the femtosecond/picosecond regimes. Three experimental detection methods are available in the laboratory. Time resolved measurements using a Streak Camera, measurements using a femtosecond up-conversion technique and transient absorption spectroscopy. In this section the excitation sources will be discussed and the detection systems available are detailed in Chapter 3.7.

3.6.1 The MaiTai Pump Laser

The SpectraPhysics MaiTai pump laser consists of two main lasers. The first laser system uses the output from a diode laser to pump Nd^{3+} ions doped in a yttrium vanadate crystalline matrix ($Nd:YVO_4$). The Nd^{3+} ions act as the gain medium and after absorption of a photon in the red or near-infrared the excited electrons decay into the upper lasing level of Nd^{3+}, the $^4F_{3/2}$ level and remain there for ~ 60 microseconds [2]. The most favourable relaxation is to the $^4I_{1/2}$ level with an emission wavelength corresponding to 1064 nm for the transition, although there are competing transitions (1319 and 1338 nm for instance) all have higher thresholds and lower gains than the

1064 nm transition and with the aid of wavelength selective optics the oscillation can be limited to this transition. The output is then converted via second harmonic generation to 532 nm. This is achieved by inserting a lithium triborate (LBO) nonlinear crystal in the beam. This visible radiation can then be used to pump the next gain medium, Titanium doped in a Sapphire matrix.

Titanium 3^+ ions are responsible for the laser action of Titanium doped sapphire. Ti:sapphire is manufactured by introducing Ti_2O_3 into a melt of Al_2O_3 (sapphire) and Ti^{3+} ions replace some of the Al^{3+} ions, thus doping the sapphire crystal. The absorption of the Titanium ions in sapphire falls between 400-650 nm and so the frequency doubled output from the Nd:YVO_4 can be used to pump this gain medium. Figure 3.2 illustrates the absorption and emission spectra of Titanium:sapphire.

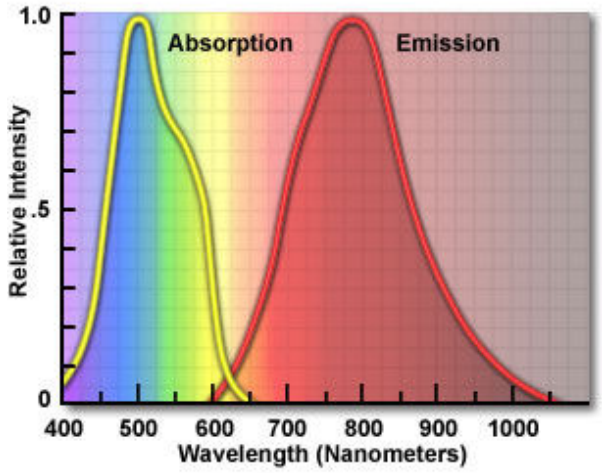

Figure 3.2 - Absorption and emission spectra of Titanium doped sapphire [3]

The emission band extends from 600 nm to 1080 nm but due to self-absorption effects the lowest possible laser wavelength is ~ 670 nm. The tuning range of the lasers is further affected by another weak absorption band (not shown) caused by the presence Ti^{4+} ions as well as the overall concentration of Ti^{3+} ions.

The laser emission from the Ti:Sapphire is at this stage CW in nature as the pump laser is CW. In order to generate ultrashort pulses a mechanism known as modelocking is used. Modelocking can be explained by looking at the modes present in a laser cavity. In a simple laser system longitudinal modes in the cavity are separated from each other by $\Delta\nu = c/2nl$, where c is the speed of light and 2nl the optical cavity length. The allowed

modes (oscillation frequencies) are thus limited by the optical length of the cavity and the bandwidth of the gain material. The output of the laser over time depends on the relative phases, frequencies and amplitudes of these modes which normally vary independently. If the relative phases of the modes were forced to stay the same, the modes would be locked together and the output becomes coherent and a short pulse is formed. The duration of the pulse depends on the number of modes that are locked together with a decrease in pulsewidth with an increase in locked modes.

Generally modelocking can be achieved by introducing some periodic amplitude modulation to the laser emission [4]. If this modulation period corresponds to the round-trip time of the laser cavity (i.e. the modulation frequency corresponds to the allowed frequency spacing of the modes) modelocking can occur. In the MaiTai, modelocking is started using an active element in the cavity. The introduction of an actively controlled element (in this case an acousto-optic modulator), which allows peak transmission every time the pulse has travelled around the cavity means that only the pulse is allowed through and experiences gain again. This eliminates the gain for other pulses and so after several roundtrips only one pulse is present.

The MaiTai uses an acousto-optic modulator (AOM) which allows repetition frequencies of around 80 MHz (defined by the optical cavity length) of the laser output. The output wavelength is selected using a prism and a slit in the region of 750 - 850 nm (800 nm default startup at maximum gain in the crystal) although with extra optics this can be extended to above 900 nm. The mode-locked output has a nominal pulsewidth of 100 fs, although this can change slightly with wavelength tuning due to group velocity dispersion and self-phase modulation in the gain medium.

Thus the MaiTai delivers 100 fs pulses at a repetition rate of 80 MHz across 750 - 850 nm. This output can be used to excite samples or be introduced into other systems to reduce the repetition rate and increase the pulse energy.

3.6.2 Regenerative Amplifier Systems

The femtosecond-laser amplifier facility has two regenerative amplifiers, a SpectraPhysics Hurricane and a Spitfire-50. A regenerative amplifier is a device to achieve strong amplification of an ultrashort optical pulse. The Hurricane produces an amplified output of 800 nm at 5 kHz and the Spitfire at 50 kHz. The use of a regenerative amplifier has two main benefits. First of all due to the nature of some the samples (for instance 100 nm thick films of polymers) the higher repetition rate of the oscillator (80 MHz) could lead to the degradation of the sample (the high peak powers in femtosecond pulses could cause thermal degradation) if exposed for a long time due to the number of pulses incident. The second benefit is that the pulse energy of the MaiTai output is not very high and by using a regenerative amplifier these pulse energies can be amplified significantly. The higher pulse energies are not necessary for spectroscopy measurements but are needed to pump the polymer laser and amplifier device to sufficiently excite the material. Another application where higher pulse energies are needed is for the generation of different wavelengths using nonlinear crystals where high pulse energies are required.

In this section only the operation of the Hurricane will be described but the general principle applies to the Spitfire as well.

The Hurricane laser-amplifier system [5] contains the seed MaiTai laser, a pump laser (SpectraPhysics Evolution), pulse stretching and compression cavities and a regenerative amplifier unit. Using these components the input energy of the MaiTai pulses can be amplified into the miliJoule energy regime. This is done by taking in pulses from a seed laser for a brief time, exposing them to gain and then dumping the pulses out of the system after several roundtrips. The control of the input and output of the seed is via Pockels Cells.

The Hurricane system uses the method of Chirped Pulse Amplification (CPA) [6] to enable higher pulse energies to be generated. The basic technique of CPA uses an input ultrashort pulse which is then stretched in its pulse duration. Pulse stretching significantly reduces the intensity (or peak power) of the pulse, this lower intensity pulse can then be

amplified using a Titanium:sapphire doped gain medium and then compressed again to its original pulse duration.

The CPA technique is needed because the original ultrashort pulse cannot itself be amplified intensely due to the inherent high peak powers present in a short duration pulse. These high peak powers can cause destructive self-focussing (caused by the non-linearity of the refractive index) within the gain medium and this thus limits the amplification that can be achieved. This means that shorter pulses cannot easily be amplified as they will destroy the gain medium, but if they are stretched in duration (leading to lower intensities as the energy is spread out in time) the amplification of the pulse will not lead to destructive self-focussing and the pulse can then be compressed externally to the amplifier medium.

In order to understand how the pulse is stretched an understanding is necessary of the nature of short pulses. The fundamental relationship between the laser pulse width and the bandwidth means that a short pulse exhibits a broad bandwidth. For Gaussian pulses this relation is $\delta\nu\,\delta\tau > 0.441$, where $\delta\nu$ is the bandwidth and $\delta\tau$ is the laser pulsewidth. This time-bandwidth relationship is a statement of the uncertainty principle. This means that for a 100 fs duration pulse at a wavelength of 800 nm the corresponding bandwidth is more than 9 nm. This broad bandwidth can be used to change the temporal characteristics of the pulse. The introduction of a diffraction grating, which disperses different frequencies at different angles thus delaying the higher frequencies (blue light) more compared to the lower frequencies (red light), the pulse is stretched with a positive Group Velocity Dispersion (GVD). The group velocity dispersion describes the relative velocities of the different wavelengths within the pulse. The positive GVD effect is also known as a positively chirped pulse. Alternatively, delaying the lower frequency light more than the higher frequencies introduces a negative chirp and this compresses the pulse.

By introducing a positive chirp to the pulse it is stretched in time, this pulse can then be amplified by as much as 10^6 in an amplifier gain medium before a negative chirp returns the pulse to its original pulsewidth. The pulse stretching and compression in the

Hurricane is performed by diffraction gratings. Figure 3.3 shows the basic layout of a pulse stretcher and compressor.

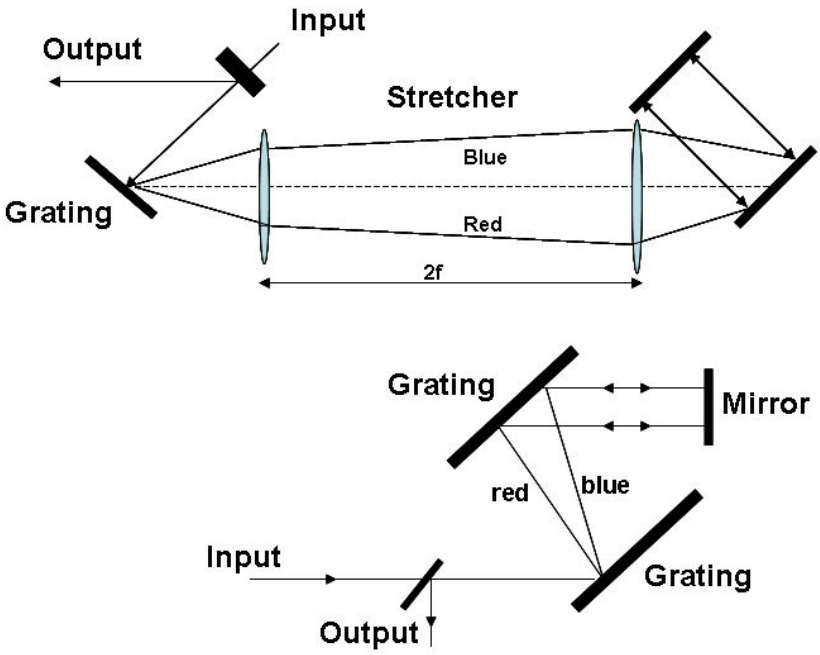

Figure 3.3 – Basic schematics of a pulse stretcher (top) and a pulse compressor (bottom).

As seen in Figure 3.3 the input is incident on a grating and the blue component travels further than the red component thus stretching the pulse. The compressor works in reverse using the gratings to make the blue component travel less distance and thus it catches up with the red light and recompresses the signal.

In the Hurricane, the amplification is provided by an amplifier cavity consisting of a Titanium:Sapphire gain medium pumped by an Evolution pump laser (which is a Diode Pumped Solid State Laser) with a repetition rate of 5 kHz. This repetition rate then determines the repetition rate of the output pulses as there is only gain available during the presence of a pump pulse in the gain medium. The Hurricane regenerative amplifier provides 5 kHz amplified 100 fs pulses. The Spitfire-50 works on a similar principle but uses a Merlin Flashlamp system at 50 kHz to pump the amplifier thus producing a higher repetition rate output. The system at the Femtosecond Laser Amplifier facility is designed to operate the Spitfire and Hurricane simultaneously (the MaiTai output is split 50/50 between them).

3.6.3 Optical Parametric Amplification

Titanium:sapphire femtosecond lasers have become increasingly useful in research since the discovery in the early 1990s of the Kerr-Lens Modelocked laser [7] which has provided the technology to computer control femtosecond lasers and thus simplifying their operation. With their wide tuning range, from ~ 690-1080nm and pulsewidths down to 20 fs commercially available there are few applications that Titanium:sapphire lasers have not been used for. Although the emission range is quite broad there are still wavelength regions which are not readily accessible by the fundamental Titanium:Sapphire output or via frequency conversion using harmonic generation. One solution to obtaining more wavelengths has been by using an Optical Parametric Amplifier (OPA).

Optical Parametric Amplification works slightly differently from a conventional laser in that it does not obtain gain from an inverted population distribution between different atomic states. In contrast an OPA derives gain from a nonlinear frequency conversion process [9].

An OPA uses nonlinear optical processes to generate variable wavelengths determined by the optical parametric amplification process. The basic principle of operation is explained here although the actual instrument is more complicated to enable the correct temporal and spatial overlaps necessary for nonlinear interactions, Figure 3.4 illustrates a typical layout of the instrument.

The Hurricane output, 100 fs pulses at 800 nm (5 kHz repetition rate), is directed into the OPA. The input laser pulse is split into two beams, a small percentage (~ 4%) is reflected into the first arm of the OPA. This light is incident on a White Light Generator unit. In this unit the pulse is tightly focussed onto a sapphire plate producing a white light continuum, the continuum is re-collimated and then directed towards the OPA crystal.

The remaining amplified seed pulse is split into two pump beams. The first part, approximately 15% of the light, is used to pump the first pass of the OPA crystal known as the pre-amplification stage. The remainder of the beam is used to pump the second-

pass or the power amplification stage of the OPA. In the pre-amplifier stage the pump beam is directed into the nonlinear OPA crystal (in this case a Barium Borate (BBO) crystal) using a mirror. This beam is then overlapped spatially and temporally in the BBO crystal which caused the continuum to be amplified by the pump beam. This generates a signal and idler beams which are reflected back on the BBO crystal (though not spatially overlapped with the pre-amplification beams to avoid interactions with this stage). These returned beams are then used as the seed pulse for the power amplification stage.

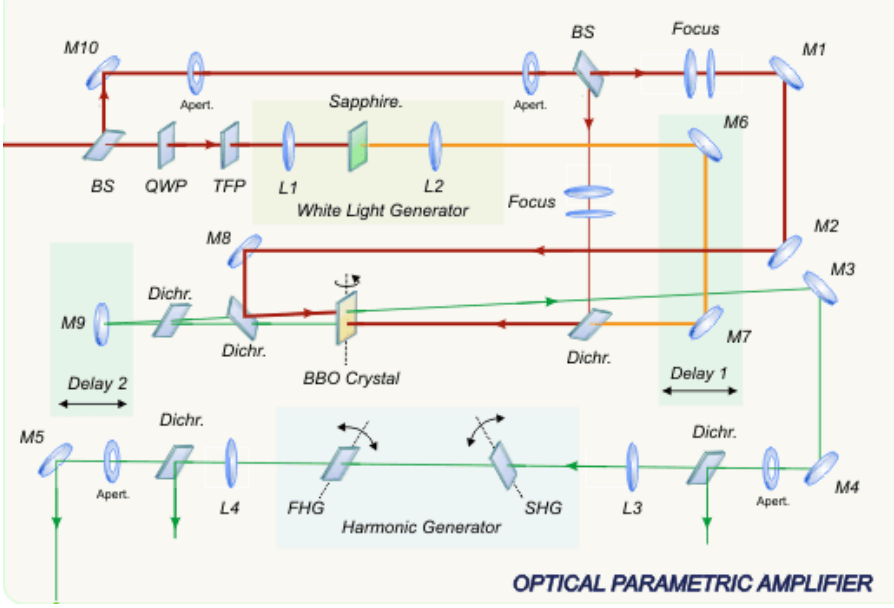

Figure 3.4 Typical Schematic of an Optical Parametric Amplifier [8]

The pump beam for the power amplification stage is then overlapped co-linearly in the BBO crystal with the signal (idler) beam in the BBO crystal for the final amplification stage. The amplified output wavelength of the signal (idler) beams are determined by the phase-matching angle of the BBO crystal. This provides wavelength tuning over a small range for both the signal and idler by changing the crystal angle. There is still some residual pump light at this stage (800 nm) which is separated from the signal and idler beams and these two beams can then be directed using dichroic mirrors to different exit ports. This mechanism produces two different wavelengths distinct from the pump beam.

The wavelength range can be extended further by use of a harmonic section of the instrument which utilises extra nonlinear crystals. The signal and idler beams can be placed through further second, third and fourth harmonic generation crystals to further

extend the available wavelengths. Sum frequency and difference frequency generation between the signal and the idler is also possible. Along with the tuning of the signal and idler this means that wavelengths are available from 200 nm to approximately 10 microns. An incredible range of wavelengths is thus available with pulses of ~ 100 fs.

The OPA was used in this research to create a 5 kHz pump and probe beam for exciting organic devices for transient absorption measurements. This allowed femtosecond spectroscopy of device properties to be studied.

3.7 Detection Systems

In order to investigate the ultrafast properties of organic samples and devices a laboratory needs not only ultrafast sources but also a fast detection system. Many electronic detection systems are limited by the electronic response of the detector or the pulsewidth of the excitation source. As described in Section 3.5 the excitation sources are sufficiently short for the investigation and so the final hurdle is to detect the emission at picosecond or (ideally) femtosecond timescales. Many photomultiplier detectors, such as those used in Time-Correlated Single Photon Counting (TCSPC) system, which are one of the fastest electronic detection systems for lifetime measurements, have detector responses of ~250 ps and in some special cases such as Micro Channel Plate photomultiplier tubes these can extend down to 50 ps. Photomultipliers are based on the direct detection of a photon incident on an inorganic semiconductor (such as Sillicon or InGaAs) and so are limited by the transit time of generated photoelectrons and subsequent electronic circuits.

The instrument response function (IRF) of a system is determined as the squareroot of the sum of the square of the detector response and the square of the excitation pulsewidth. Thus using a 50 ps detector response and a laser width of 100 fs the IRF is limited by the detector response. Thus in order to lower detection response times, classical detectors such as photomultiplier tubes alone are not sufficient for the application. Other methods with faster electronic responses or involving all-optical methods which can remove the limitations of the electronics on the IRF are thus necessary.

In the Femtosecond Laser Amplifier Facility there are three main detection systems. These are the Hamamatsu Streak Camera, the FOG100 femtosecond up-conversion system and a transient absorption setup. The streak camera is based on an detector system based on electronics to record a measurement and the last two utilise interactions between 100 fs pulses as the detection reference. These three instruments and techniques will be described in this section.

3.7.1 Streak Camera Detection

A streak camera is a powerful tool for simultaneously probing both the lifetime kinetics and emission spectrum of a sample upon excitation. The Hamamatsu FESCA C6860 streak camera is capable of detecting lifetimes from ~500 fs to 2 ns [9].

Samples investigated using the streak camera were excited using 100 fs pulses thus the instrument response of the streak camera is determined by the limits of the streak system. The emission of the sample was collected and focussed into a Chromex spectrograph (controlled by the Streak camera software) via a pair of lenses. The spectrograph redirects the emission onto the entrance slit of the streak camera.

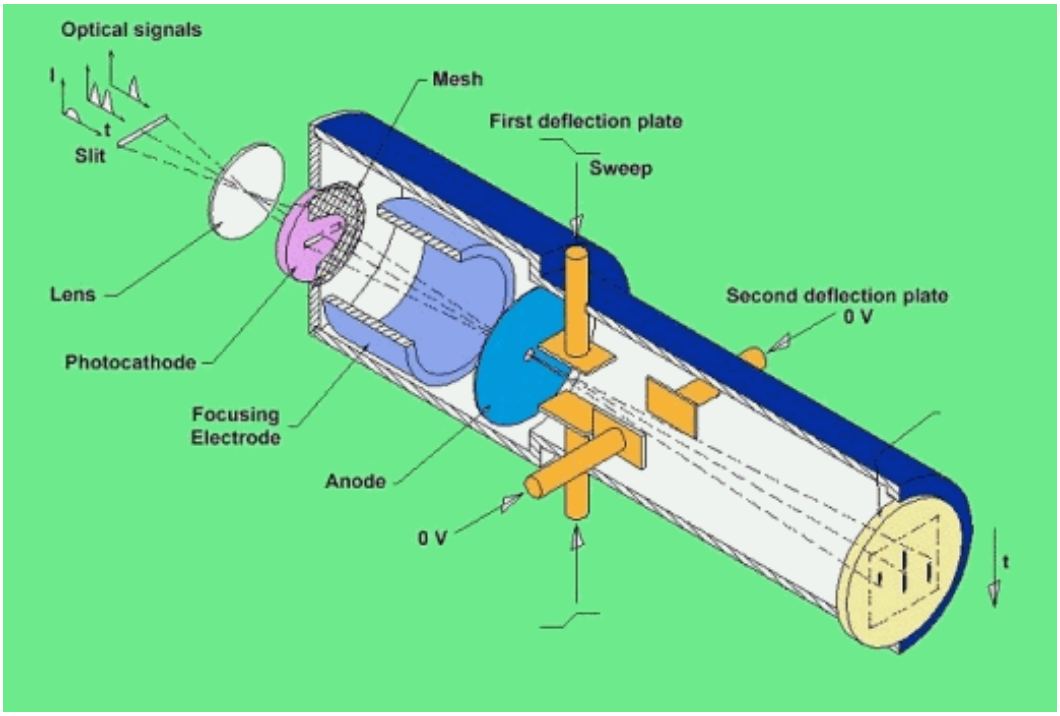

Figure 3.5 – Schematic of a Streak Camera Tube

The incident light is dispersed inside the spectrograph using a diffraction grating. This light is then incident on the streak camera slit and via a lens the emission encounters a photocathode and is converted into electrons. These electrons are then focussed towards the anode and after passing through the anode are subject to a sweeping electric field. This field is caused by a voltage being swept down the plate the electrons are accelerated at different times depending on their arrival. These electrons are then incident upon a phosphor screen and the emitted photons from the phosphor screen are recorded by a CCD camera. Figure 3.5 only shows the streak tube up to the phosphor screen. The sweeping of the field means that the image recorded by the CCD camera is a two-dimensional measurement of the intensity as a function of wavelength and time (x-axis emission spectra and y-axis temporal profile).

The two-dimensional image captured can be controlled in both the wavelength and time resolution and range. The wavelength control is via the spectrograph where different gratings with higher numbers of grooves will provide a more dispersed signal thus increasing the wavelength resolution but with a reduced range. The largest range measurable using this system was a 134 nm wide spectrum, the shortest was 25 nm. The time ranges available to the streak camera are dependent on the sweep voltages used. The streak camera has 6 preset time ranges from 0-40 ps to 0-2 ns.

The refresh rate of the streak camera is synchronised to the 80 MHz MaiTai output. This causes the image to refresh every 12 ns so any longer lived fluorescence than 12 ns would show up as a background emission in the next image.. The temporal resolution is dependent on the stability of the MaiTai laser as the Streak Camer is optically triggered and any change in the risetime of the pulses would lead to a jitter in the streak camera time resolution. The use of the streak camer in this work was atypical in that the excitation laser repetition rates were significantly lower (50 kHz) than the refresh rate. Normally the same frequency is used to optimise the time resolution but no significant difference was experienced between excitation at 50 kHz and 80 MHz for the time resolution

The simultaneous measurement of emission spectra and decay kinetics makes the streak camera images a powerful tool for studying the emission of a sample. A typical recorded image is shown in Figure 3.6 along with the separated lifetime and spectral data. The typical instrument response of the streak camera was determined by recording using a scattered excitation pulse and was typically 1-2 ps.

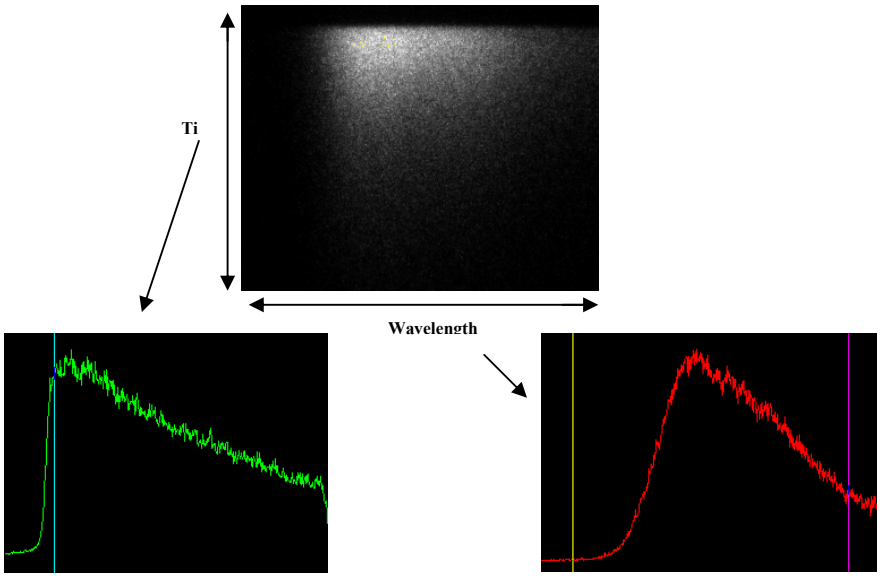

Figure 3.5 – A typical streak camera image (Top). The temporal profile (bottom left) is the integration across the y-axis. The spectral profile (bottom right) is obtained by integrating over the desired x-axis range.

3.7.2 Femtosecond Up-conversion Technique

As described above, the limitations of detection using a streak camera result from the use of electronics which have an operating speed which is limited by the electronics. The best streak cameras commercially available are able to measure ~ 500 fs [10]. However many interesting phenomena occur below this, such as the breaking of chemical bonds over timescales as short as 100 fs.

The drive to create shorter pulses from lasers has led to many novel detection methods for ultrafast pulses. Femtosecond lasers pulse durations cannot be measured using electronics due to the inherent slower speed of the electronic circuits. To measure ultrafast pulses new all-optical techniques have had to be created. The most widely used technique to characterise optical pulses is the autocorrelation technique [11] where the optical pulse is compared to itself. In order to perform time-resolved measurements in the 100 fs regime an optical technique based on the interaction between optical pulses (similar to autocorrelation) is used. The interaction this time is in a nonlinear crystal and compares the signal to be measured (of any lifetime) with a 100 fs reference beam. This means that the limiting factor should be the pulsewidth of the laser and not the speed of the detection electronics. In order to achieve this detection limit a technique called femtosecond up-conversion (sum frequency generation) is used. This technique is also called femtosecond optical gating and works on the principle of interacting two light pulses within a nonlinear crystal to create a third wavelength whose amplitude is related to the intensity of the initial pulses.

The femtosecond up-conversion technique (described in [12,13]) utilises laser induced fluorescence along with sum frequency generation of this emission and a reference beam. A femtosecond laser pulse produces fluorescence which is incident upon a nonlinear crystal, sum frequency generation only occurs if both this fluorescence emission and a delayed reference pulse are temporally overlapped in the crystal (Figure 3.6). The generated sum frequency signal is detected via a monochromator onto a PMT working in single photon counting mode leading to a high sensitivity in the measurement.

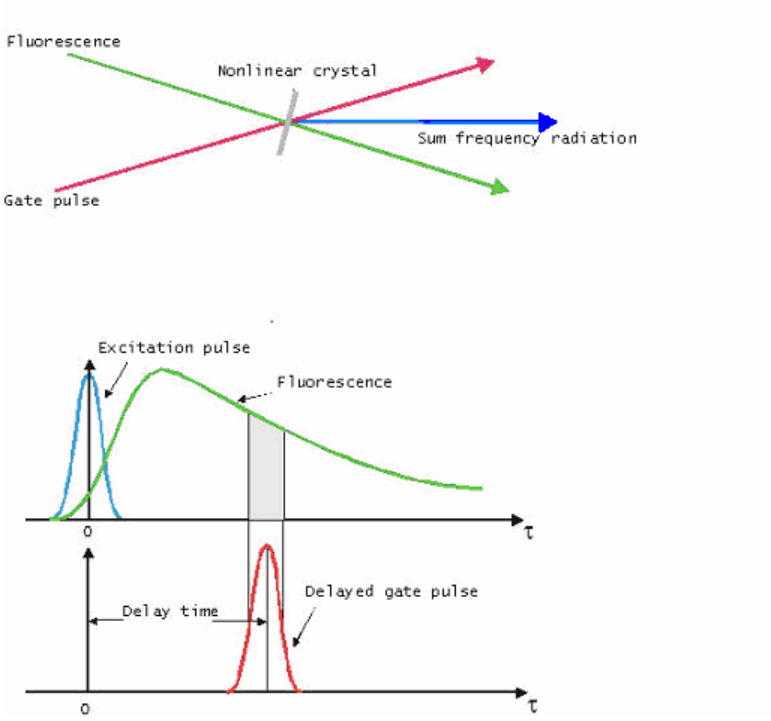

Figure 3.6- Schematic layout of fluorescence up-conversion. Sum frequency radiation is generated in a nonlinear crystal (upper section) during the time that a delayed laser pulse is present (lower section).

By controlling the optical delay of the reference beam compared to the excitation pulse the fluorescence rise and decay can be detected at a wavelength determined by the monochromator settings and the angle of the crystal (this angle and the desired wavelength and thus the monochromator setting are pre-calculated), as the reference beam is set to one wavelength the adjustment of the angle of the nonlinear crystal allows the detection wavelength to be tuned in the emission wavelength range. The intensity of the fluorescence signal is proportional to the sum frequency signal as the reference beam does not change its intensity. The temporal response of the system can be determined by the convolution of the excitation and reference pulses and is as such independent of any detection electronics. The temporal resolution if 100 fs pulses are used is typically < 200 fs due to broadening in the crystal

This technique has been simplified by using a instrument created for this purpose. The FOG100 instrument from CDP systems was the first commercial instrument to use fluorescence up-conversion as a detection method.

A schematic layout of the FOG100 is shown in Figure 3.7. In the femtosecond laser amplifier facility a femtosecond oscillator source (wavelength 750-850 nm, 80 MHz repetition rate) was used as well as the output from the two regenerative amplifiers with outputs of 800 nm at 5 kHz and 50 kHz. For illustration purposes the excitation laser is taken to be set at 800 nm and have a pulsewidth of 100 fs. The repetition rate is not important except that of course for lower rates the signal count is lower, though for materials which are easily photo-damaged a lower repetition rate is preferable to avoid sample degradation.

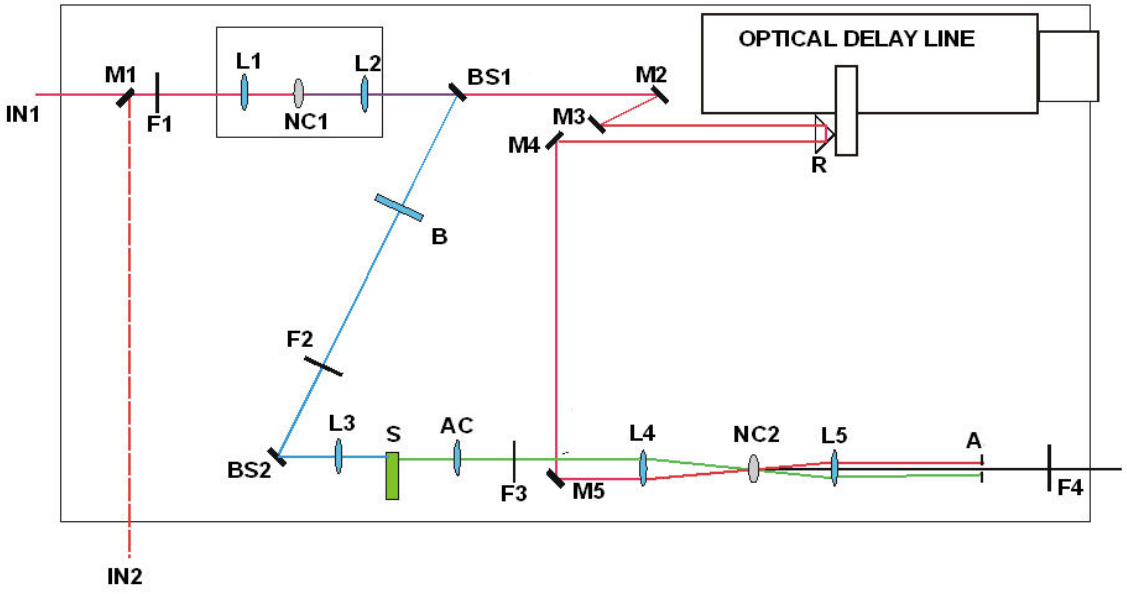

Figure 3.7- Schematic of the FOG100 optical setup.

A femtosecond laser beam is steered into the instrument via port 1 or 2. It is then directed and focussed with mirror M1 and lens L1 onto crystal NC1 which is a BBO crystal cut for second harmonic generation of 750-850 nm light when placed in the beam. The 800 nm laser beam generates a 400 nm signal and leaves a residual 800 nm beam. These two beams are thought of as one pulse split into two and are then collected by the second lens L2. These beams are incident upon a dichroic beamsplitter BS1 and the 800 nm beam, referred to as the gate or reference beam, travels on via some mirrors to the retroreflector set on a delay line and back again parallel to the incoming beam via two mirrors onto lens 4.

The dichroic beamsplitter BS1 directs the 400 nm excitation light towards the sample chamber via the Berek waveplate B (a polarisation compensator which allows the polarisation of a beam to be changed). The excitation light is directed via a secondary beamsplitter BS2, to further filter any possible 800 nm light, and focussed onto the sample by lens L3. The sample can be solid (transparent or reflective) or liquid though in the research carried out for this thesis only solutions and thin films on quartz substrates were studied and so no reflective mirrors were needed to redirect emission which would be emitted back towards the excitation path. L3 focuses the excitation beam onto the sample and an achromatic collecting lens AC is used to collect the emission. This emission is then filtered using filter F3 to eliminate the 400 nm excitation light such that only the emission is left. The emission is then directed onto lens L4.

Lens 4 simultaneously focuses the reference beam and the emission from the sample onto the second nonlinear crystal NC2, a BBO crystal cut for sum-frequency generation. By spatially and temporally overlapping the reference beam and the emission a sum-frequency signal is generated which travel normal to the plane of the nonlinear crystal. The lens L5 collects the signals and directs them towards the detection monochromator. The signal is passed through an aperture to discriminate as much as possible the more divergent emission and reference beams and a further filter F4 allows only the sum frequency generated (up-conversion) signal through. This up-conversion signal is then incident via a slit into a monochromator set for the required sum-frequency signal and a PMT measures the signal intensity at the monochromator set wavelength.

The signal intensities are recorded by the Lumex software whilst the optical delay line scans across the fluorescence rise and decay to a maximum of a 2 ns temporal range (determined by the length of the delay line). This method is highly adaptable to different samples and allows detection of fluorescence using a temporal resolution not easily matched using electronic systems.

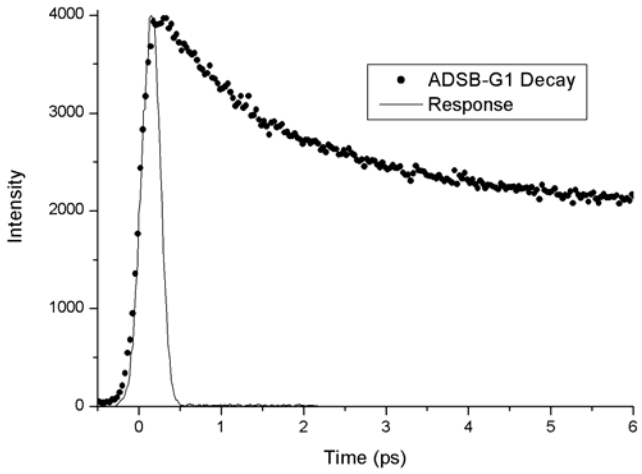

Figure 3.8 – Test data of the FOG system showing a decay of the conjugated dendrimer ADSB-G1 and the response of the system (~ 250 fs)

Figure 3.8 shows test data highlighting the capabilities of the FOG100. The decay of a conjugated dendrimer is studied and exhibits a fast decay which is easily observed and the response function of the system is shown to be ~250 fs.

There are some drawbacks in that only one wavelength can be measured at a time and the changing of the wavelength requires some manual optimisation of the crystal angle. Figure 3.8 shows test data highlighting the capabilities of the FOG100.

3.7.3 Transient Absorption

It is useful to probe the absorption as well as emission following ultrafast photoexcitation and this too can be achieved with an all-optical measurement. Time-resolved measurements normally use a single excitation pulse to probe transitions from the ground state to an excited state and then measure the decay back to the ground state. Transient absorption however is based on the probing of the excited state (i.e. its absorption). An initial pump pulse is incident on a sample and excites an electron into an excited state. Before this excitation can decay back to the ground state a second pulse excites the electron into a higher excited state. This technique allows us to determine the properties of the excited state levels as well as the properties of the excitations in the excited state. This technique is also known as the pump-probe method.

The basic layout of the transient absorption setup is illustrated in Figure 3.8. The output from the OPA is set to a pump wavelength and a probe wavelength. The green pump wavelength is chopped at half the pulse repetition rate to let every second pulse excite the signal. The probe beam can be either a white light continuum or a chosen wavelength (for a particular application). The pump beam travels along an arm with a retroreflector on a delay stage whilst the probe beam is directly incident on the sample. This allows the optical delay between the two pulses to be controlled.

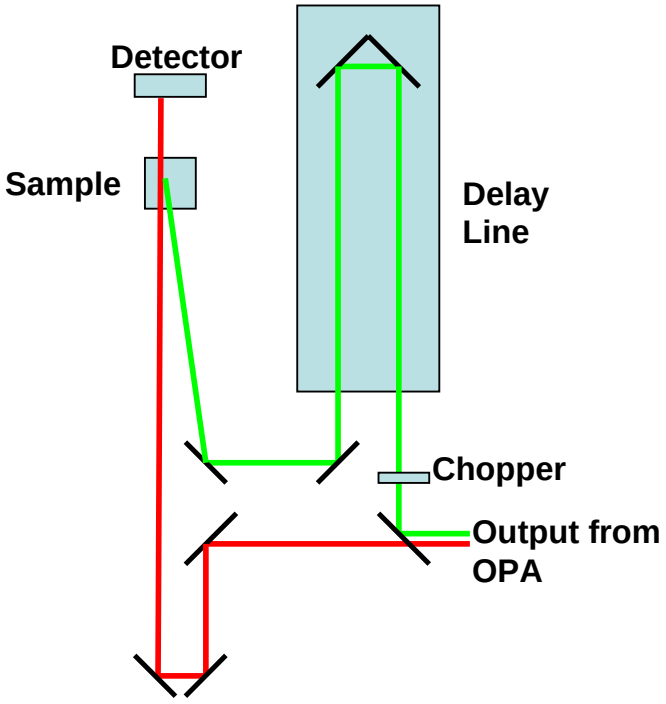

Figure 3.8 – Transient Absorption Setup. The output wavelengths from the OPA travel in two arms of the setup. The green Pump beam travels via a retroreflector on a delay stage onto the sample and the red Probe beam is directed via mirrors onto the sample.

The pump and probe beams are spatially overlapped onto the sample (to ensure interaction) and the probe beam is then detected by a silicon photodiode. When the probe pulse is incident on the sample whilst the pump pulse has generated an excited state the probe beam intensity will be affected. The next probe beam to pass through will not be affected as there is no pump beam present for every second pulse, this acts as a reference beam. The two signals are detected via a lock-in amplifier setup taking the ratios of the probe beam with pump on/off as these are at two separate frequencies. The transient absorption method detects the interaction of two pulses, the pump beam causes an excited state in the sample and the probe beam interacts with this beam. By scanning the pump

beam delay stage across this interaction the kinetics can be measured using an optical method. This should provide a temporal resolution of several 100 fs.

Chapter 3 References

[1] JR Lakowicz, Principles of Fluorescence Spectroscopy, Chapter 10, Page 291, Kluwer Academic, Second Edition (1999)

[2] SpectraPhysics MaiTai Manual

[3] http://micro.magnet.fs.edu/primer/java/lasers/tsunami/index.html

[4] HA Haus, *IEEE Journal of Selected Topics in Quantum Electronics*,**24**,388 (1999)

[5] Hamamatsu SpectraPhysics Hurricane Manual

[6] JV Rudd, G Korn, S Kane, J Squier, G Mourou, P Bado ,Optics Letters, 18,2044 (1993)

[7] Spence DE, Keane PN, Sibbet W, Optics Letters 16, 42, (1991)

[8] http://www.chem.kuleuven.ac.be/mds/optical_parametric_amplifier.htm

[9] Streak Camera C6860 Manual

[10] Hamamatsu website www.hamamatsu.co.uk

[11] LP Barry, PG Bollond, JM Dudley, JD Harvey, R Leonhardt, *Electronics Letters* **32**,1922 (1996)

[12] J.Shah:, IEEE Journal of Quantum Electronics, **24**, 276 (1988)

[13] M.A.Kahlow, W.Jarzeba, T.P.DuBruil and P.F.Barbara, Review of Scientific Instruments, **59**, 1098 (1988)

Chapter 4

Spectroscopic Studies of Conjugated Polymers and Dendrimers

4.1 Introduction

The discovery of electroluminescence in poly(*para*-phenylene vinylene) (PPV) [1] has led to much research into the photophysical properties of conjugated polymers. This research has been focused on probing the relationship between the chemical structures of these conjugated polymers and their ability to emit light. The diversity of organic chemistry means that if this relationship between structure and the resulting photophysics can be understood, conjugated structures could be tailored to the required photophysical properties for an application.

The diversity of organic compounds is limited only by the discovery of a synthesis route to the required polymer. Long polymer chains are created by first producing a precursor polymer, made by polymerization of a monomer unit. This precursor polymer then undergoes thermal conversion to the long chain polymer. Some conjugated polymers can be synthesized from different precursors (monomer repeat units which are then added together to form the polymer chain) and this can also lead to slight differences in properties. Optical spectroscopy is a powerful tool for investigating the relationship between material structure and photophysical properties

The work carried out in this Chapter was as part of a wider investigation into the photophysical properties of different materials and their potential applications. The research was focused on studying the materials used within the Organic Semiconductor Centre (OSC) at the University of St Andrews for applications such as OLEDs and laser devices. The materials studied were the conjugated polymer MEH-PPV as well as novel

conjugated dendrimers. The effect of conjugation breaks in MEH-PPV was studied by observing the temperature dependence of steady state absorption as well as by time-resolved photoluminescence.

Conjugated dendrimers were studied in order to gain a better understanding of the photophysics of these new materials. As explained in Chapter 2.7 these novel materials have been used primarily within OLED applications as a light-emitting layer. The relationship between chemical structure such as the nature of the conjugation across the dendrimer and the photophysical properties of the dendrimer can provide an insight as to new structures for future study. A highly efficient phosphorescent dendrimer was also studied. This Iridium based compound has been studied in order to improve the understanding of the ultrafast fluorescence lifetimes which have not been reported before from these materials.

This work was started as part of the Ultrafast Photonics Collaboration (UPC) based at the University of St Andrews. The materials studied in this Chapter were provided by the research group of Dr Paul Burn at the University of Oxford with whom the research group collaborated for many years in order to create better conjugated polymers and dendrimers.

This Chapter presents the work done as an initial photophysical study of materials before the work focused on the study of devices such as lasers and amplifiers based on these materials.

4.2 The Effect of the Degree of Conjugation on the Photophysical Properties of MEH-PPV

Following the discovery of electroluminescence of PPV [1] much research has been carried out on the photophysics of PPV and its derivatives [2-11]. In particular spectroscopic studies of MEH-PPV have been performed using many different techniques yet the results raised considerable debate on the nature of the excited state. It was discovered that the preparation of the sample is vital to achieving consistent experimental conditions. Correct sample preparation and storage is also important for sample stability during an experiment as degradation can lead to quenching of emission. Different solvent

environments also interact differently with the polymer chains depending on their conformation [12-18].

The degree of conjugation of MEH-PPV is known to affect the photophysical properties [19] as it alters the electron delocalization properties of the chain. The research investigates the temperature dependence on the steady-state absorption and time-resolved luminescence of partially and fully conjugated MEH-PPV. The temperature dependence is a useful tool for observing polymer chains as at lower temperatures (towards 0K) an ideal polymer chain is expected to be planar. As the temperature (and thus energy) rises, entropy causes the chain to twist creating breaks in the conjugation [20-24]. The breaks in conjugation in polymer chains are due to either chemical defects along the chain or the folding or twisting of the chain causing a break in conjugation.

4.2.1 Partially and Fully Conjugated MEH-PPV

To better understand the nature of excited states in conjugated polymers the conjugation along a polymer chain was varied. Studies of the photophysical properties with this variation could lead to a better understanding of the excited state position on the chain. Conjugated polymers are a special class of semiconductors and this study would provide information on the extent of electron delocalization. Inorganic semiconductors are known to have extended/delocalized excited states, whereas small conjugated molecules have very localized excited states. By studying the effect of conjugation on the photophysics of a polymer the relationship between the chemical structure and the location of an excited state can be probed and further insight gained into the electron delocalization in these materials.

The conjugated polymers used in this work are two different MEH-PPV structures. As can be seen in Figure 4.1 the structure of MEH-PPV can be adjusted by replacing some of the vinylene linkages with single bonds and hydrogen atoms. The polymers here had 34% and 0% of the linkages replaced. The polymers were synthesized using base catalyzed elimination of a precursor polymer which replaced the chosen percentage of leaving groups with hydrogen [25].

The temperature dependence of the absorption and emission properties of these conjugated polymers enables a study of the effect of the conformation of the polymer chain. When a polymer solution is cooled there is a wavelength shift in the absorption and emission spectra.

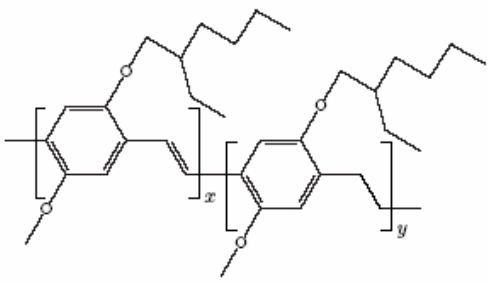

Figure 4.1 -The structure of partially and fully Conjugated MEH-PPV. For the fully conjugated chain the ratios of repeat units is x=1, y=0 with no replaced linkages. For the partially conjugated chain the ratio is x=0.66, y=0.34.

In most conjugated polymers a red-shift of the absorption and emission is seen on cooling [26-28] although a few cases of blue-shifts have been reported as well [29,30]. Previous studies of MEH-PPV have shown it to red-shift with a decrease in temperature [31,32]. An explanation of the red-shift is that as the sample temperature is reduced, the thermal energy in the chain decreases and this reduces the energy available to twist the chain. This effectively flattens out the polymer backbone and removes the breaks in the conjugation caused by these twists leading to longer segments of conjugated chains. For the partially conjugated polymer chain this straightening of the polymer chain reduces the breaks in conjugation caused by twisting and any further breaks in conjugation would be primarily due to the chemical defects introduced.

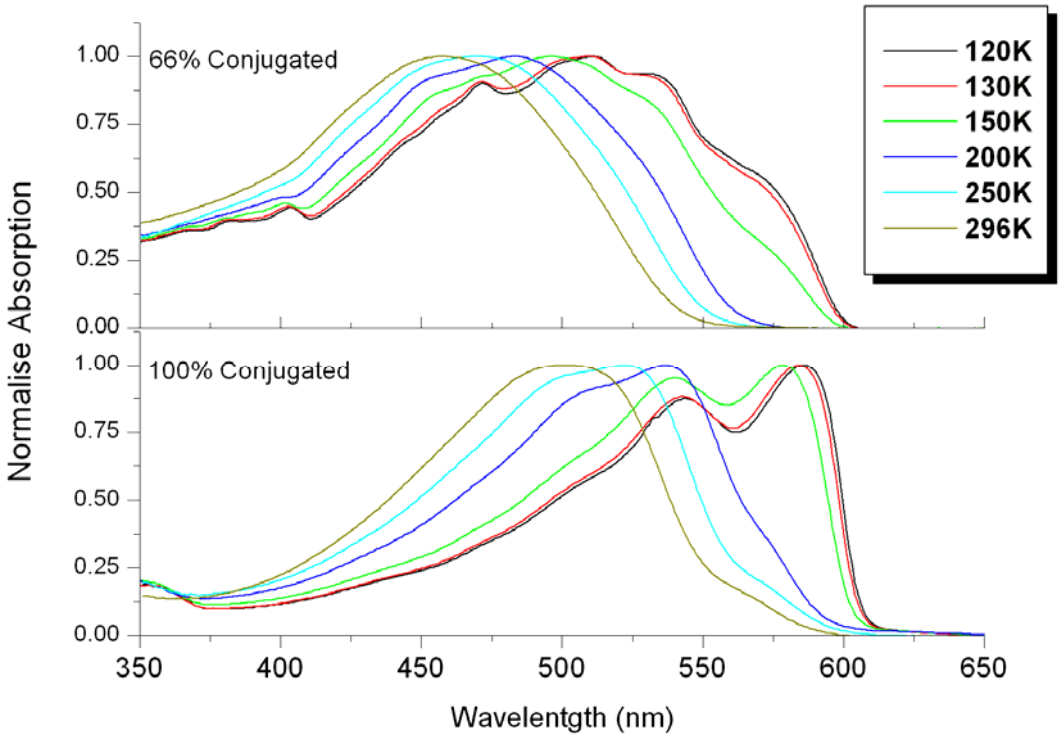

Figure 4.2 - Temperature Dependent Absorption of partially and fully conjugated MEH-PPV dissolved in 2-MeTHF

4.2.2 Temperature Dependent Absorption Spectra

The two MEH-PPV samples were dissolved in 2-methyl-tetrahydrofuran (2-MeTHF), this is often used as a solvent for cryogenic experiments as it forms an optical glass below 135K. The absorption spectra shown in Figure 4.2 were measured in dilute solution. With the reduction in temperature the absorption red-shifts and the spectra become more structured. The absorption is also seen to increase slightly (not shown due to normalisation) and this is thought to be due to solvent shrinkage at low temperatures.

There is a marked difference between the structural changes of the two polymers. The fully conjugated chain (bottom panel) has a large red-shift with the decreased temperature with the peak of the absorption changing by 82 nm. A marked increase in vibronic structure is also observed and the edge of the absorption towards 600 nm becomes very steep at low temperatures. The absorption in the range of 450-500 nm decreases considerably as the absorption peak is red-shifted. The partially conjugated

polymer (top panel) exhibits a smaller red-shift in the peak absorption wavelength of 55 nm and the spectra show a less obvious change in vibronic structure, some structure is observed but the overall shape of the spectra do not change significantly beyond broadening towards the red.

The fully conjugated MEH-PPV behaved significantly differently from that of the partially conjugated MEH-PPV. They both exhibited a red-shift in their absorption spectra indicating that the polymer chains were straightening as the thermal energy available to twist the chains was decreased [26,28].

In the fully conjugated MEH-PPV the straightening of the chain creates less breaks in conjugation and leads to longer segments of conjugation. Longer segments absorb lower energies thus leading to more absorption in the red. The increase in segment length also explains the vibronic structure change. When the creation of the longer segments reaches a limit, the individual segments within the chain should be absorbing at similar energies as they are of similar length. The vibronic structure of these segments will therefore coincide and causes the appearance of the structured spectra as the majority will exhibit similar conjugation lengths.

The straightening of the chains in the partially conjugated MEH-PPV does not cause a marked increase in the structure of the spectra as the breaks in conjugation are not primarily caused by conformational disorder. As the temperature decreases the conformational breaks are reduced but the chemical defects remain constant. There is no significant increase in conjugated segment lengths as these are determined by the chemical breaks. This causes the spectra to widen instead of shifting as radically as the fully conjugated MEH-PPV where the conjugation breaks are almost solely due to the chain conformation. A red-shift does occur as some of the chains which have breaks due to conformation will lengthen, but there will still be many shorter segments due to the chemical breaks. Thus the spectra are broad as there are still many different segment lengths on the chain.

4.2.4 Temperature Dependent Time-Resolved Photoluminescence

In order to study the evolution of the photoluminescence after it is excited, time-resolved measurements are performed. In order to study the dynamics of the polymer chain after ultrafast excitation with a 100 fs pulse, a streak camera system was used as described in Chapter 3.5. The study of the emission decay dynamics could provide information on the movement of the excitations along the chain from higher energy segments to low energy segments and the time within this occurs.

The excitation pulses used were the frequency-doubled output from the MaiTai oscillator tuned to 415 nm. As no steady-state spectrometer was available for cryostat measurements, temperature dependent photoluminescence was recorded using the streak camera. The recordings of the spectra were obtained from the whole image of the Streak Camera as this provides a time-averaged spectra (over a 2 ns window) which approaches the shape of the steady state spectra as the decay dynamics of the MEH-PPV are known to be less than the 2 ns time window used.

Figure 4.3 illustrates these quasi-steady state spectra. Similar to the earlier absorption measurements a red-shift in the spectra is observed with a more structured vibronic emission shape. As seen in the steady state absorption the lowering of the temperature leads to emission from the lower energy segments of the chain as the conjugated segments increase in length (and hence lower in energy). This is seen for both partially and fully conjugated spectra. The vibronic structure of the emission of the partially conjugated MEH-PPV is more pronounced than in the absorption but is still broader than the fully conjugated MEH-PPV due to the larger number of segment lengths inherently present due to chemical defects.

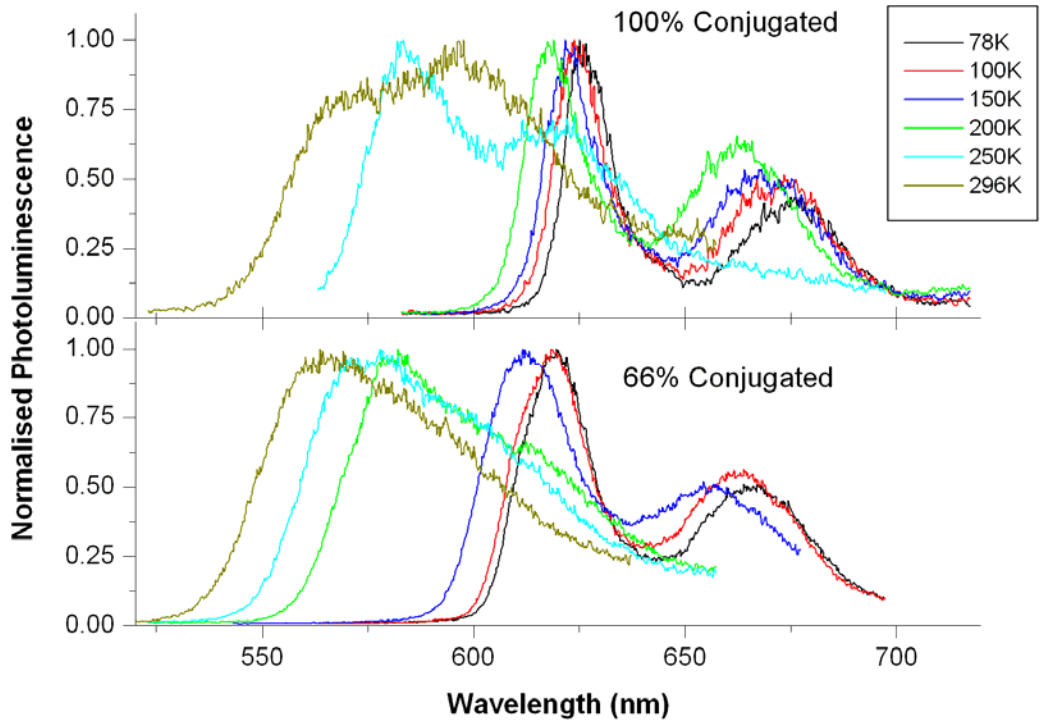

Figure 4.3 - Temperature Dependent Photoluminescence of Fully and Partially Conjugated MEH-PPV in 2-MeTHF

The main difference between the partially and fully conjugated spectra is the temperature where the emission red-shifts. The red-shift and vibronic structure in the emission at 200 K for the fully conjugated spectrum is far more pronounced than for the partially conjugated spectrum. This is not totally unexpected as for the fully conjugated MEH-PPV the breaks in conjugation are due to chain twists primarily so the straightening of the chain will produce longer segments quicker than in the partially conjugated MEH-PPV where the straightening of the chain still sees chemical defects break the conjugation. The partially conjugated spectra thus red-shifts at lower energies towards the red as longer segments are inherently only present when the chain is almost straight.

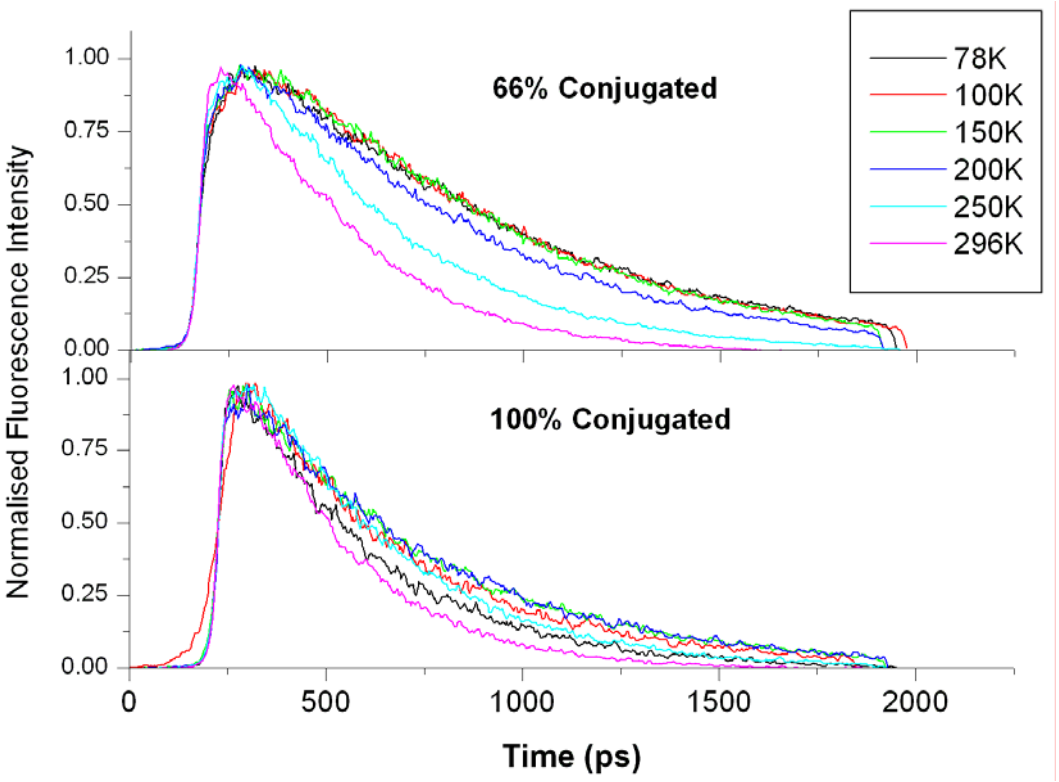

Figure 4.4 Temperature dependent lifetime of partially and fully conjugated MEH-PPV observed over a 2 ns window

Figure 4.4 demonstrates the average emission dynamics (averaged 5 nm either side of the peak emission wavelength) for the two MEH-PPV polymers. At room temperature the emission dynamics of the two polymers are very similar in lifetime though the partially conjugated MEH-PPV is slightly longer-lived. There is a marked increase in the emission lifetime observed in the partially conjugated MEH-PPV whereas the fully conjugated MEH-PPV broadens slightly and then at very low temperatures decreases again.

The faster decay observed for the fully conjugated MEH-PPV can be attributed to either a faster radiative rate, higher K_R, or a higher non-radiative rate, K_{NR}, where there is faster diffusion to quenching sites.

The partially conjugated emission dynamics broaden considerably as the temperature of the sample is decreased. The inherent chemical defects are the most likely cause. At room temperature there are many short segments caused by either breaks in

conjugation due to chain twisting or chemical defects. At room temperature excitation migration is hindered by these breaks but it is similar for the fully conjugated polymer. As the chain straightens with lowered sample temperature the partially conjugated chain sees less conformational defects but overall will still have the inherent chemical defects introduced into the chain. This means that as the chain flattens out the conformational conjugation breaks between the numerous chemical defects disappear. There is still an ensemble of segments of varying length but they are mainly due to chemical defects. Perhaps the excitation migration along the chain is easier via a conformational defect compared to a chemical defect which would cause the lengthening of the lifetime observed. Further work needs to be performed on this in order to better understand the mechanisms involved.

The partially conjugated lifetimes converge to a limit, which is reached between 200 K and 150 K. This is likely where the majority of the conformational breaks have been flattened and a further decrease in temperature will not change the chain properties sufficiently for further lifetime changes.

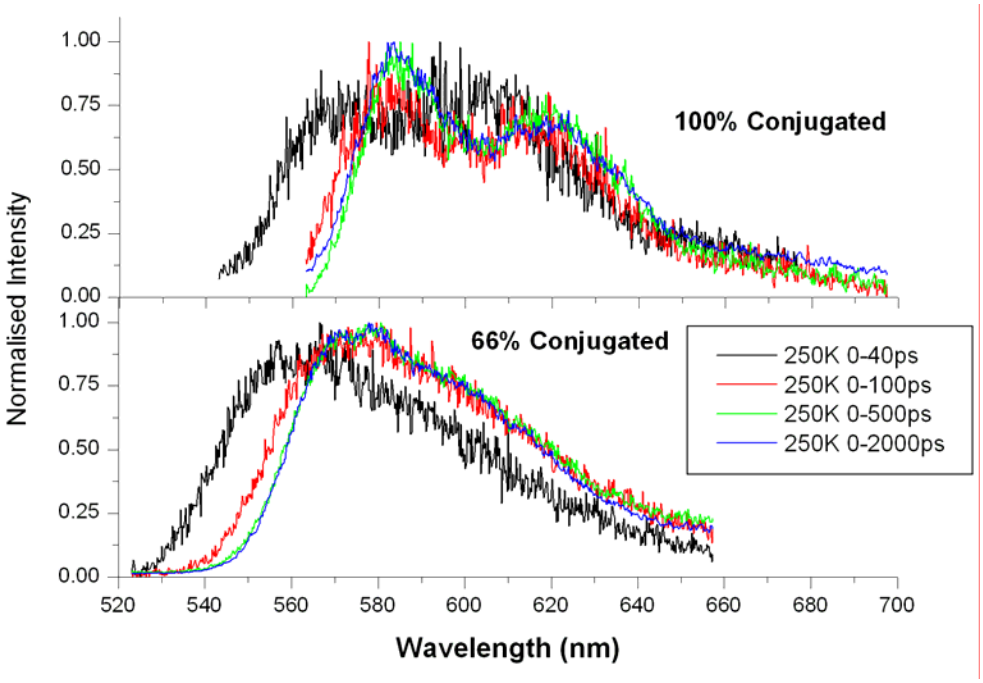

Figure 4.5 Evolution of the emission spectra of partially and fully conjugated MEH-PPV over time (measured at 250 K)

By studying the evolution of the emission spectra we can determine over what timescales the excitation migration occurs as this is seen in the wavelength shift in the spectra. As can be seen in Figure 4.5 the spectra have been recorded over different time-ranges from 0-40 ps to 0-2 ns, the graph chosen was for the 250 K temperature but the behaviour is typical for all time temperatures. For the fully conjugated material the migration is very fast and the only real difference is noticed in the 0-40 ps timescale. After 40 ps the spectra are very similar and so the excitation migration occurs in approximately 40 ps. For the partially conjugated spectra the emission spectra change slightly slower as expected but within 100 ps they are broadly similar in appearance to the time averaged spectra.

4.3 Novel Dendrimer Materials

In recent years, conjugated dendrimers have been used to produce more efficient OLED devices. As described in Chapter 2.5 dendrimers can be tuned to specific properties by altering the various constituent components. Colour tuning has been demonstrated and LED devices in the red, green and blue have been produced using identical processing properties [33,34]. The chromophore in the dendrimer can thus be easily substituted whilst the processing properties, which are defined by the surface groups stay the same. The much smaller size of the dendritic molecules compared to conjugated polymer chains means that there are no long chains of various conjugation. The conjugation should be similar for each dendrimer with known breaks uniform to all molecules of the same type.

By extending the branching (ie the number of dendrons) in a dendrimer higher generations of dendrimers are produced. The addition of further branching allows fine control of the spacing of the chromophores on the nanometre scale. Carrier mobility has been controlled within LEDs by controlling the generation of branching of the dendrimer. Much work has been performed on these materials and by finely controlling dendrimer properties LED devices of high efficiencies have been demonstrated.

Two different types of dendrimer were studied, one was fluorescent and the other phosphorescent.

4.3.1 Fluorescent Dendrimers

The fluorescent dendrimers studied were an amino-cored distyrylbenzene (ADSB) and benzene cored distyrylbenzene (BDSB), where the core is defined as the three distyrylbenzene units attached to the central unit (Nitrogen atom or benzene ring respectively) as seen in Figure 4.7. Stilbene units are used as dendrons and the surface groups are t-butyl units, which allow good solubility in common solvents such as toluene, THF and chlorobenzene. The dendrimer could be branched by adding further dendron generations as seen in Figure 4.7, this increases the size of the molecule and effectively allows control over the spacing of adjacent cores and thus their interaction. The ADSB dendrimer studied here was the G1 generation as shown in Figure 4.6 and the G2 generation for the BDSB dendrimer.

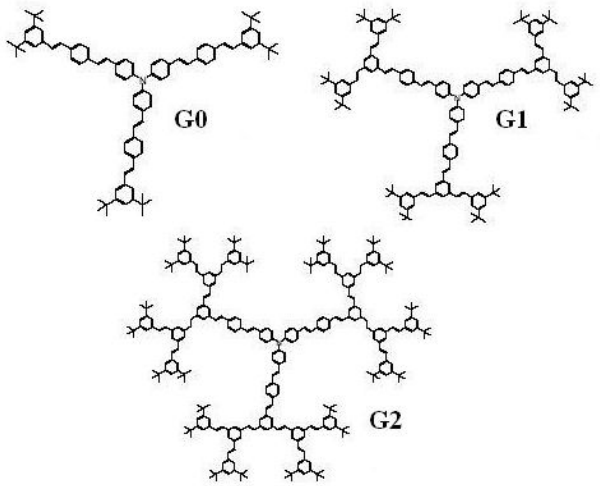

Figure 4.6 – Structure of three generations of the nitrogen cored A-DSB, B-DSB is similar but has a benzene ring at the centre.

These dendrimers have been modelled using coupled electronic oscillator calculations [35] in order to better understand the effect the core unit has on a similar dendrimer structure. The model predicted that for BDSB the excited state would be present on the DSB units of the core and that the meta positioning of these DSB chromophores surrounding the benzene ring effectively blocked electron delocalisation between the three DSB units. The nitrogen cored ADSB was predicted to have a strong coherence between these units suggesting delocalisation across all three units and across part of the central core.

Measurements of the anisotropy were performed in order to study the polarised fluorescence properties of these dendrimers. The benzene core is known to create a break in the conjugation but there is some delocalisation across the nitrogen core. An optical excitation onto these materials creates an electron-hole pair on a small conjugated segment and this localised pair can then contribute to either incoherent hopping of the energy between segments of the dendrimer or collective excitations. For energy transfer between segments the transition dipole of the molecule should reorient and lead to a depolarisation of the emission. Thus if there is delocalisation across two or more segments delocalisation must have occurred.

For the ADSB dendrimer the effect of changing the excitation wavelength on the steady state anisotropy is illustrated in Figure 4.7. The anisotropy at lower excitation wavelength is ~0.04 and this rises to 0.06 when the excitation is shifted to the peak of the absorption (need absorption graph find on server data was not available on this laptop). Excitation at lower wavelengths is partially absorbed by the dendrons and this leads to a lower anisotropy due to a loss of some excitations getting to the core. An anisotropy of 0.05 is very low and reveals that the emission is depolarised and thus the transition dipole has reoriented itself after excitation occurs as the excitation spreads across the core.

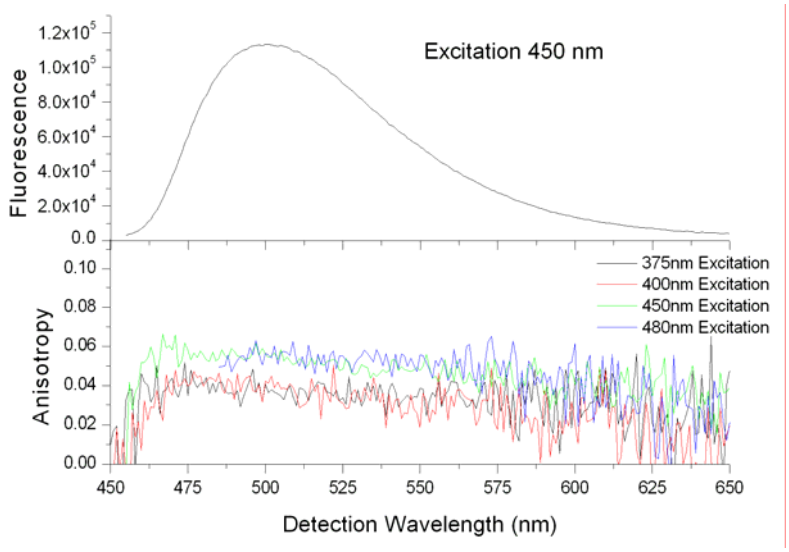

Figure 4.7 – Photoluminescence of ADSB-G1 (top) and the anisotropy of ADSB-G1 as a function of excitation wavelength.

In order to investigate the speed at which this occurs a time-resolved study using the femtosecond up-conversion technique (described in Chapter 3.7) was performed on this system. Figure 4.8 exhibits the polarised lifetime emission curves and anisotropy at 480 nm after excitation at 400 nm. The system had a 250 fs response function and as can be seen the anisotropy is found to stay flat at 0.06 almost immediately after excitation. This suggests that the depolarisation of the emission (and thus the reorientation of the transition dipole) occurs within 250 fs. This is an extremely fast depolarisation and shows that the excitation delocalises within 250 fs across the core.

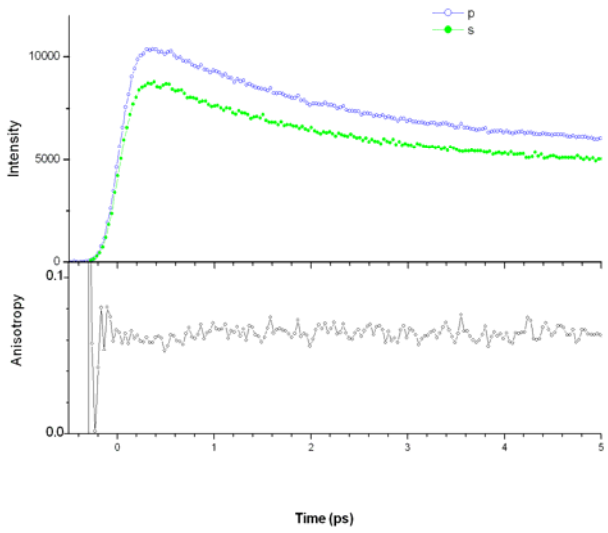

Figure 4.8 - Anisotropy measurement of ADSB on a 5 ps timescale. The excitation wavelength was 415 nm and the emission was observed at 480 nm

Work on the ultrafast depolarisation of these dendrimers has been studied using a similar technique and the G0 and G2 generations of ADSB [36,37]. The rotational diffusion is not thought likely occur within 250 fs due to the size of the molecule and this fast rearrangement was seen for G0 and G2 as well. Ultrafast depolarisation of the ADSB-G1 is thus observed as it must decay from an initial value of 0.4 and the mechanism involved is likely the reorientation of the transition dipole as the energy hops between segments of the dendrimer.

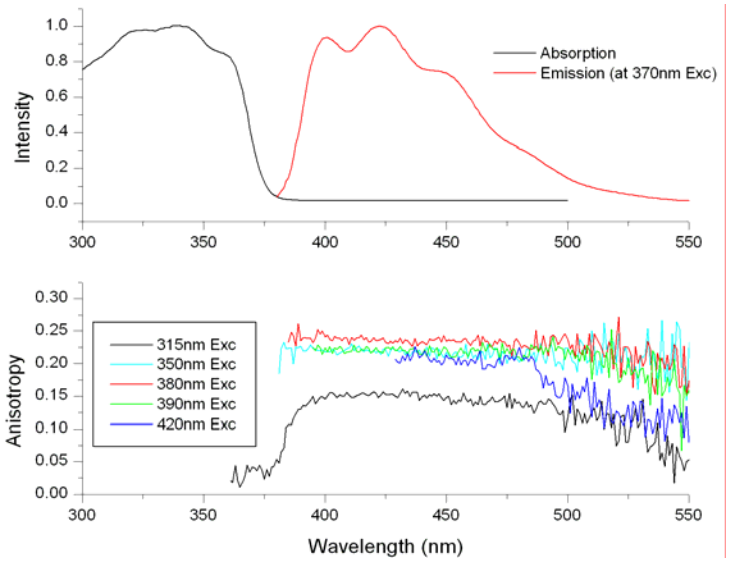

Figure 4.9 – BDSB G2 absorption and emission spectra (top) and anisotropy as a function of excitation wavelength (bottom).

Further anisotropy investigations were performed on BDSDB-G2. Figure 4.9 demonstrates the steady-state anisotropy behaviour of the BDSB-G2 dendrimer. The excitation at 315 nm has a lower anisotropy as the excitation is absorbed by the dendrons compared with the predominantly the core at higher wavelengths. The anisotropy is lower for the 420nm excitation but that is very weakly absorbed as it overlaps with the emission.

The anisotropy for BDSB-G2 is found to be quite high (~ 0.25 for excitation at 380 nm) and consistent across the spectrum. The fluorescence is thus not depolarised as fast as for the ADSB-G1. A femtosecond up-conversion study performed and the results are illustrated in Figure 4.10

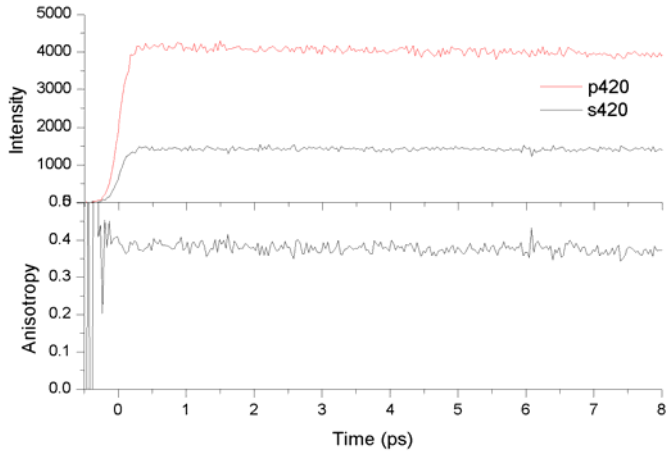

Figure 4.10 – Anisotropy measurement of BDSB-G2 on an 8 ps timescale. The detection wavelength was 420 nm and the excitation wavelength 370 nm.

The anisotropy decay here starts at 0.4 as expected and very slowly decays from this. No ultrafast depolarisation is observed and the slower decay towards the steady state anisotropy value is thought to be due to rotational diffusion of the molecule.

This difference in the anisotropy behaviour of two very similar molecules highlights the effect small changes in the chemical structure can produce. When a nitrogen atom is present in the core of the DSB dendrimer intersegment interactions occur on an ultrafast timescale. If the core incorporates a benzene ring instead the resulting intersegment interactions are very different. The measurements also clearly verify the calculations of the excited state interactions from the modelled dendrimer system [35].

4.3.2 Phosphorescent Dendrimers

Phosphorescent dendrimers have received much interest in recent years as an efficient route to extracting more efficient light output from a dendrimer. These dendrimers usually contain a transition metal complex as the core. Iridium based complexes are highly efficient phosphorescent emitters and quantum efficiencies for 100% internal electroluminescence efficiency have been reported [38]. Dendrimers with an iridium complex core have demonstrated highly efficient OLEDs using solution processing fabrication [39]. Blue and red phosphorescent materials have been found to be

less efficient mainly due to a lower strength of the phosphorescent state and faster non-radiative deactivation.

In order to better understand the dynamics of the singlet-triplet energy states the fluorescence signal of phosphorescent dendrimers was studied. Even though the emission is expected to be from the phosphorescent triplet state the excitation has to transfer to this via intersystem crossing after optical excitation into the singlet state. This is known to occur very efficiently and fast but some fluorescence signal is still expected to be visible in the very initial stages of the excitation transfer from the singlet to the triplet state. Despite the importance of phosphorescent dendrimer to OLED applications so far no fluorescence from singlet excited states has been reported from iridium complex based dendrimers due to the efficient transfer to the triplet state. By using an ultrafast excitation and detection system the fluorescence signal can be probed.

The dendrimers studied were the *fac*-tris(2-phenylpyridine) iridium(III) [$Ir(ppy)_3$] cored dendrimer which is a green emitter and ($G1ppy_2$)btpIr (name) a red emitter. The study was performed using the femtosecond up-conversion technique. The excitation pulse was a 400 nm 100 fs pulse at a 50 kHz repetition rate. Figure 4.11 illustrates the absorption and emission of the green dendrimer as well as its structure.

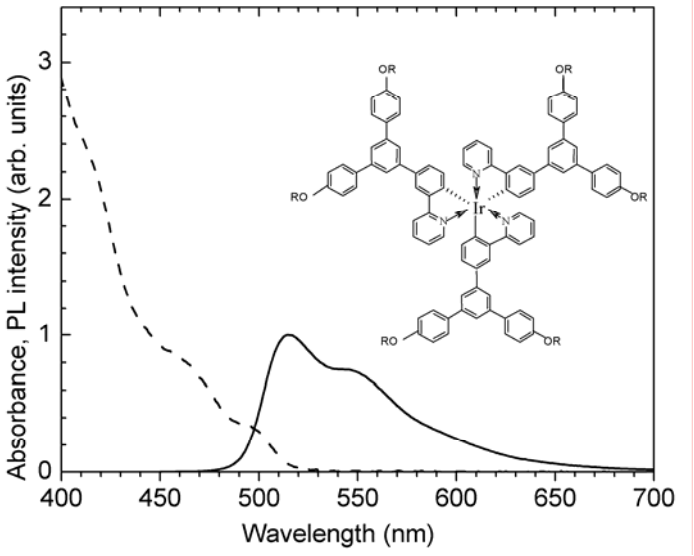

Figure 4.11 – The absorption and emission of *fac*-tris(2-phenylpyridine) iridium(III) [$Ir(ppy)_3$] and its chemical structure.

Figure 4.12 shows the time resolved results for the green dendrimer. The photoluminescence lifetime for 460 nm is almost identical to the response function of the system with a fitted 20 fs component (although this is limited by the resolution and should be taken as an approximate value). As the detection wavelength is increased the lifetimes become slower with a longer lived component forming which is the phosphorescent state, the 490nm data exhibits a 180 fs component. Fits to higher wavelength data provide a time constant of 240fs for the longer wavelengths for the emission of the singlet state.

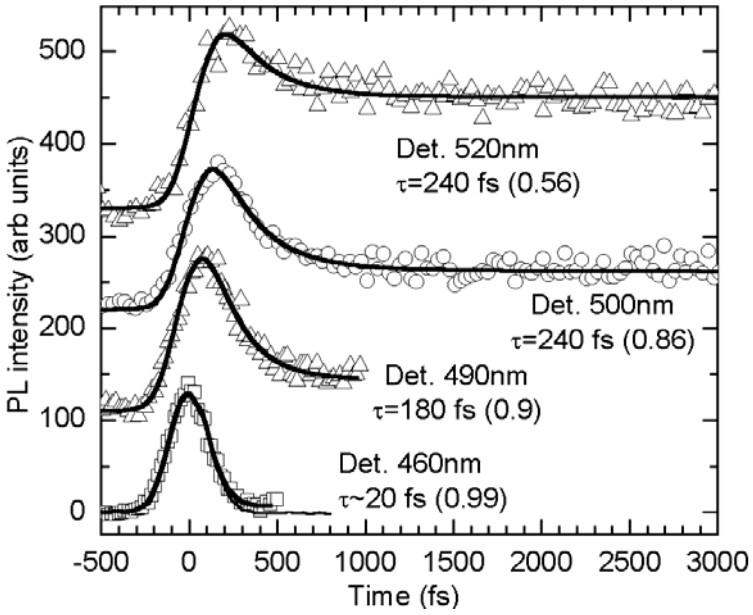

Fig. 4.12. PL decay kinetics (left panel, symbols) of the $Ir(ppy)_3$ dendrimer in toluene detected at 460, 490, 500 and 520 nm after excitation at 400 nm. Kinetics are offset for clarity. Thick solid lines are the best fits with a sum of an exponential decay and a long component, the time constant and the pre-exponential factor of the fast decay component are given.

This singlet emission is the first reported from a highly efficient phosphorescent dendrimer and gives an insight into the decay dynamics of these short lived states.

4.4 Conclusion

In this Chapter the effect of conjugation was investigated in MEH-PPV using temperature dependence. Steady-state absorption and emission properties vary with a decrease in sample temperature and this is due to the straightening of the polymer chain as the thermal energy of the polymer decreases and the effect of conjugation breaks is observed. Red-shifts in emission and absorption are less pronounced as chemical defects are introduced due to the presence of more shorter chain segments compared to fully conjugated chains.

Time-resolved studies of the emission spectra show that the excitation migration to the longer chain segments occurs within 40 ps for fully conjugated MEH-PPV and slightly longer for partially conjugated MEH-PPV. The emission lifetime was not altered significantly for the fully conjugated sample whereas for the partially conjugated sample the lifetime was lengthened considerably. This can be explained by a longer excitation migration to a lower energy segment if more chemical defects are in place. No anisotropy change was observed within a 2 ps time resolution of the equipment suggesting that any effect of the excitation occurs within this timeframe.

Studies of several novel dendrimers provided some insight into the dynamics of the excitation produced on it. Anisotropy studies of two fluorescent dendrimers ADSB-G1 and BDSB-G2 were conducted with a variation of the excitation wavelength. ADSB-G1 exhibited an ultrafast depolarisation of the emission within 250 fs (attributed to intersegment interactions) compared to no fast depolarisation in the similar BDSB-G2 molecule.

The ultrafast emission properties of two phosphorescent dendrimers were studied. The singlet emission of *fac*-tris(2-phenylpyridine) iridium(III) [$Ir(ppy)_3$] cored dendrimer was observed and is the first reported fluorescence emission from a phosphorescent dendrimer. The singlet emission has a decay constant of ~240 fs before emission is transferred to the phosphorescent triplet state. A red emitting dendrimer was studied but results were inconclusive.

Chapter 4 References

[1] J. Burroughes, D. D. C. Bradley, A. R. Brown, R. N. Marks, K. Mackay, R. H. Friend, P. L. Burn, and A. B. Holmes. *Nature*, 347, 539, (1990).

[2] Samuel IDW, Rubles G, Collison CJ, *Physical Review B*, **52**, 11573 (1995)

[3] Hayes GR, Samuel IDW, Phillips RT, *Physical review B*, **52**, 11569 (1995)

[4] N. T. Harrison, D. R. Baigent, I. D. W. Samuel, and R. H. Friend. *Physical Review B*, **53**, 15815, (1996).

[5] J. M. Leng, S. Jeglinski, X. Wei, R. E. Benner, and Z. V. Vardeny. *Physical Review Letters*, **72**, 156, (1994).

[6] S. Huen, R. F. Mahrt, A. Greiner, U. Lemmer, H. Bassler, D. A. Halliday, D. D. C. Bradley, P. L. Burn, and A. B. Holmes. *Journal of Physics Condensed Matter*, **5**, 247, (1993).

[7] H. B¨assler and B. Schweitzer. *Accounts of Chemical Research***, 32**, 173, (1999).

[8] G. D. Scholes, D. S. Larsen, G. R. Fleming, G. Rumbles, and P. L. Burn. *Physical Review B*, **61**, 13670, (2000).

[9] U. Rauscher, H. B¨assler, D. D. C. Bradley, and M. Hennecke. *Physical Review B*, **42**, 9830, (1990).

[10] M. Yan, L. J. Rothberg, E. W. Kwock, and T. M. Miller. *Physical Review Letters*, **75**, 1992, (1995).

[11] N. S. Sariciftci, editor. *Primary Photoexcitations in Conjugated Polymers: Molecular Exciton Versus Semiconductor Band Model*. World Scientific Publishing, (1998).

[12] V. Doan T. Q. Nguyen and B. J. Schwartz. *Journal of Chemical Physics*, 110, 4068, (1999).

[13] C. J. Collison, L. J. Rothberg, V. Treemaneekarn, and Y. Li. *Macromolecules*, 34, 2346, (2001).

[14] D. Hu, J. Hu, and P. F. Barbara. *Journal of the American Chemical Society*, 121, 6936, (1999).

[15] J. Yu, D. Hu, and P. F. Barbara. *Science*, 289, 1327, (2000).

[16] D. Hu, J. Yu, K. Wong, B. Bagchi, P. J. Rossky, and P. F. Barbara. *Nature*, **405**, 1030, (2000).

[17] T. Huser, M. Yan, and L. J. Rothberg. *Proceedings of the National*

Academy of Sciences of the United States of America, **97**, 11187, (2000).

[18] T. Huser and M Yan. *Journal of Photochemistry and Photobiology A: Chemistry*, **144**, 43, (2001).

[19] P Wood, IDW Samuel, GR Webster, PL Burn, *Synthetic Metals*, **119**, 571 (2001)

[20] G Rossi, RR Chance, R Silbey *Journal of Chemical Physics*, **90**, 7594 (1989)

[21] KS Schweizer, *Journal of Chemacal Physics*, **85**, 4181 (1986)

[22] SN Yaliraki, R Silbey, Journal of Chemical Physics, **140**, 1245(1996)

[23] Kohler BE, Samuel IDW, *Journal of Chemical Physics*, **103** ,6248(1995)

[24] Wood P, Samuel IDWm, Schrock R, Christensen RL, *Journal of Chemical Physics*, **115**,10955 (2001)

[25] G. R. Webster. *Advanced polymers for light emitting diodes*. PhD thesis, University of Oxford, (2000).

[26] S. H. Lim, T. G. Bjorklund, and C. J. Bardeen. *Chemical Physics Letters*, 342, 555, (2001).

[27] J. Yu, M. Hayashi, S. H. Lin, K. K. Liang, W. S. Fann, C. I. Chao, K. R. Chuang, and S. A. Chen. *Synthetic Metals*, 82, 159, (1996).

[28] O. Ingan¨as, W. R. Salaneck, J. E. ¨ Osterholm, and J. Laakso. *Synthetic Metals*, 22, 395, (1988).

[29] J. R. Linton and C. W. Frank. *Synthetic Metals*, 28, C393, (1989).

[30] M. Severin and O. Ingan¨as. *Journal of Chemical Physics*, 105, 8446, (1996).

[31] M. Zheng, F. Bai, and D. Zhu. *Journal of Photochemistry and Photobiology A: Chemistry*, 116, 143, (1998).

[32] A. K. Sheridan, J. M. Lupton, I. D. W. Samuel, and D. D. C. Bradley. *Chemical Physics Letters*, 111, 531, (2000).

[33] M.Halim, I.D.W.Samuel, J.N.G.Pillow,P.L.Burn, *Synthetic Metals*, **102**, 1113 (1999)

[34] J. N.G. Pillow, M. Halim, J.M. Lupton, P.L. Burn, I.D.W. Samuel, *Macromolecules* **32,** 5985 (1999)

[35] *JM Lupton, IDW Samuel, PL Burn, S Mukamel, Journal of Physical Chemistry B*, 106, 7647 (2002)

[36] O Varnavski, G Menkir, T Goodson, PL Burn, *Applied Physics Letters*, 77, 1120 (2000)

[36] O Varnavski, G Menkir, T Goodson, PL Burn, IDW Samuel, JM Lupton, R Beavington *Applied Physics Letters*, 77, 1120 (2000) (Erratum)

[38] C. Adachi, M.A. Baldo, M. E. Thompson, S. R. Forrest, Journal of Applied Physics **90**, 5048-5051 (2001).

[39] S.-C. Lo, N.A.H. Male, J.P.J. Markham, S.W. Magennis, P.L. Burn, O.V. Salata, I.D.W. Samuel, “, Advanced Materials, **14,** 975-979 (2002).

Chapter 5

Ultrafast Conjugated Polymer Lasers

5.1 Introduction

In recent years, conjugated polymers have become an attractive new gain medium for lasers that are tuneable across the visible spectrum [1-8]. Conjugated polymers exhibit high fluorescence quantum efficiencies and little concentration quenching, permitting their use in the solid state. The broad emission spectra of conjugate polymers has been used to tune the emission from a conjugated polymer by controlling the film thickness or the laser structure [9,10].

The high gain available from conjugated polymers in the visible spectrum indicate that conjugated polymer laser are compatible with the low-cost polymer optical fibres (POF), leading to their potential use as light sources for short-haul communication networks [11,12].

Even though much research has been carried out on lowering the laser threshold by varying the resonator configurations but the temporal dynamics of conjugated polymer laser are not well studied. The broad spectra of these materials make them a potential candidate for ultrafast photonics as the generation of a short laser pulse calls for a gain medium which operates over a wide range of optical energies. This is because of the energy-time uncertainty principle, $\Delta E \Delta t > h/4\pi$. Where Δt is the time duration of the laser pulse, ΔE are the resultant optical energies it exhibits and h is Planck's constant. For a short laser pulse to exist this means a large range of photon energies must be available in the gain material. Such broad emission ranges with high gain are known to exist in conjugated polymers and so a study of the temporal laser dynamics was performed to investigate the ultrafast nature of the emission from a conjugated polymer laser

The work in this chapter is aimed at studying the temporal dynamics of two-dimensional distributed feedback lasers using MEH-PPV as a gain material. Studies using both a Streak Camera and a femtosecond up-conversion technique are used and

pulsewidths of the polymer laser are observed to decrease to 410 fs. A model is described which is used to explain the behaviour of the reduction in pulsewidth as the buildup of amplified spontaneous emission. Further work on a novel encapsulated laser device is also performed and is shown to support short pulses down to 6 ps pulses.

5.2 Gain Properties

The gain exhibited by conjugated polymers can be exhibited in several ways: Amplification of an initial intensity signal after passing through a gain medium, an increase in transmission in transient absorption, the presence of amplified spontaneous emission (ASE) or through lasing. Each of these is observed only if gain is present and the different experiments will be briefly discussed except lasing which is covered in more detail in Chapter 5.3.

The amplification of an input signal in one pass (i.e no feedback) is discussed in more detail in Chapter 6 as this would imply an optical amplifier. Amplification in conjugated polymers in solution has been reported with a gain of ~ 40 dB/cm have [13].

Transient absorption was discussed in Chapter 3 and is a technique for analyzing the time dependence of the gain. An incoming ultrashort pulse arrives at the sample and excites the medium creating a population inversion. The probe beam then arrives after this excitation and is amplified. This leads to a change in transmission, as the time delay between these pulses is increased, which is measured and from this the gain can be calculated [14]. The transmission of the probe signal is measured through the sample with the pump on (T_{on}) and the pump off (T_{off}) and this can be related to a change in the induced absorption of the medium:

$$\frac{\Delta T}{T} = \frac{T_{on} - T_{off}}{T_{off}} = -\Delta\alpha d \qquad \text{Equation 5.1}$$

where $\Delta\alpha$ is the induced absorption change and d is the thickness of the sample the light passes through. The induced absorption change is related to the excited state population and the absorption cross-section and so this measurement allows the direct observation of

the time dependent excited state population and the absorption cross section. A negative change in $\Delta T/T$ is due to photoinduced absorption where the probe beam is absorbed by the excited state of the sample and promotes the excitation to a higher energy state. A positive change can be attributed to either photobleaching or by stimulated emission. Photobleaching is the process where the absorption at the probe wavelength is reduced due to the depletion of the ground state by the pump.

Another manifestation of gain in a material is amplified spontaneous emission (ASE). This is when spontaneously emitted photons are amplified by stimulated emission in the region being optically pumped, as shown in Figure 5.2.

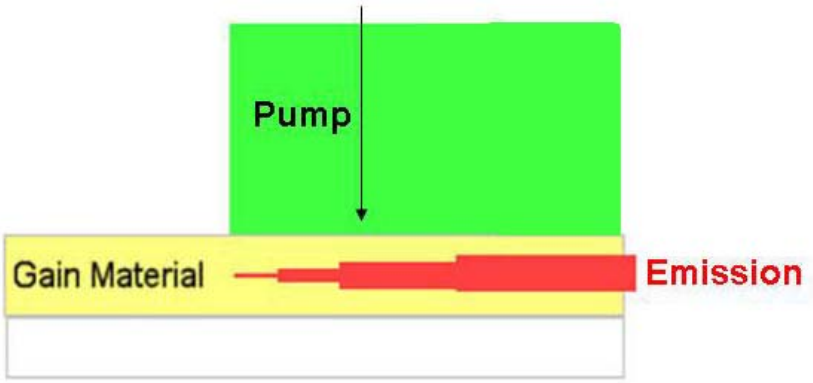

Figure 5.2 Amplified Spontaneous Emission in a thin film

By pumping a small region of a conjugated polymer on a substrate, spontaneous emission is amplified by stimulated emission and the gain can be studied by measuring the emission from the edge. As photons with a wavelength at the peak of the gain experience preferential amplification the emission spectrum narrows in width. Although this is an indirect measure of gain [2], gain narrowing has been observed in a variety of materials such as polyfluorenes, polyphenylenevinylene (PPV) and polyparaphenylene (PPP) [15]. Gains of 60 cm-1 have been observed [2] and further work has shown that the wavelength of ASE can be controlled by varying the thickness of the waveguide layer [16], emission was tuned over a 31 nm range in a MEH-PPV waveguide.

5.3 Conjugated Polymer Lasers

A laser has two components; a gain medium and a resonator structure which provides feedback such that oscillations can build up. Lasers normally consist of a solid gain medium placed between two or more mirrors to create a cavity within which the emission can travel and be amplified. Dye (small molecule) and solution based conjugated polymer lasers have been demonstrated using these microcavities. For solid samples a structure with cleaved edges could also be used as a resonator providing it has some form of internal waveguiding as the internal reflections from the cleaved edges provide sufficient feedback to sustain lasing.

With the advances in OLED technology and with devices with high luminescence efficiency becoming common the development of an organic semiconductor laser has become an area of much research using similar architectures to those used for OLEDS. In order to study the processes involved in such devices the primary research so far has been performed using excitation by photopumping. Due to the large amount of energy needed to create a population inversion it is easier to study the stimulated emission and gain properties using optical excitation methods.

Stimulated emission was first detected in conjugated polymer in solution [17], quickly followed by studies involving diluted [18,19] and undiluted solid thin films [20] leading to lasing observed in both solution and solid films. So far research has produced an insight into the device geometries that will allow the laser threshold to be reduced as well as the material properties that will be required to make the first electrically driven laser. Due to problems with current injection, charge transport as well as the lack of sufficient material gain, electrically driven lasing in a conjugated polymer device has not been achieved yet.

Several geometries of organic lasers have been studied (Figure 5.3), first of all the microcavity laser [21]. In a microcavity laser the gain medium (in this case the organic semiconductor) is placed inside a Fabry-Perot resonator. The resonator cavity length determines the wavelength of emission and is set to be within the emission spectra of the gain medium. When excited, the light output is coupled to cavity modes and this causes spectral narrowing of the output [22] allowing control over the emission [23]. One such

microcavity laser is the Distributed Bragg Reflector (DBR), which has the gain material surrounded by alternating layers of high and low refractive index, in essence two broadband mirrors. These layers can be created to be chirped and thus allow several different modes to exist within the gain medium. DBR lasers have been studied using dye-doped polymers [24] and polyfluorenes [25]. Microcavity lasers are relatively easy to produce as their structure is similar to OLEDs. The geometry also means they will emit perpendicular to the substrate on which the device is fabricated. Because the gain medium is a film sandwiched between two mirrors the laser threshold can be quite high but this can be reduced somewhat by using highly reflective mirrors.

Figure 5.3 – Different possible laser resonator structures

A different resonator structure to the cavity are spherical or ring microlasers (see Figure 5.3). Emission is coupled to resonant modes of the structure due to its small size and these "whispering gallery" modes are confined around the circumference of the cavity. Single mode lasing has been achieved by varying the diameter of the ring and laser threshold as low as 100 pJ have been reported [2]. These types of lasers have been made using organic as well as inorganic gain media and their main advantage has been an easy fabrication route as well as low thresholds. Their main drawback is that the output emission does not have a very good beam quality.

In order to improve the laser thresholds of organic lasers the light emission has to be better controlled within the gain medium. This can be achieved by having some form of waveguide present within the resonator using wavelength scale microstructures. The microstructures alter the propagation of the light. This is caused when the light in the waveguide modes is diffracted from periodic scattering centres by Bragg scattering. Using a periodic modulation of the waveguide thickness as shown in Figure 5.3 the propagating light is scattered out of the waveguide (perpendicular to the substrate) or

back along its previous path. This kind of device is known as a distributed feedback laser DFB.

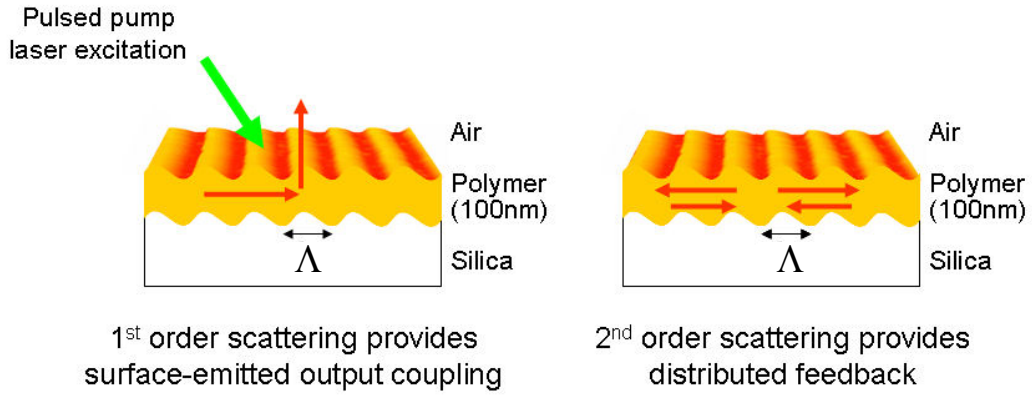

Figure 5.3 - Bragg Scattering in Distributed Feedback Lasers

Different orders of Bragg scattering have different effects. First order Bragg scattering couples light out of the waveguide and the second order couples together counter-propagating modes. Bragg scattering is defined by:

$$\frac{2\pi}{\lambda}\sin(\theta) = \pm\frac{2\pi n_{eff}}{\lambda} \pm m\frac{2\pi}{\Lambda} \qquad \text{Equation 5.2}$$

where n_{eff} is the effective refractive index of the waveguide , Λ is the fundamental period of the grating and m is an integer. This equation is derived from momentum conservation in the plane of the waveguide. The Bragg vector $k_G=2\pi/\Lambda$ is based on multiple integers to account for grating effects. The first order m=1 as mentioned before causes light to be scattered out of the waveguide which is important for laser output but the second order m=2 effect governs resonator feedback. Second order Bragg scattering couples together counter-propagating modes and controls the amount of feedback present in the device. Thus by simply incorporating a periodic modulation to the interface between the substrate and material, as shown in Figure 5.2, both feedback and output coupling is addressed.

DFB lasers work on the principle of feedback being distributed across an area. By using periodic structures which reflect (second order Bragg scattering) some of the light back and forth inside a certain area enough feedback occurs to promote lasing action. For

conjugated polymer lasers this type of periodic structure can be created on the substrate on which the gain material is to be deposited, thus making this technology compatible with current manufacturing processes for OLED device. Another advantage is that this architecture has shown to have lower laser thresholds which leads itself to the possibility of future electrical devices.

Inorganic DFB lasers date back to the 1970s [26] and are a key component in the data transmission market due to their highly stable (yet tuneable) single frequency output. The term DFB implies a particular form of a laser where the feedback is induced by a uniform one-dimensional periodic modulation. However with the advent of two and three-dimensional modulation architectures which provide better light constraint and improved threshold conditions the term is used for many different types of laser based on periodically modulated feedback. With the advances in photonic crystal technology over the recent years novel architectures have been developed which have enabled lower laser thresholds to be achieved.

Conjugated polymer DFB lasers were first demonstrated using one dimensional gratings on silica [27] with a spin coated film of BuEH-PPV. The emission wavelength was defined by the grating period and this is true for all DFB lasers. Conjugated polymer lasers on a flexible substrate [3] were demonstrated which illustrate the potential diversity of application of devices based on conjugated polymers.

MEH-PPV as a gain material has been studied in more depth in recent years using one and two dimensional DFB structures [9, 28]. In a one-dimensional (1-D) DFB laser the periodic modulation is in one direction only as can be seen from Figure 5.3. This means that the feedback occurs only in one direction. The output coupling in these structures is at a well-defined angle but the grating provides no control of the direction in the plane and this leads to a fan-shaped emission.

A novel tuneable laser based on the 1D-DFB structure [9] has been demonstrated which highlights the broad gain available from conjugated polymers. In this case a chirped grating was created in which the period of the modulation of the DFB structure varies with position. The wavelength which undergoes feedback and output coupling in a Bragg grating depends on the grating period and so the emission can be tuned by

translating the grating such that the pump beam is incident on different grating periods. In this way lasing was demonstrated over a 20 nm wavelength range. This highlights the broad gain available in these materials.

A superior laser is created by using two perpendicular gratings as shown in Figure 5.4, which exhibits feedback in two perpendicular directions. There are several important advantages to this. First is that the laser threshold is found to be decreased due to the decrease in effective mode volume and laser thresholds have been reduced to 10 nJ in these structures [29,30]. Secondly the output beam is well defined as the output is perpendicular to two gratings, this has led to near-diffraction limited emission [30].

Conjugate polymer 2D-DFB lasers exhibit lower thresholds than most other laser geometries and much research has gone into reducing these thresholds by either using different materials [31, 10] or improved DFB structures [32].

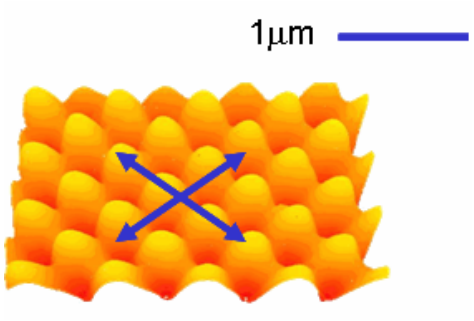

Figure 5.4 – Two-dimensional laser structure

5.4 Temporal Dynamics Of A Two-Dimensional Polymer Laser

Conjugated polymer lasers based on distributed feedback structures have been shown to exhibit lowered laser thresholds compared to other geometries. The lasing properties of these devices have been studied since the first demonstration of lasing from a conjugated polymer but few studies [33,34] have been made of the temporal dynamics of laser emission when optically pumped by a pulsed laser.

In recent years picosecond ASE pulses have been studied [35,36] as well as the dynamics from a microcavity laser [37]. The lifetimes of the pulses was found to decrease to several picoseconds in these cases though no further narrowing was seen.

The laser studied was a 2D-DFB surface emitting distributed feedback laser with a known low laser thresholds. The DFB structure consisted of a two-dimensional "egg-box" corrugated structure in a silica substrate as shown in Figure 5.5. The gratings had a period of 409 nm in both directions and a peak-trough height of 100nm. Thin films of poly[2-methoxy-5-(2'-ethylhexyloxy)-1,4-phenylene vinylene] (MEH-PPV, Covion) were spin coated onto these substrates. The thickness of these layers as determined by a Dektak 3 was ~ 120 nm.

In order to study the temporal and spectral dynamics of these laser devices they were first studied using the Streak Camera described in Chapter 3.7.

5.4.1 Streak Camera Results

In order to study the dynamics of a 2D-DFB MEH-PPV laser the streak camera and attached spectrograph were used. The laser excitation was provided by the output from the Spitfire regenerative amplifier of 800 nm 100 fs pulses at 50 kHz. This output was frequency doubled to 400 nm to excite the MEH-PPV laser, as shown in Figure 5.5 this is not at the peak of the absorption but should provide sufficient excitation. The experimental layout is shown in Figure 5.6.

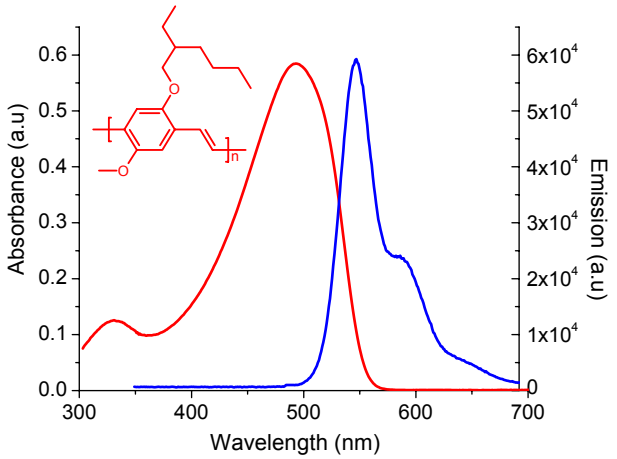

Figure 5.5 – MEH-PPV absorption and emission spectra with the chemical structure of MEH-PPV inset.

The conjugated polymer laser was placed in a vacuum chamber and held under a vacuum of 10^{-5} mbar to prevent contact with water and oxygen quenching the emission. Two lenses were used to capture, collimate and then focus the emission from the polymer laser onto the imaging spectrograph and via this onto the streak camera. The temporal response of the streak camera was measured using the detection of a 100fs excitation pulse. The spot size of the excitation beam was measured using a beam profiler and was found to be 150 μm in diameter.

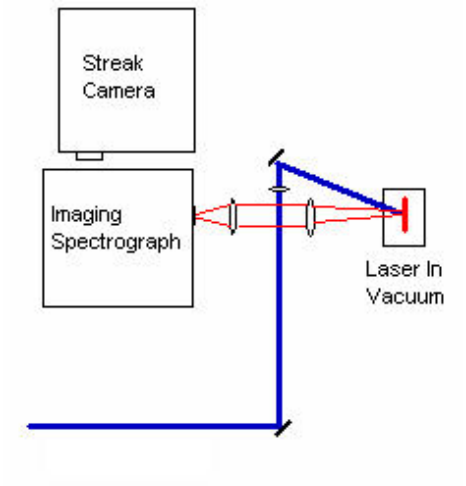

Figure 5.6 –Streak Camera experimental layout.

In order to study the lasing behaviour of this device the excitation energy was increased from almost nothing to well above laser threshold. The effect of the grating on the narrowing of the pulses can be seen by comparing the lifetime of the MEH-PPV thin film on the substrate with no DFB grating present and the film on the grating structure. Figure 5.7 illustrates the lifetime differences from on-grating lifetime (at an excitation energy below threshold of 0.6 μJcm^{-1}) and the thin film MEH-PPV lifetime on the substrate alone. The rise in emission is significantly faster for the film on the grating by almost 30ps. This is attributed to the scattering of the emission in the DFB structure. The film lifetime of both is similar to that reported for spontaneous emission [38] of 180 ps although the lifetime on grating was slightly less at the same excitation density compared to that when excited observed off the grating. For clarity all lifetimes were normalised and overlapped at an initial 10% of the peak intensity during the rise of the fluorescence to study the change in temporal dynamics.

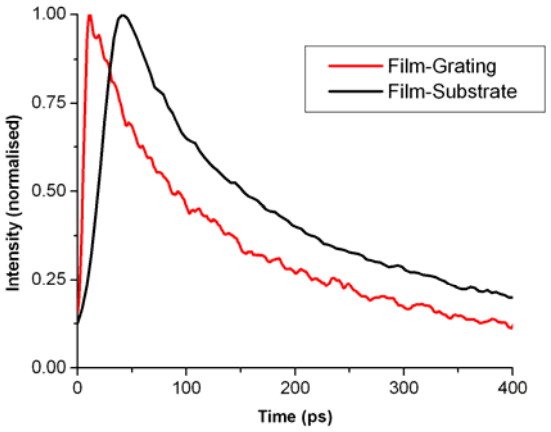

Figure 5.7 – Lifetime dynamics of the MEH-PPV film deposited on the DFB grating structure or on a non-etched are of substrate

Increasing the excitation energy demonstrated a clear lifetime shortening with the lifetime dropping from ~180 ps to less than 80 ps below threshold as can be seen in Figure 5.8. The noisy data is due to the small amounts of emission at these low excitation densities that could be collected, in part due to the vacuum chamber setup defining how close the capturing lens could be placed, as well as the general low emission at these pump densities. As shown in Figure 5.8, the emission lifetime shortens until lasing action is observed at a pump density of ~2.6 μJcm^{-2}, where the pulse is shortened to ~ 10 ps.

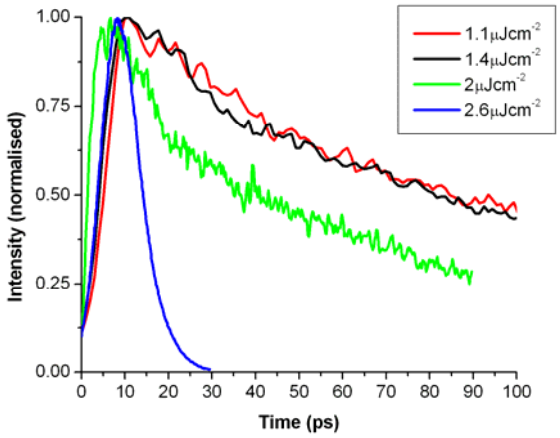

Figure 5.8 – Decay Dynamics at low excitation densities

Figure 5.9 clearly shows that spectral narrowing has occurred and although this could be due to ASE the output from the laser was visible as the well-known cross-emission from a 2D-DFB laser. Further increase in the excitation energy density to more than twice the threshold shows a further line narrowing which is limited by the resolution of the system.

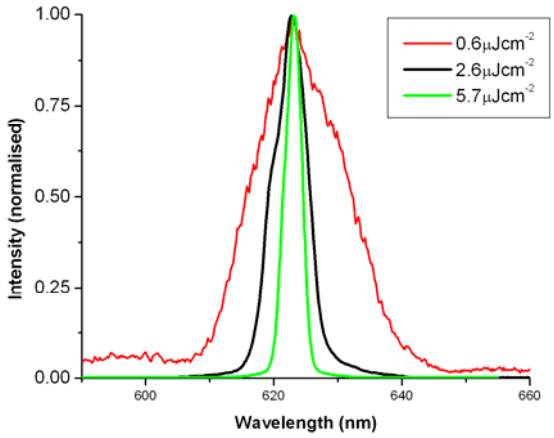

Figure 5.9 – Spectral Emission from a 2D-DFB laser below and at threshold

As the excitation energy is increased further above threshold the pulse width narrows further from 10.4 ps towards the resolution limit of the streak camera as defined by the response function as shown in Figure 5.10. The response function was measured to

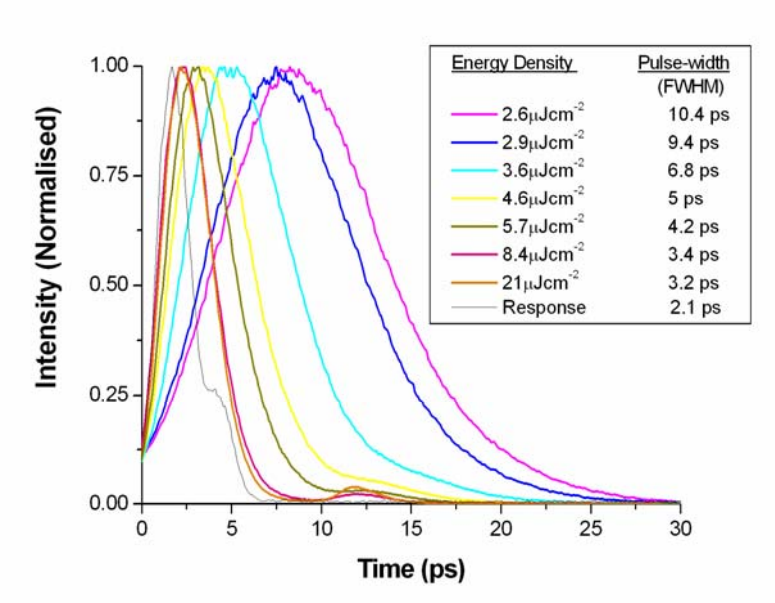

Figure 5.10 – Temporal dynamics of a 2D-DFb laser above lasing threshold, table of pulsewidths inset

be ~ 2 ps. A small reflection off the back of the substrate is responsible for the small tail of the response function.

The response of the system limited the detection of lifetimes below 2 ps. Although the streak camera is specified to measure with a resolution of 500 fs this is however dependent on the jitter of the laser to which it is synchronised (in this case the synchronisation is performed using optical triggering). The synchronisation laser used was part of the output from the MaiTai oscillator at 80 MHz and the excitation was provided by the MaiTai seeded Spitfire regenerative amplifier at 50 kHz. Normally a streak camera would be synchronised to the repetition rate of the excitation laser and we believe this is one of the first demonstrations of a measurement taken using a streak camera synchronised with a repetition rate significantly above that of the excitation pulses.

Ultrafast pulses from a 2D-DFB MEH-PPV laser were observed and this shows that short pulse generation is supported in these materials.

5.4.1.1 Modelling of the lasing dynamics

In order to investigate the dynamics observed in the previous section a model based on simple rate equations was created. The model describes the upper state population density and the photon density within the laser. A similar model has been used to describe the dynamics observed in a microcavity laser [37] with Alq_3:DCM although the model used here does not take into account the energy transfer of the blend as we use a conjugated polymer neat film.

The rate equations for the upper state population N(t) and the photon density S(t) are:

$$\frac{dN}{dt} = -S(t)V_{gr}[\sigma_{SE}N(t)] - \frac{N(t)}{\tau_{exc}} \qquad \text{Equation 5.3}$$

$$\frac{dS}{dt} = S(t)\Gamma V_{gr}[\sigma_{SE}N(t) - \alpha_{abs}] - \frac{S(t)}{\tau_{ph}} \qquad \text{Equation 5.4}$$

Equation 5.3 describes the dynamics of the upper state population N(t) using only terms describing the stimulated emission rate and the spontaneous exciton decay. The 100 fs excitation pulse is assumed to produce an instantaneous population inversion (gain-switched operation). V_{gr} is the group velocity of light in the waveguide, taken to be ~$2x10^{10}$ cms^{-1}, α_{abs} is the absorption loss taken as 100 cm^{-1} and τ_{exc} is the exciton decay time constant of 180 ps. The initial population density N(0) values were calculated from the energy of the excitation pulses in the experiment and the initial photon density S(0) was taken as 0.001% of this value to approximately represent the number of photons spontaneously emitted into the laser mode within the short duration of the pump pulse. The initial photon density was found to have little effect on the calculated pulse widths with a variation of less than 5% over a change of six orders of magnitude for the initial photon density.

The photon density dynamics as described by Equation 5.4 includes terms for the stimulated emission and the lifetime of the photons in the resonator. The photon lifetime

τ_{ph} can be expressed as a function of the group velocity and a loss factor combining the absorption and scattering of photons.

$$\tau_{ph} = \frac{1}{V_{gr}\alpha_{loss}} \qquad \text{Equation 5.5}$$

Where α_{loss} represents the losses from absorption and scattering of the photons and is taken to be 250 cm^{-1}, more than twice that of the absorption loss as Bragg scattering of the photons is expected to be a large contributing factor in a DFB structure. The light confinement factor Γ of the 2D-DF laser structure was calculated to be 0.4 [39].

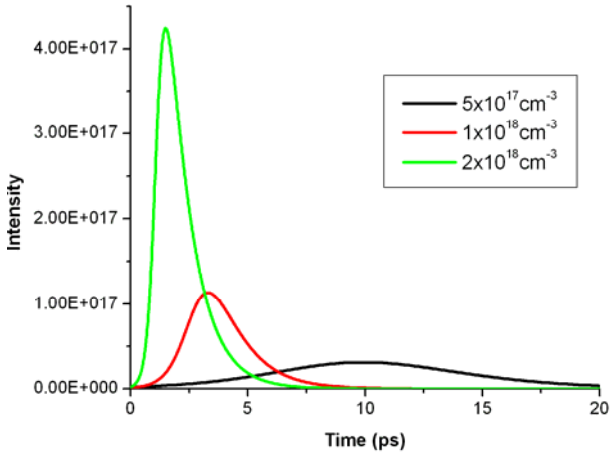

Figure 5.11 – Theoretical plots of photon density for different initial population inversions.

Figure 5.11 illustrates the results from the theoretical modelling with different initial population inversions based on the excitation densities used in the experiment. As can be seen at around threshold ($5x10^{17}$ cm^{-3}) with further narrowing of the pulse towards 2-3 ps at the higher excitation densities. The stimulated emission cross section found to best model the dynamics was σ_{SE} $3x10^{-16}$ cm^{-1}, this is comparable to other reported values [40] These results agree with the experimental pulsewidth narrowing observed can be explained as the growth of ASE in the resonator structure. At higher excitation densities the model predicts pulse narrowing below the picosecond regime though this was not observed, however the limitation of the streak camera resolution is 2 ps and so this is not unexpected.

5.4.2 Femtosecond Up-Conversion Results

As described in the previous section the streak camera resolution of ~ 2 ps may have limited the detection of pulsewidths below this response function. In order to study these pulses in more detail a conjugated polymer 2D-DFB laser was studied using the up-conversion technique described in Chapter 3.

The laser structure studied was the same grating used in the Streak Camera studies described above with a similar thickness film of MEH-PPV (Covioon) and again placed in the vacuum chamber to avoid exposure to air and water during the measurements.

The experiment was performed using 50 kHz amplified pulses from the Spitfire. The 80 MHz MaiTai oscillator was not a candidate excitation source as the high repetition rate led to fast degradation of the laser at the high pumping densities needed to achieve lasing. This meant that the signal counting rate was slow as it was limited to the repetition frequency of the optical excitation. The lasers were thus pumped at 400nm and the emission was studied at the lasing wavelength. Compared to the Streak Camera method the spectra are more difficult to obtain and an Ocean Optics USB Spectrometer was used to verify the emission output such that the wavelength was known for the frequency conversion angle.

Upon pumping the 2D-DFB MEH-PPV laser the time dynamics were recorded. It was found that the emission prior to lasing was very weak and very difficult to collect but that once the excitation was above the lasing threshold a strong emission was seen with the characteristic cross beam profile of these lasers. This output was then directed towards the up-conversion crystal and overlapped with the gate beam. Figure 5.12 illustrates the observed features.

The emission below threshold was not measurable using the setup configured for collecting laser emission this was because the available collected emission from the grating was too weak to interact in the up-conversion crystal. The lasing threshold was found to be ~ 5 μJcm^{-2}, slightly higher than found earlier for the streak camera results.

The emission was measured at 620 nm (lasing output found using the Ocean Optics spectrometer), no emission was measured 4 nm either side. The spot size of the excitation pulse was measured to be 75 μm, this is half the size that was used before but could not be easily expanded due to the position of the tightly focussing lens used in the setup.

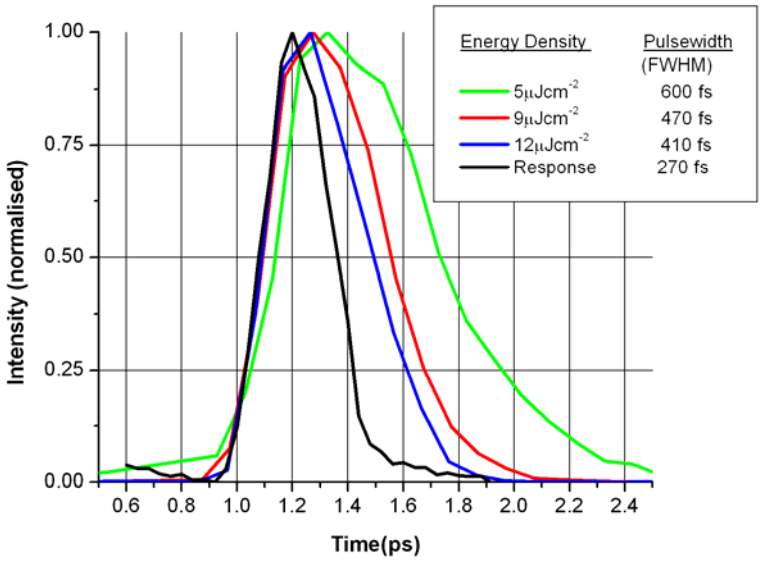

Figure 5.12 – Femtosecond up-conversion results from a 2D-DFB Laser. As the excitation density was increased the laser duration decreased to 410fs. The response function was measured to be ~ 270 fs.

The measured response of the system was ~ 270 fs with the excitation pulse at 400 nm and the gate pulse at 800 nm. The observed pulsewidths as shown in Figure 5.12 demonstrate sub-picosecond pulsewidths (not limited by the resolution of the system). Weak lasing was observed visually from about 4 μJcm^{-2} with the emergence of the cross-beam profile but it was not until the excitation energy was raised to 5 μJcm^{-2} did a signal become measurable with a pulsewidth of 600 fs. Increasing the energy of the excitation pulse leads to a pulse narrowing towards the response function with the shortest observed pulse of 410 fs at an excitation energy of 12 μJcm^{-2}. It was found that if the energy was raised above this the polymer film would be photodamaged within 20 seconds which meant that no measurements could be made.

Using the model used in Section 5.4.1.1 we get similar agreement with the pulse widths of 600 fs, but lower pulsewidths could not be reproduced by the model as higher excitation energies reproduced pulses of 600 fs at best.

5.5 Dynamics of an Encapsulated Polymer Laser

As mentioned previously the conjugated polymer DFB lasers were studied in vacuum as exposure to oxygen and water quenches the emission of most polymer thin films. In OLED applications the need for encapsulation has been overcome by using a transparent cathode material known as indium tin oxide (ITO) which is sputtered on top of a quartz substrate. This allows the organic layer of the device to be sandwiched between the cathode and the metal anode and yet still emit light through the transparent contact. Encapsulation is a well known technique to seal devices to avoid degradation effects caused by exposure to air or water (humidity). For OLED applications the encapsulation normally involves the use of a chemical "getter" which acts as a hydrophilic agent for any air or water that gets into the device and effectively protects the device for many hours (thousands of hours commercially). The use of a "getter" here is impractical but conventional encapsulation can be performed using optical adhesives.

Encapsulation involves the use of an UV-cured epoxy resin to seal off the edges of the devices. In order to study the feasibility of creating these devices for commercial applications work has been carried out at the Organic Semiconductor Centre to study encapsulation of conjugated polymer DFB lasers. The 2D-DFB lasers studied previously were created by spin coating a thin film of MEH-PPV onto a silica substrate which had a DFB structure etched into it. Encapsulation of the silica substrates was not available as the use of epoxy would mean the substrate would be very difficult to clean and possible lead to the grating to be damaged for further use. As these gratings are difficult to produce this was not a viable experiment.

However an alternative technology was available to produce laser structures in a polymer thin film using a soft lithography technique. Soft lithography describes methods of pattern transfer from a master substrate to a polymer thin film via pressure contact. A 2D-DFB laser structure has been created previously using the solvent-assisted

micromoulding (SAMIM) route of soft lithography [41]. The pattern transfer means that the thin film on a quartz substrate does not have the DFB structure at the polymer/substrate interface but at the polymer/air(vacuum) interface instead.

An encapsulated laser was produced by spin coating a thin MEH-PPV film (~100 nm depth) onto a quartz substrate. A solvent-assisted micromoulding process transferred a ~30 nm peak-trough grating structure into the polymer film. An optical adhesive (Norland 68) was applied over this structure and a microscope cover slip was placed on top of the structure. The optical adhesive spreads out as pressure is applied and air is pushed out of the device. Once the glue is hardened this leaves a 2D-DFB laser that can be used without the need for a vacuum chamber. The application of the glue and subsequent pressure does not appear to deform the polymer structures produced enough to limit their use.

A side-effect of the encapsulation is that the mode profile of the waveguided light is changed somewhat as the relative index of refraction of the polymer/air interface is now replaced with a polymer/optical adhesive interface. This changes the waveguide layer properties and actually makes the mode profile more symmetric within the MEH-PPV film as the substrate structure has a refractive index structure of substrate/polymer/optical adhesive of 1.47/1.8832/1.56 compared to 1.47/1.8832/1 for the non-encapsulated device where the mode sits nearer the polymer/substrate interface.

5.5.1 Experimental Results

The encapsulated laser was studied using the Streak Camera. The excitation laser used was the 50 kHz output of the Spitfire frequency doubled to 400 nm. The experimental setup was identical to Figure 5.6 for the earlier experiment except the sample is not in the vacuum chamber. The laser dynamics of the encapsulated laser are shown in Figure 5.12 with the emission centred at 621nm.

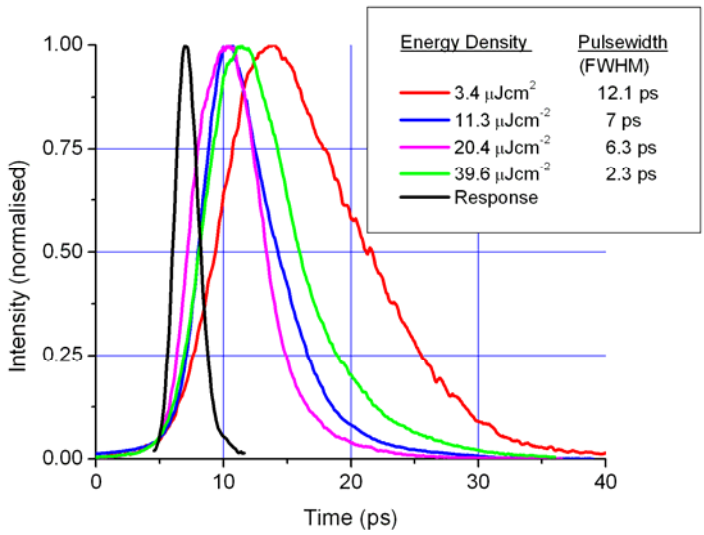

Figure 5.12 – Encapsulated laser dynamics

The pulse widths observed for the encapsulated lasers shows that lasing threshold was ~ 3.4 μJcm^{-2} and the laser pulse had a 12.1 ps duration The recorded emission was very weak at threshold and no emission could be captured below the lasing threshold. The weak emission is likely due to the grating structure only being ~30 nm deep meaning the interaction of the Bragg scattering is much weaker thus less efficient. At threshold the pulse width is just above 12 ps wide and this reduces to 6.3 ps at ~ 6 times the threshold (20.4 μJcm^{-2}). When the excitation density was further increased to ~ 40 μJcm^{-2} the pulse width was seen to broaden slightly. The response was again ~2 ps and thus the response function did no limit the experimental resolution.

The equations described in Section 5.4.1.1 was used to model this emission although there were a few changes to the parameters used. The pulsewidths recorded were longer than those seen previously using the quartz substrate grating structures and this can be attributed to the less efficient Bragg scattering which can be modelled by decreasing the light confinement factor Γ to 0.3. Another likely scenario is that the encapsulation used was not perfect and thus some quenching occurred via air left within the device after encapsulation or entered during the experiment. The encapsulated lasers worked for several days without degradation in the output and so the more likely case is for air trapped within the device. This would mean that photoinduced absorption is likely to play a larger part in the gain region and this would lead to a reduction in the stimulated

emission by reducing the available upper state population. The best agreement was found by reducing N(0) by a factor of 4.

The model however does not reproduce the broadening of the pulsewidth at very high excitation densities. The cavities found within a DFB structure are usually of the order of 150 μm in length [Barlow] but as the Bragg scattering is not as good for shallower grating structures the emission inside the excited area could travel outwards and set up a second cavity on the edge of the first cavity, this could lead to gain competition between the cavities. Another potential broadening mechanism is the onset of independent single grating lasing [30,35) which has a lower spectral and spatial coherence compared to the two-dimensional laser mode structure.

In order to further study the encapsulated lasers an attempt was made to measure the dynamics in the up-conversion setup. No measurements were recorded successfully as the laser emission degraded in less than 10 seconds which was insufficient time to perform a scan. The reason behind this is unclear, the excitation energies used were slightly higher than for the streak camera observations although the onset of lasing was at a similar excitation density compared to the shortest pulsewidth measured for the streak camera (20 μJcm^{-2}). Potentially imperfect encapsulation could explain this but as the devices worked in the streak camera this is unlikely. The higher pump energies most likely caused photodegradataion in the polymer film when focussed tightly.

5.6 Conclusion

The temporal dynamics of two-dimensional distributed feedback polymer lasers have been studied here and have been shown to be able to support ultrashort pulse generation. The pulsewidths observed shorten in pulsewidth from a longer lifetime below threshold to the shortest possible pulsewidth significantly above threshold. Using a combination of streak camera data and femtosecond up-conversion results the dynamics were studied from the MEH-PPV lifetime at very low thresholds down to the shortest measured pulse of 410 fs. This is to our knowledge the first study of the dynamics of a

conjugated polymer laser culminating in the shortest reported pulsewidth in a gain-switched conjugated polymer laser of 410 fs.

The results observed were modelled using a simple rate equation model based on the growth of amplified spontaneous emission which implied a stimulated emission cross-section of $\sigma_{SE} = 3x10^{-16}cm^{-1}$ which is comparable to other values reported for similar conjugated polymers.

Further studies of a novel encapsulated conjugated polymer laser device exhibited longer pulsewidths of 6 ps but still demonstrated the potential for ultrashort pulses in these easily fabricated structures.

These results show that MEH-PPV gain-switched lasers can support ultrashort pulse generation and potentially opens the path to modelocking in conjugated polymer lasers.

References for Chapter 5

[1] N. Tessler, *Advanced Materials*. **11**, 363 (1999)

[2] M. D. McGehee, A. J. Heeger. *Advanced Materials*, **12**, 1655, (2000).

[3] C. Kallinger, M. Hilmer, A. Haugeneder, M. Perner,W. Spirkl, U. Lemmer, J. Feldman, U. Scherf, K. Müllen, A. Gombert, V. Wittwer, *Advanced Materials* **10**, 920 (1998)

[4] S. Riechel, C. Kallinger, U. Lemmer, J. Feldmann, K. Gombert, V. Wittwer, and U. Scherf, *Applied Physics Letters*, **77**, 2310 (2000)

[5] G. A. Turnbull, T. F. Krauss, W. L. Barnes, and I. D. W. Samuel, *Synthetic Metals*, **121**, 1759 (2001)

[6] G. A. Turnbull, P. Andrew, W. L. Barnes, I. D. W. Samuel, *Physical Review B*, **64**, 125122 (2001)

[7] C. Bauer, H. Giessen, B. Schnabel, E.-B. Kley, C. Schmitt, U. Scherf, and R. F. Mahrt, *Advanced Materials*, **13**, 1161 (2001)

[8] W. Holzer, A. Penzkofer, T. Pertsch, N. Danz, A. Brauer, E. B. Kley, H. Tillmann, C. Bader, H.-H. Horhold, *Applied Physics B*,. **74**, 333 (2002)

[9] G. A. Turnbull, T. F. Krauss, W. L. Barnes, and I. D. W. Samuel, *Synthetic Metals*, **121**, 1759 (2001)

[10] R. Xia, G. Heliotis, P.N. Stavrinou, DDC Bradley, Applied Physics Letters, **87**,031104 (2005)

[11] Khoe G D, *IEEE J. Sel. Top. Quantum Electron.* **6**, 1265-1272 (2000).

[12] Monroy T I *et al. Opt. Fiber Technology,* **9**, 159-171 (2003).

[13] J. R. Lawrence, G. A. Turnbull, I. D.W. Samuel, Applied Physics Letters **80**, 3036 (2002).

[14] McBranch DW, Sinclair MB, *Primary Photoexcitations in Conjugated Polymers*, Chapter 20,. World Scientific Publishing Co, (1997)

[15] F. Hide, M. A. Diaz-Garcia, B. J. Schwartz, M. R. Andersson, Q. Pei, and A. J. Heeger. *Science*, **273**, 1833, (1996).

[16] A. K. Sheridan, G. A. Turnbull, A. N. Safonov, and I. D. W. Samuel. *Physical Review B*, **62**, 929, (2000).

[17] D. Moses, Appl. Phys. Lett. **60**, 3215 (1992).

[18] T. Pauck, R. Hennig, M. Perner, et al., Chem. Phys. Lett. **244**,171 (1995).

[19] M. Yan, L. J. Rothberg, E. W. Kwock, and T. M. Miller, *Interchain excitations in conjugated polymers*, Phys. Rev. Lett. **75**, 1992 (1995).

[20] M. Yan, L.J. Rothberg, F. Papadimitrakopoulos et al, Physical Review Letters, 72, 1104 (1994)

[21] N. Tessler, G. J. Denton, and R. H. Friend, , Nature **382**, 695 (1996).

[22] Tsutui T, Takada N, Saito S, Ogino E, *Applied Physics Letters*, **65**, 1868 (1994)

[23] Lidzey DG, Pate MA, Whittaker DM, Bradley DDC, Weaver MS, Fisher TA, Skolnick MS, *Chemical Physics Letters*, **263**, 655 (1996)

[24] Kaminow IP, Weber HP, CHandross EA, Applied *Physics Letters*, **22**, 497 (1971)

[25] Virgilil T, Lidezey DG, Grell M, Bradley DDC, Stagira S, Zavelani-Rossi M, de Silverstri S, *Applied Physics Letters*, **80**, 4088 (2002)

[26] CV Shank, JE Bjorkholm, H Kogelnik, Applied Physics Letters, 18, 395 (1971)

[27] M. D. McGehee, M. A. Diaz-Garcia, F. Hide, R. Gupta, E. K. Miller, D. Moses, A. J. Heeger, Applied Physics Letters, **72**, 1536 (1998)

[28] GA Turnbull, P Andrew, WL Barnes, IDW Samuel, *Applied Physics Letters*, **82**, 313 (2003)

[29] Riechel S, Kallinger C, Lemmer U, Feldmann J, Gomber A, Wittwer V, Scherf U, *Applied Physics Letters*, **77**, 2130 (2000)

[30] GA. Turnbull, P. Andrew, M. J. Jory, W. L. Barnes, and I. D. W. Samuel, Physical Review B **64**, 125122 (2001)

[31] G Heliotis, SA Choulis, G Itskos, R Xia, R Murray, PN Stavrinou, DDC Bradley, *Applied Physics Letters*,**88,** 081104 (2006)

[32] AE Vasdekis, GA Turnbull, IDW Samuel, P Andrew, WL Barnes, *Applied Physics Letters*, **86**, 161102 (2005)

[33] Stagira S, Zavelani-Rossi M, Nisoli M, DeSilvestri S, Lanzani G, Zenc C, Mataloni P, Leising G, Applied Physics Letters, 73, 2860 (1998)

[34] van den Berg SA, 't Hooft GW, Eliel ER, Physical Review A, 63,063809 (2001)

[35] Kallinger C, Riechel S, Holderer O, Lemmer U, Feldmann J, Berleb S, Muckl AD, Brutting WJ, *Journal of Applied Physics* , **91**, 6367 (2002)

[36] Lee CW, Wong KS, Huang JD, Frolov SV, Vardeny ZV, *Chemical Physics Letters*, **314**, 564 (1999)

[37] Koschorreck M, Gehlhaar R, Lyssenko VG, SWoboda M, Hoffmann M, Leo K, *Applied Physics Letters*, **87**, 181108 (2005)

[38] Hayes GR, Samuel IDW, Phillips RT, *Physical Review B*, **52**, 11569 (1995)

[39] G Barlow and A. Shore private communication

[40] Holzer W, Penzkofer A, Schmitt T, Hartmann A, Bader C, Tillmann H, Raabe D, Stockman R, Horhold HH, *Optical Quantum Electronics*, **3**3, 121 (2001)

[41] Lawrence JR, Turnbull GA, Samuel IDW, *Applied Physics Letters*, **82,** (2003)

[47] GA. Turnbull, P. Andrew, M. J. Jory, W. L. Barnes, and I. D. W. Samuel, Phys. Rev. B **64**, 125122 (2001).

Chapter 6

Conjugated Polymer Amplifiers

6.1 Introduction

The recent advances in organic lasers (as seen in Chapter 5) have demonstrated that the emission from these laser devices is compatible with polymer optical fibre (POF) based communication networks. This technology is seen as a viable low-cost platform for use in improved performance in local area networks [1] as the transmission wavelength range for POF based networks overlaps with the emission wavelengths of conjugated polymer lasers. However, losses are not as low as those for the telecommunication wavelengths in silica fibres. The useful range of these networks depends on the distance the signal can travel before transmission and splitting losses inherent in the network deteriorate the signal. An amplifier device that boosts the signal at certain stages along the network is thus required.

In modern communications the signal is boosted by devices such as the Erbium Dope Amplifier (EDFA) and inorganic Semiconductor Optical Amplifiers (SOA's). They compensate for the losses in the silica fibre network and enable signal regeneration, wavelength selection and conversion as well as all-optical switching to occur. Conjugated polymers have demonstrated high optical gain over a broad spectral range in the visible spectrum [2-6] and as such could be used as a broadband gain material for an optical amplifier for POF based networks or passive planar light wave circuit technology [7-11].

With the rapid increase of data-communications, direct to the individual user, silica-based optical systems are struggling to provide low-cost, high performance networks. In this increasingly-competitive market, polymer technology is considered an interesting low-cost alternative with simple processing properties. Combined with cheap and importantly low-loss polymer optical fibres, such as polymethylmethacrylate

(PMMA) [7,8], lasers and amplifier devices based on conjugated polymers have become an area of much interest.

Another area in which conjugated polymer based devices are being considered as a technological route are in personal area networks (PANs), such as those found in automobiles. At present the automotive industry utilizes the 650 nm low loss window of PMMA fibres in its MOST and Byteflight protocols [12]. Easier installation (alignment) and maintenance of visible wavelength devices are also substantial benefits of the technology.

A major advantage of conjugated polymers is their solubility in a wide range of solvents. By dissolving the material in an appropriate solvent, the solution can be easily processed, for example by spin-coating, inkjet printing or micromoulding [13-15] making mass fabrication a real prospect. The presence of gain in conjugated polymers has been established, by transient absorption [2-4] and lasing [16-18]. Optical amplification in a conjugated polymer device, where an input signal is amplified via stimulated emission within an optically pumped gain volume before being emitted as a higher intensity pulse, has thus far only been reported in a dilute solution [19]. Although dye doped polymer fibres and rib waveguide structures have recently been investigated as amplifiers [20-25], light-emitting conjugated polymers offer several potential advantages. Unlike small organic chromophores, conjugated polymers exhibit little concentration quenching, allowing high chromophore densities to be used. Solid state films from conjugated polymers also have the potential for electrical excitation [16,17] by exploiting similar technology to OLEDs. So far however there has been no known report of a practical solid-state conjugated polymer optical amplifier device.

6.2 Broadband Conjugated Polymer Optical Amplifiers

The mechanism for gain in conjugated polymers was discussed earlier in Chapter 2.3. For optical amplification to occur, a photon has to travel through a gain medium which has been excited to supply gain via a population inversion. The methods available for studying these processes depend on the device structure of the optical amplifier.

Conjugated polymers can be studied in solution and as thin films but due the differences in the two states with respect to distances between polymer chains and rigidity of the polymer chain (in solution it can twist freely compared to the solid-state) the gain properties will also differ. Whether in solution or in the solid-state, conjugated polymers are optically pumped to create a sufficiently large population inversion to exhibit gain via stimulated emission.

In order to study gain in a polymer solution the sample is placed in a quartz cuvette. Gain is only observed if the input signal and the pump beam are overlapped or no gain would be available to the signal. In the solid state, polymer thin films are generally no more than a few hundred nanometers thick. Overlapping the signal and pump beams in solution is more readily achieved as the thin polymer films create only a small volume in which to overlap the beams and access the gain of the material. Thin polymer films are also amorphous in nature and cleaving does not produce well defined edges as are seen in inorganic structures. Edge-coupling of light to obtain a larger overlap volume for the gain is thus almost impossible due to ragged nature of the polymer film edge. As the direct overlap of the input and pump beams is difficult to achieve with thin films, gain measurements are generally performed using the gain-stripe method described in Chapter 5.2. This is not an ideal geometry for an amplifier device as there is no external input signal, as the probe beam is produced via spontaneous emission generated by the pumping of the polymer film. For a practical solid-state amplifier an input signal must be guided into and out of the gain region.

In this work, polymer amplifiers were first studied using a solution amplifier and later work on a novel solid state geometry was performed. The research into broadband optical amplifiers was performed as part of the Ultrafast Photonics Collaboration [26]. This collaboration between various research institutes and industrial partners has as one of its aims the increased cooperation between different research groups in order to better utilize the different resources available at its member institutions. Part of this work was performed in collaboration with the Experimental Solid State Physics (ESSP) Group at Imperial College London. Novel gain materials were provided by the ESSP and were studied at the experimental facilities of the Organic Semiconductor Centre (University of St Andrews). The coupling grating structures of the solid state amplifier were fabricated by Dr William Whelan-Curtin and Andreas Vasdekis at the Microphotonics and Photonic

Crystals Research Laboratories at the University of St Andrews. The discussion on the optimization of the gain materials has been provided by Dr George Heliotis who has studied these materials in depth along with Dr Ruidong Xia and Dr Yanbing Hou. The measurements of the F8BT and RedF/F8BT materials were performed with the assistance of Dr George Heliotis.

This Chapter will first review the first reported optical amplification in a conjugated polymer [19] before outlining work on a solution optical amplifier using poly(9,9-dioctylfluorene-*co*-benzothiadiazole) (F8BT) as a gain material. Further work to realize a solid-state optical amplifier device is then discussed with improvements in device geometries and tailored gain material properties via blending of the proprietary RedF (Dow Chemical) material with F8BT. Solid-state amplification in a device with an input and output coupler is demonstrated with gain as high as 18 dB with a 300 μm long gain channel between the couplers. Further comparison work using MEH-PPV as a gain material is then outlined which exhibited a maximum gain of 21 dB in a 1mm long gain channel.

6.3 Solution Optical Amplifiers

Optical amplification in solution can be probed using the experimental setup described in Chapter 3.5. The use of a tuneable dye laser allows the conjugated polymer solution to be probed for gain over a broad wavelength range.

This technique was used to measure the first polymer solution amplifier [19]. In this first demonstration the solution amplifier was based on the conjugated polymer, poly-(2-methoxy-5-(3',7'-dimethyloctyloxy)-paraphenylene-vinylene (OC_1C_{10}-PPV). Gain was measured as high as 43 dB inside the 1cm cuvette. Gain curves were recorded with a gain higher than 30 dB available over a 70 dB range. The gain was found to depend on the concentration of the dilute solution.

This concentration dependence was explained by a combination of two mechanisms. For lower concentrations the pump beam is thought to be too weakly

absorbed to produce a sufficient excitation density necessary for significant gain to take place. For higher concentrations the pump beam is absorbed too strongly in the first few millimetres of the cuvette and this leads to a poor overlap with probe beam. Concentration quenching is not thought to contribute as substantial gain has been seen in undiluted solid-state materials [27].

The broad gain seen in this simple experiment demonstrated the potential for polymer broadband amplifiers. The solution amplifier measurement is a useful way of measuring the broadband gain obtainable in potential materials. Considering that no broadband gain had been reported since the initial solution amplifier an investigation into a novel gain material was undertaken.

6.3.1 F8BT Solution Optical Amplifier

In recent years a new family of conjugated polymers known as polyfluorenes have been studied [28,29] which exhibit gain across the visible spectrum. In order to test whether these materials would be suited as broadband optical amplifiers, two related materials were studied. These two proprietary materials were provided by Dow Chemical and were Lumation F8BT and RedF. The structure of the green-emitting poly(9,9-dioctylfluorene-*co*-benzothiadiazole) Lumation F8BT is shown in Figure 6.1. No structure has been made publicly available for the proprietary RedF but it is known to have F8BT incorporated into the chain together with a red chromophore, Figure 6.4 illustrates the absorption and emission spectra of F8BT.

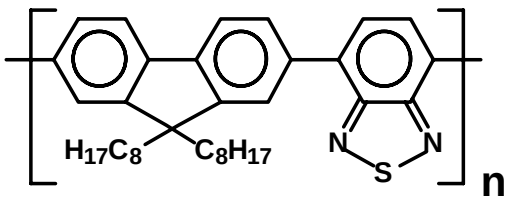

Figure 6.1 - Molecular structure of F8BT

As can be seen in Figure 4 there is a distinct overlap of the spectra of these materials suggesting that the RedF that much of the absorption of the RedF co-polymer is due to F8BT and transfers energy from the F8BT to an unidentified red chromophore for emission. Both materials exhibit high absorption peaks at ~ 337nm providing a good match to the pump laser of the solution amplifier setup.

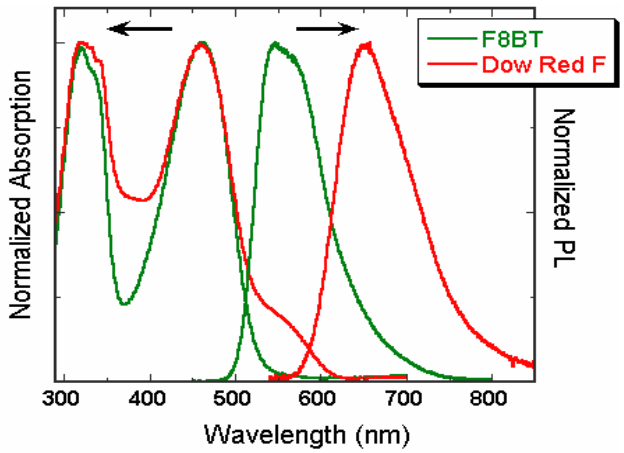

Figure 6.2: Absorption and Emission Spectra of Dow RedF and F8BT
(provided courtesy of Dr G. Heliotis, Imperial College)

In the solution amplifier setup as described in Chapter 3.5 uses nitrogen pumped tuneable dye laser. This allows a broad range of wavelengths to be studied using different dyes. A pump beam at 337 nm is split into two and excites the solution as well as a dye solution whose emission us tuned to the desired wavelength using gratings.

The F8BT solution amplifier was probed between 535 nm and 585 nm. As a concentration dependence of the gain was reported previously [19] various concentrations were studied. Figure 6.3 illustrates the gain curves recorded between 535 nm and 585nm for dilute concentrations of F8BT of 1.5 - 5 mg/ml.

F8BT exhibited gain from 535 nm to 585 nm, the omission of data in the 8nm gap between 562 nm and 570 nm was due to the lack of appropriate laser dye available to cover this probe beam wavelength range. At a high concentration of 5 mg/ml a gain of 15-25 was observed, as the concentration is decreased the gain at first increases with gain

over 30 dB recorded across a wide range for a 3 mg/ml solution. A further dilution of the sample to 1.5 mg/ml significantly reduced the observed gain to ~10 dB. This is attributed to the concentration dependence discussed previously.

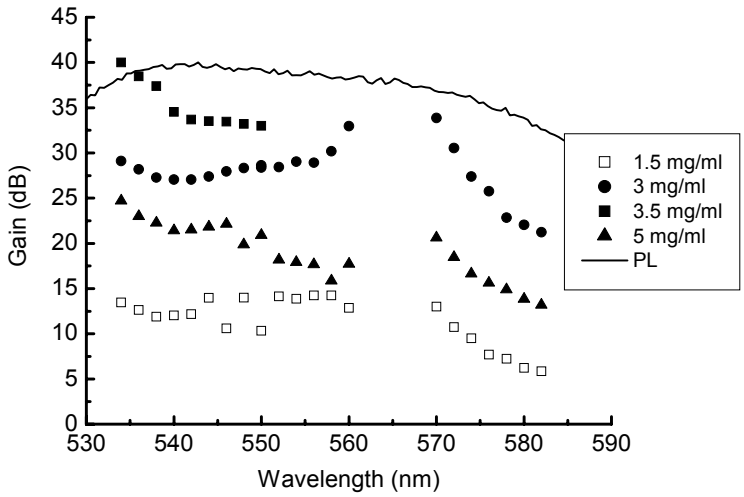

Figure 6.3: The gain spectra for a range of F8BT solution concentrations. The photoluminescence spectrum is overlaid as a reference.

Gain of up to 40 dB was measured in the 3.5 mg/l solution (data for this concentration was initially only recorded up to 550 nm later measurements were precluded due to limited sample supply) and as can be seen for the 3 mg/ml concentration the observed gain is ~ 30 dB or above from 535 nm to 570nm.

In this experiment the effect of the gain was also observed by capturing the amplified output using a CCD detection system. Figure 6.4 illustrates the probe beam amplification at a wavelength of 537nm. The top panel illustrates the probe signal passing through the F8BT solution with no pump exciting the gain region. The polymer chains are thus mainly in their ground state and so there is very little interaction between the probe and the solution (aside from some small losses attributed mainly to absorption and reflection). This is because the absorption of the input probe wavelength in the F8BT is almost negligible [28,29]. When the solution is optically pumped stimulated emission leads to a gain region through which the probe beam passes and is amplified by a factor

of 3460, corresponding to a gain of 35.4dB/cm. The bottom panel shows the polymer emission spectrum when there is no probe beam present.

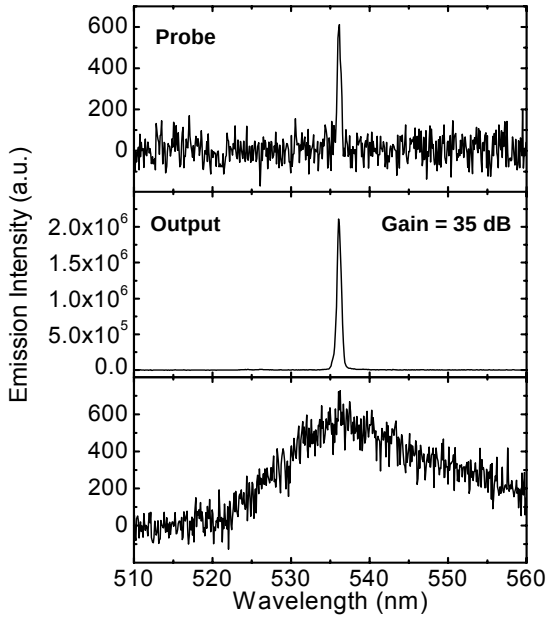

Figure 6.4: Top: Probe pulse before amplification. Middle: probe pulse after amplification Bottom: photoluminescence spectrum of F8BT.

The gain of the 3 mg/ml amplifier solution was also studied as a function of the probe energy and the results are shown in Figure 7. The energy of the probe beam, at 543nm, is increased from 0.5 nJ to 1 μJ and the gain is seen to substantially decrease from its peak value of ~29 dB cm^{-1} due to the influence of gain saturation. This is a common amplifier property and is caused by a strong probe beam extracting a significant fraction of the stored excitations. The theoretical fit in Figure 6.5 is modeled using the expression for a homogeneously-saturated pulsed amplifier [30].

$$E_{OUT} = E_S \ln\left[1+\exp\left(\frac{E_{IN}}{E_S}-1\right)\exp(G)\right] \qquad \text{(Equation 6.1)}$$

E_{OUT} is the energy extracted from the amplifier, E_{IN} is the input probe energy, G is the small signal gain coefficient and E_S is the saturation energy. Using Equation 1 a theoretical fit is found to match the behaviour of the optical amplifier and obtain a small

signal gain G = 28.4 ± 0.6 dB at λ = 543 nm and a saturation energy of ~ 636 nJ (indicated by the dashed line in Figure 6.5), corresponding to an energy density of 2.12 mJ/cm^2.

The amplification in conjugated polymers is obtained from stimulated emission from a four level laser system comparable to that described for organic laser dyes [30,31]. The stimulated emission cross-section σ_{SE} can then be determined from Equation 6.2 for the gain coefficient.

$$G = \sigma_{SE} N_{ex} l \qquad \{\text{Equation 6.2}\}$$

Where N_{ex} is the excitation density and l is the length of the amplifier. From this the F8BT stimulated emission cross-section is found to be σ_{se} = 1.7 ± 0.1 x 10^{-16} cm^2.

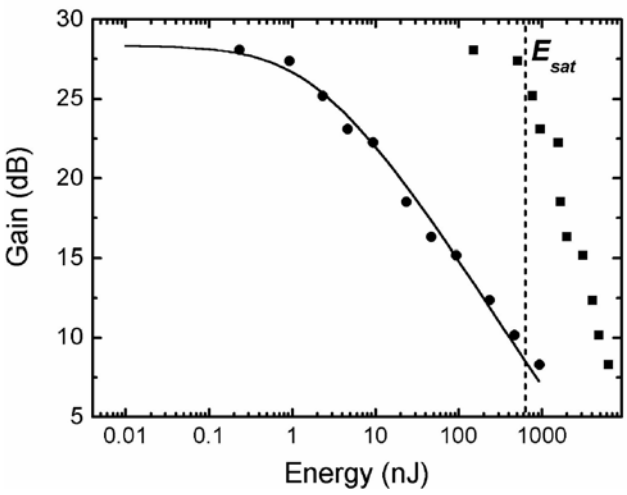

Figure 6.5: Gain Saturation curve of the 3 mg/ml sample. The solid line is a theoretical fit using Equation 6.1. The dashed line illustrates the saturation energy.

This value is comparable with those reported for polyparaphenylenevinylene, PPV (1 x 10^{-16} cm^2) [32], a range of dialkoxy and dialkyl substituted phenylenevinylene and phenylene-ethynylene polymers (≤ 2 x 10^{-16} cm^2) [33] and established laser dyes such as Rhodamine 6G and pyrromethene 650 (≤ 3 x 10^{-16} cm^2) [22]. The value is slightly less than estimated from amplified spontaneous emission measurements [28] in F8BT solid films. But in a solid film there is a higher density of chromophores and this could easily lead to a higher stimulated emission cross-section.

Figure 6.5 also illustrates the F8BT solution amplifier gain as a function of output energy (solid squares). As expected, the amplifier gain drops to half of its initial small-signal value (i.e. $G = G_0 - 3$ dB) when the output signal becomes equal to the saturation energy. Then using Equation 6.2 we can calculate an excitation density of ~3.8×10^{16} cm^{-3} for the 3 mg/ml F8BT solution.

The saturation energy can then be used to obtain an estimate of the stimulated emission cross-section σ_{se} of 3.8 x10^{-16} cm^{-2} which agrees well with values reported for poly(p-phenylenevinylene) (PPV) of 1×10^{-16} cm^{-2} [6] and OC_1C_{10}-PPV 5.3×10^{-17} cm^{-2} [19].

Thus the potential for polymer materials for future broadband optical amplifier devices has been established across over 100 nm (~ 90 THz) range from 535-640 nm with a gain of approximately 30 dB across this spectrum, using two different polymers as demonstrated in Figure 6.6.

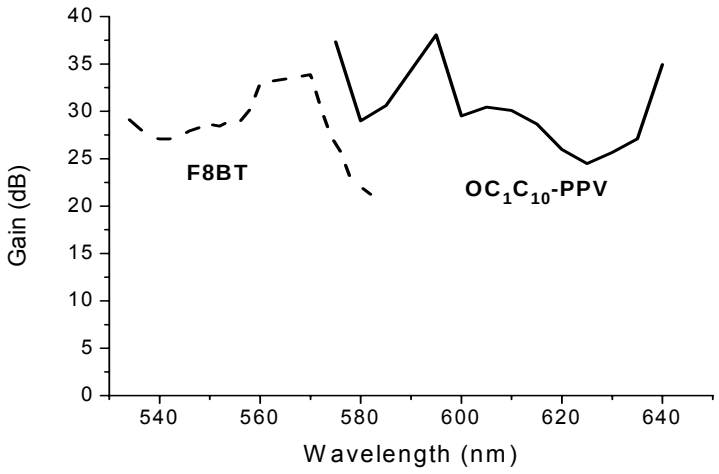

Figure 6.6: The gain curves for 3 mg/ml F8BT and 2 mg/ml OC_1C_{10}-PPV (data taken from [19])

Another material that was studied was RedF mentioned before. This is a proprietary chemical from Dow Chemicals which has demonstrated high gain in previous work [21-22]. In the solution amplifier experiment no amplification was measured in solutions of RedF using this solution amplifier technique. A likely explanation is that the absorption at 337 nm is not efficiently transferred along the chain. Even though F8BT makes up part of the RedF chain and acts as an absorbing species in this chemical the

gain could not be accessed. Any excitation at 337 nm is unlikely to be easily internally transferred via energy migration to the red chromophore and this can explain the lack of gain measured in this experiment

6.4 Solid State Amplifiers

Solution based gain is a useful tool for studying material gain properties but a solid state device would be much more useful. The next challenge once gain has been demonstrated in solution is to access this gain in the solid state. Measurements of gain in solid state organic semiconductors have previously been reported based on transient absorption measurements through sub-micron thick films, or indirectly over longer path-lengths via amplified spontaneous emission (ASE). These measurements so far have not provided any control over the probe signal. Measurements through a thin film cannot extract significant gain from the small volume the probe signal interacts with and the ASE studies use a produced by spontaneous emission. In order to successfully demonstrate gain in a device the probe signal has to be controlled into and out of the gain region. An amplifier device with input and output coupled light has as yet not been demonstrated using conjugated polymers.

6.4.1 Input and Output Couplers

For an optical amplifier device to operate the probe beam must interact with an excited region. In inorganic semiconductor amplifiers the layers can be easily cleaved leading to well defined facets which mean that optical input in devices such as ridge waveguides is easily input coupled. Organic materials deposited on substrates are not easily cleaved due to their amorphous nature and thus input coupling is an issue with these devices.

In order to couple a probe beam into and out of a polymer thin film the system used in this work uses Bragg gratings, similar to the laser gratings in Chapter 5, to couple a probe beam into a waveguide through a gain region and then couple it out. The grating period defines the angle at which a wavelength is coupled into the waveguide. In a DFB laser the grating provides feedback as well as the output coupling, here the gratings are

only illuminated with the probe signal and so no lasing occurs on the grating structures. The schematic of the amplifier gratings is shown in Figure 6.7.

The amplifier unit consists of one input coupler and one output coupler with a waveguide area between them where an optical pump can excite the polymer film as the probe beam passes through, thus providing a gain region. Different distances between input and output couplers were produced to investigate gain changes over different distances or probe propagation. The output coupler grating axes are angled ~ 20^0 with respect to the input coupler in order to avoid feedback (and hence lasing) between these two gratings which was seen in earlier work, it also spatially separated the amplified signal from any surface reflections present.

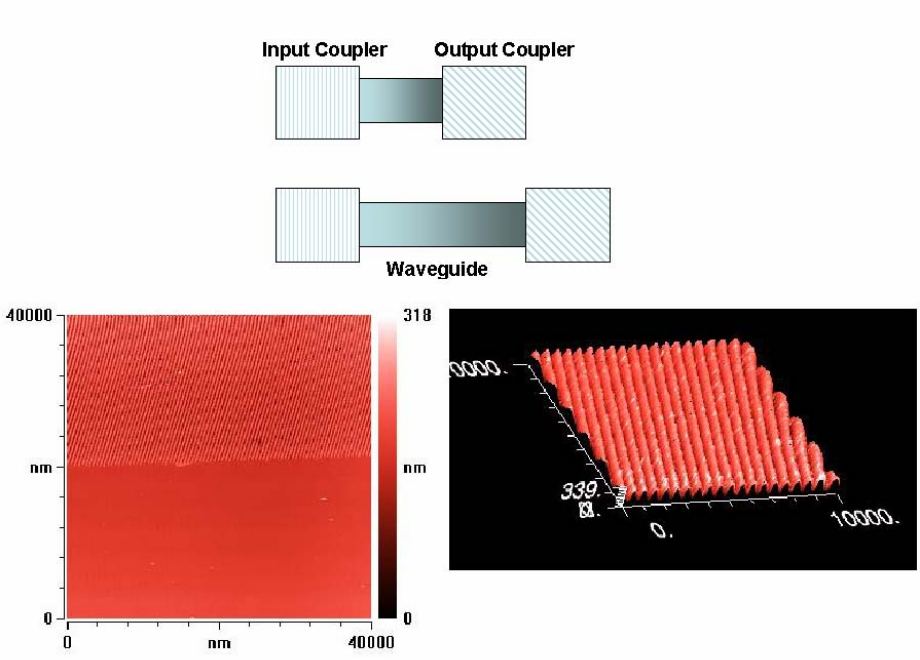

Figure 6.7 – Top: Input and output gratings were produced with different channel lengths Bottom: AFM images of the grating structures.

The optical amplifier is created by spin-coating a polymer thin film on top of a silica substrate with the grating structures fabricated on it. To create the coupler on the silica substrate a film of PMMA is deposited on the substrate and the coupler gratings are defined by electron beam lithography in this film. The pattern is then transferred to the substrate using reactive ion etching (RIE). The patterns created can be seen in the bottom panel of Figure 6.7 in an Atomic Force Microscope (AFM) image.

Figure 6.8 shows a schematic of one semiconducting polymer optical amplifier. The amplifiers comprise a thin (~ 120 nm thick) conjugated polymer blend film spin-coated on a silica substrate on the input and output Bragg gratings that are designed to couple the signal to/from the fundamental TE (transverse electric) propagating mode of the waveguide structure. For an optical amplifier, it is necessary to ensure that laser oscillation does not occur, as this depletes the inverted population that is needed to amplify the signal. The grating couplers can in principle also act as individual DFB laser structures (this was dealt with by avoiding direct pumping of the grating areas) or as feedback mirrors for light propagating in the film plane. The gratings were fabricated with dissimilar periods to avoid feedback of the same wavelengths across the waveguide and act as a laser, thus depleting the gain available. In this experiment, the grating periods were $\Lambda_1 = 440$ nm for the input and $\Lambda_2 = 480$ nm for the output-coupler, as these gratinigs provided the best coupling characteristics and were chosen to couple in the probe at a slight angle from normal and the difference between the grating periods is to ensure no feedback between the gratings. The input coupler grating period is offset from the resonance condition for the wavelength of coupling in the probe using Bragg scattering in the grating. Although the input coupler efficiency is thus slightly reduced this was done intentionally to enable coupling at an angle from the normal as this is almost impossible in a vacuum chamber and the reflections caused by the windows and the substrate of the amplifier are problematic for detecting the output signal as well as interfering with the probe placement onto the grating coupler.

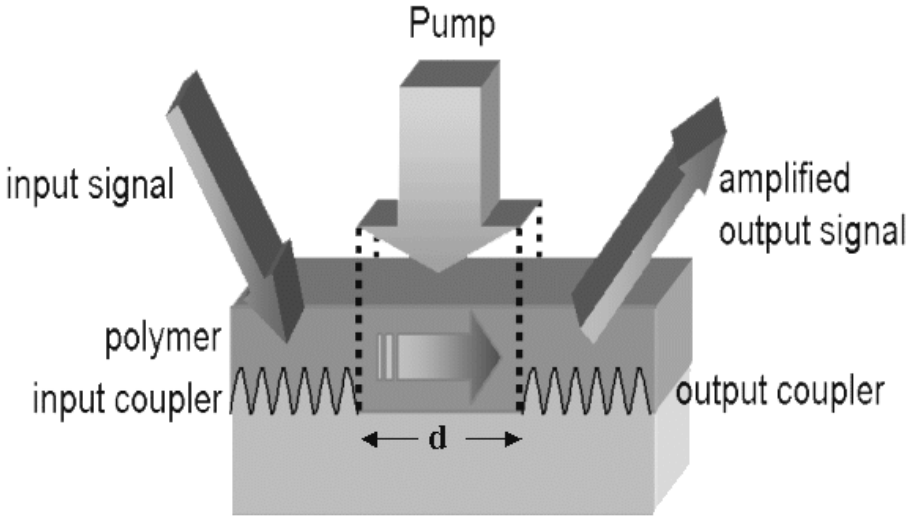

Figure 6.8 Schematic of the optical amplifier design

As Figure 6.8 illustrates, the weak input signal (λ_{signal} = 660 nm, 100 fs pulse duration and with adjustable intensity) was incident on the input coupler and after coupling via the first grating it propagated through the transversely pumped (λ_{pump} = 510 nm, 100 fs pulse duration, adjustable intensity) gain region. The resulting amplified signal was then coupled out by the second grating and its intensity monitored as a function of the input signal and transverse pump intensities. Amplifiers with three different gain lengths were studied. The spacing between the couplers were d = 100, 200 and 300 μm.

6.4.2 RedF/F8BT Gain Material

As mentioned earlier, a family of polyfluorenes, has been extensively studied [21,22] in terms of their electronic and optical properties. Two of these F8BT and RedF have been studied as solution amplifiers but only F8BT was found to amplify over a broad wavelength range. Work performed by our collaborators at Imperial College (Dr George Heliotis, Dr Ruidong Xia and Dr Yanbing Hou) found that the RedF exhibited high gain but that its gain could be accessed better by blending with F8BT [28]. Optical pumping as used for the solution amplifier setup at 337 nm is also not ideal as there are too many internal energy transfers before the excitation is transferred to an emissive site and the losses involved will restrict access to the available gain.

These two materials exhibit broad photoluminescence and gain spectra and a blend of two of these materials, F8BT and Dow RedF, provides a high net gain in the low-loss spectral window of PMMA fiber, (i.e. ~ 650 nm). Figure 6.9(a) shows the absorption and PL spectra for F8BT and Dow RedF. The shaded region highlights the spectral overlap between the absorption of Dow RedF and the emission of F8BT. Such an overlap is required for Förster energy transfer, which can enable strong gain in a region of low ground-state absorption in organic semiconductors. The energy transfer to longer

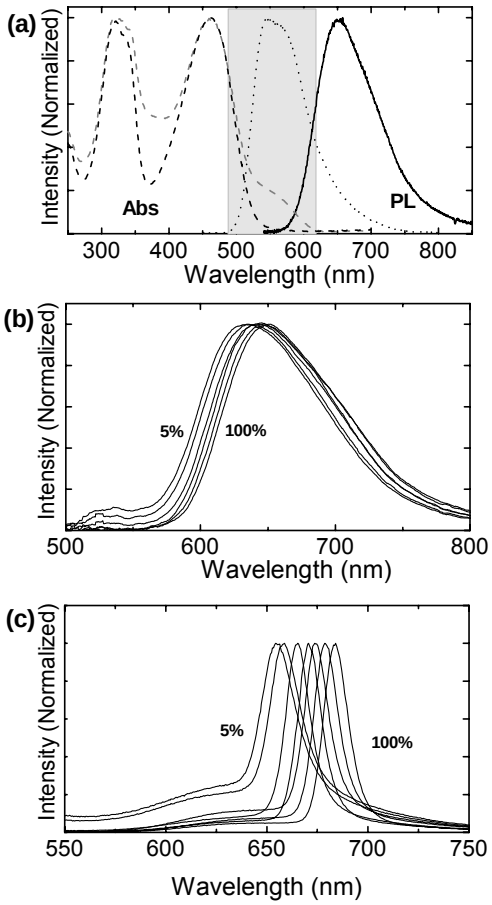

Figure 6.9: (a) The absorption and photoluminescence spectra of F8BT and Dow RedF (b) Normalized PL spectra for varying blend composition from 5% by weight to 100% Dow RedF with a 32nm peak shift between the extremes (c) ASE spectra [data provided by Dr George Heliotis]

wavelengths can in some cases lead to emission quenching due to charge separation but this is not the case for Dow RedF /F8BT blends [28].

Figure 6.9(b) shows the PL spectra of F8BT: Dow RedF blends as a function of RedF concentration. For blends of < 20% Dow RedF there is a small peak at 540 nm associated with F8BT emission which implies incomplete energy transfer at low dopant concentration. With increased concentration of Dow RedF, the peak of the PL is red-shifted by 32 nm. The corresponding ASE spectra in Figure 6.9(c) show a similar trend. Dilution of the Dow RedF places the emission peak into the wavelength region of low-loss PMMA fibers. The dilution also causes the photoluminescence quantum efficiency and excited state lifetime to increase, along with a decrease in the ASE threshold and

optical losses (2.8 cm^{-1} at 30% blend). The best overall characteristics were found in the 40% blend which was then selected as the gain material to be used for the solid state amplifier. The work in this section on the optimization of the gain material was performed by the ESSP group at Imperial College.

6.4.3 Experimental Setup

In order to investigate a solid state amplifier an input probe beam and a pump beam are required. The approach in this work was to use the femtosecond laser-amplifier facility to perform transient absorption measurements of the gain dynamics of the amplifier. This allow us to probe both overall gain as well as the obtain insights into the lifetime of the gain.

The 100 fs pump (510 nm) and probe (660 nm) pulses were produced at 5 kHz by the optical parametric amplifier (OPA), pumped by the Ti:Sapphire regenerative amplifier. The pump beam was attenuated with neutral density filters, and traveled via a delay line to be focused onto the polymer film in the channel between the output and input coupler to produce a gain region. For each channel length the pump area was changed to cover the entire area between the input/output gratings. The probe pulse was coupled into and out of the structure using the gratings and then detected by a photodiode. The pump beam was chopped at 2.5 kHz and synchronous detection of the probe was used (using lock-in amplifiers). Measurements were performed with the amplifier structures in a vacuum chamber at $5x10^{-5}$ mbar to prevent degradation of the polymer film due to contact with air or water.

The gain was determined by measuring the intensity of the signal at 660 nm after passing through the polymer amplifier when the pump beam was turned on, relative to the measurement performed when it was turned off. The data are corrected for the background photoluminescence emitted by the polymer when the pump was on (which can also be guide into the output coupler during excitation) measured in the absence of the probe signal.

6.4.3 RedF/F8BT Solid State Amplifier

Three different amplifier devices of varying channel lengths were studied. All three devices were found to amplify the probe pulse to some degree depending with the channel length. The gain was studied by varying the pump energy in order to probe the gain mechanism and effect of varying the channel lengths. The input probe energy was set to ~ 10 pJ and the corresponding amplification was measured as described before. Figure 6.13 demonstrates the gain curves for the three different length devices.

The observed gain versus pump intensity dependence is as expected from theory and is typically seen in inorganic semiconductor optical amplifiers (SOAs) [24]. In the three structures the gain rises with increasing pump intensity until gain limiting processes start to dominate. As Figure 6.10 shows, the three amplifiers have quite different characteristics: The gain rises faster with pump energy density and reaches much larger values as the channel length d increases. A maximum gain of 18 dB (similar to typical inorganic SOAs) was achieved with the d = 300 μm amplifier. The 200μm and 100μm amplifiers yielded maximum gains of 15dB and 6dB respectively.

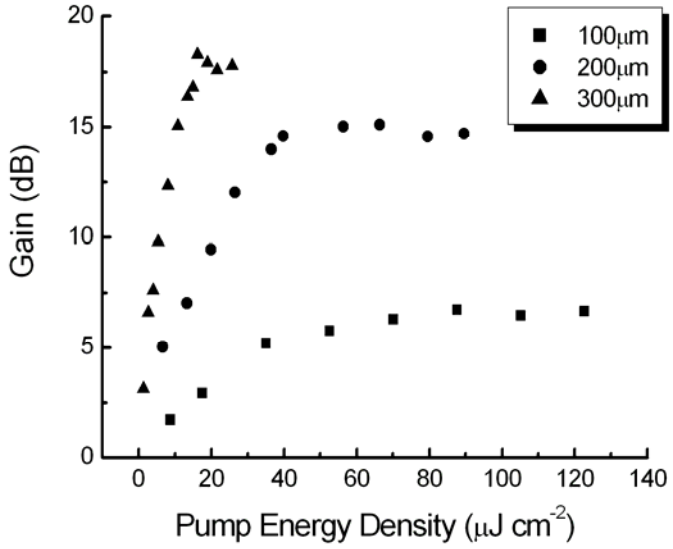

Figure 6.10: Variation of the amplifier gain as a function of pump energy density for the different polymer structures with device length s of (a) 100 μm, (b) 200 μm and (c) 300 μm.

Each of the curves in Figure 6.10 exhibits a gradual rise in the gain until gain limiting factors affect this rise causing a flattening of the. Gain limiting mechanisms can be gain saturation, ASE and exciton-exciton annihilation. Excitation densities above ~ 100 μJ/cm^2 for the 100 μm channel amplifier (Figure 6.10(a)) corresponds to a regime where the exciton density is sufficient to fully populate the red chromophore segments. The gain in this structure is thus limited by chromophore density, a conclusion supported by the observation that the background PL saturates at a similar excitation density. The results show further that saturation occurs at progressively lower pump energy density for the longer structures: This suggests that exciton-exciton annihilation or other intensity dependent processes cannot play the dominant role. Similar trends in the gain curves of inorganic SOAs are usually assigned to the faster onset of gain saturation and/or generation of ASE as the gain length increases, this is also believed to be present in these organic amplifier devices.

In an ideal amplifier the gain (in dB) at constant pump intensity should scale linearly with the channel length but this is not observed here. This is likely due to the data being acquired from three structures that possess differences in alignment, grating characteristics and/or polymer film quality. The creation of the grating structures in silica is not straightforward and this work was performed with gratings that were still being perfected in terms of quality (as can be seen by the ragged edge seen on the AFM image in the bottom panel of Figure 6.7). This affected particularly the grating coupling efficiency. For these RedF/F8BT amplifier structures the coupling efficiency was at best ~1% for these structures from measurements of the probe transmission. The study of these devices was limited in that no amplifiers were created with channel lengths longer than 300 μm.

The probe energy dependence of the gain was also studied and a typical curve is shown in Figure 6.11. This curve illustrates the typical gain saturation for an amplifier with channel length of 100μm. The data can be fit with Equation 6.1 and a probe saturation energy of 0.45nJ (1.8mJ/cm^2) is calculated. The good fit of the theory with experiment indicates the amplifier operates in a conventional way. Equation 6.2 can then

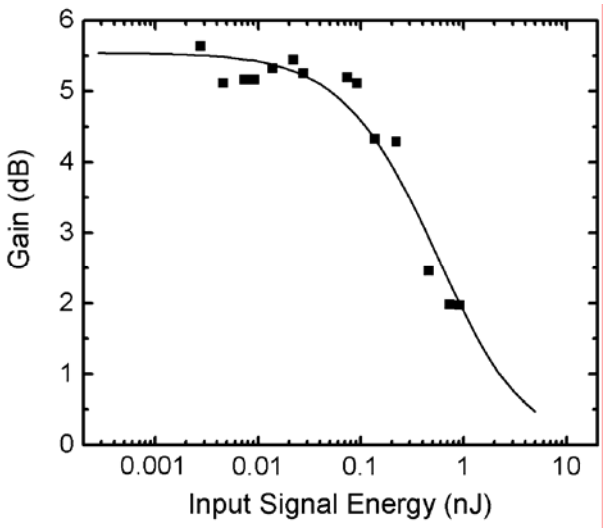

Figure 6.11: Gain saturation curve for the d = 100 μm amplifier. Experimental data (filled squares) are fit (solid line) to the expected theoretical dependence

be used to calculate the stimulated emission cross-section of the blend of $\sigma_{SE} = 2 \times 10^{-16}$ cm^2.

The use of the transient absorption experimental setup meant that the delay line on the optical pump arm could be used to find the temporal overlap of the pump and probe pulses (this had to be done due to the 100 fs pulses used). It also meant that it could be used to record the temporal response of the amplifiers. Figure 6.12 demonstrates a typical set of gain dynamics for the 300 μm channel. All the curves exhibit fast rise-times for the gain and the initial decay of the gain becomes faster with higher pump density. As the pump density increases ASE and exciton-exciton annihilation start to become important factors in the gain dynamics.

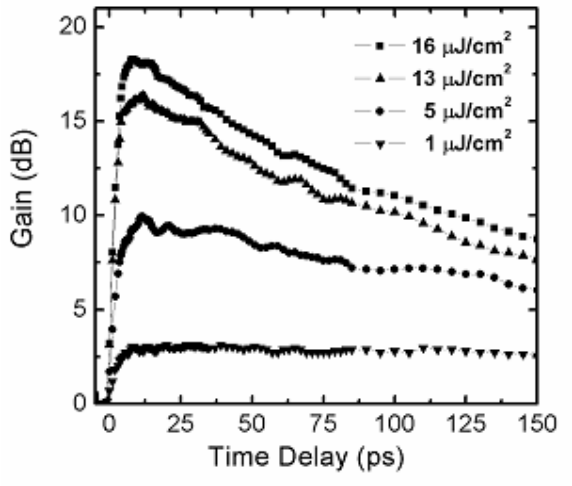

Figure 6.12: Gain dynamics for the 300 μm amplifier.

The temporal dynamics are useful to record the length of time gain is achievable but were also used to probe the mechanisms present in the amplifier.

This work is to date the first conjugated polymer amplifier device with structures for input and output demonstrating gain in the solid-state.

6.4.3.1 MEH-PPV Solid State Amplifier

In Chapter 5, MEH-PPV was used as a gain material for organic lasers and was shown to have high gain present as well as the ability to exhibit this gain over a sub-picosecond timescale. To further probe the possibilities of solid state optical amplifiers this material was chosen as a useful broadband emitter with known gain properties. It is also chemically very similar to OC_1C_{10}-PPV studied earlier as a solution amplifier.

The MEH-PPV (ADS 100RE) was dissolved in chlorobenzene and spin coated onto a substrate to form a thin film of ~100 nm. The input and output couplers were produced with much better success [35] leading to better coupling efficiencies. Transmission measurements were performed which determined a coupling efficiency of ~20% and waveguide losses of 60 cm^{-1} at 630 nm.

The MEH-PPV optical amplifier exhibited gain of up to 21 dB at 630 nm as well as ~15 dB at 615 nm and 650 nm demonstrating that high gain is available over a large gain region and in channel lengths of up to 1 mm. The available wavelength for probe beams were dependent on the output of the OPA and as such further wavelength where difficult to achieve without changing the pump wavelength.

This result demonstrates that these devices can readily supply high gain from conjugated polymers over distances as long as 1mm. The differences in the dynamics of when gain is available are due to material properties. Figure 6.16 shows the gain versus time for an amplifier device with a channel length of 622 μm. When compared to a similar device (shorter channel length of 30 0mm) for the RedF/F8BT blend shown in Figure 6.13 the gain is present for longer in the blend material (more than 150 ps) compared to the MEH-PPV amplifier where useful gain decays in roughly 50 ps. The time over which gain is present in a pulsed optical amplifier is very important because any jitter in the arrival of pulses may lead to a reduction in gain. Thus longer gain lifetimes are preferred. The mechanism responsible for the gain being present for longer is due to the energy transfer that occurs between the F8BT and the RedF and the associated lifetimes. The energy transfer in the blend compared to the energy transfer along the polymer chain means that exciton annihilation is more likely to inhibit gain in the MEH-PPV amplifier leading to faster gain decay.

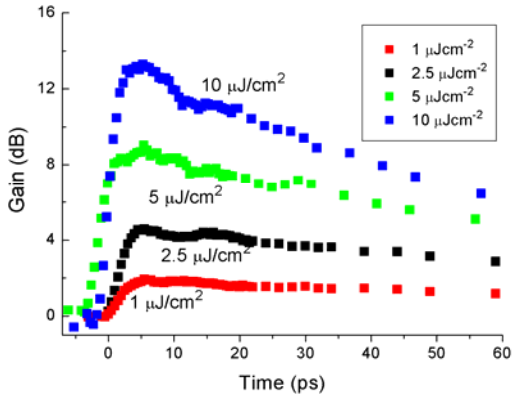

Figure 6.13- The observed gain plotted against the time delay between pump and signal pulses in a 622μm long wave guide.

The gain as a function of pump energy density for the 622 μm amplifier is shown in Figure 6.14. The gain curve is very similar to that of the 300 μm device of the RedF/F8BT blend with almost identical pump energy densities for the gain saturation and a value of the maximum gain which is only slightly higher.

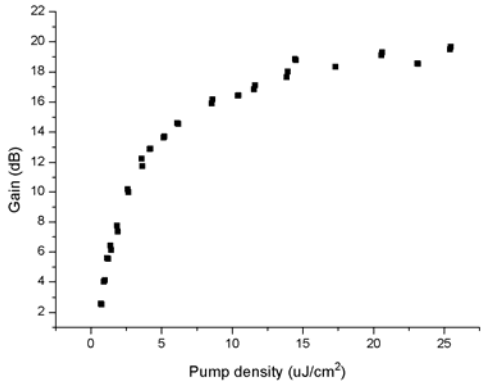

Figure 6.14 – Gain as a function of pump energy density of a 622μm long MEH-PPV amplifier device.

6.5 Conclusion

In this chapter the optical amplification in solution and solid-state organic optical amplifiers made from semiconducting polymers was demonstrated. In solution a a gain of ~ 30 dB was observed from 530 nm to 575 nm using the polyfluorene F8BT was observed.

A solid state RedF/F8BT optical amplifier device with input and output couplers has been demonstrated. A peak gain of 18 dB in a 300 μm channel length (at 660 nm) was observed A solid state optical amplifier based on the prototypical conjugated polymer MEH-PPV exhibited gain of 21dB in a 1 mm channel length (at 630nm). Gain at 615 nm and 650 nm in this amplifier were ~15dB once again demonstrating broadband amplification but this time in the steady state.

These results show that semiconducting polymers are very promising materials for optical amplification and are a natural extension of available semiconducting polymer optoelectronic devices. Such amplifiers are expected to have excellent compatibility with polymer optical fibre and polymer lightwave circuits, making them useful components for polymer photonics.

The time over which gain is available is also an important factor to be considered for devices. Ideally gain needs to be present for long enough (and at high enough values) to effectively amplify the optical pulse traveling through. This means that the longer lifetimes found in the blend are more suited to this application. Shorter gain lifetimes could lead to problems involved in pulse jitter if during operation a pulse is delayed by a few tens of picoseconds this may mean less amplification in the MEH-PPV amplifier. Longer gain lifetimes relax restrictions in pulse arrival and would be beneficial for potential devices.

References for Chapter 6

[1] Koike Y, Ishiguro T, Sato M, Nihei E. *Pure & Applied Optics*,**7**, 201(1998)

[2] M Yan, LJ Rothberg, F Papadimitrakopoulus, ME Galvin, TM Miller, *Physical review Letters*, **72**, 1104 (1994)

[3] BJ Schwartz, F Hide, MR Andreson, AJ Heeger, *Chemical Physics Letters*, **265**, 327 (1997)

[4] GJ Denton, N Tessler, NT Harrison, RH Friend, *Physical Review Letters*, **78**, 733 (1997)

[5] T Granlund, M Theander, M Berggren, M Andersson, A Ruseckas, V Sundstrom, G Bjork, M Granstrom, O Inganas, Chemical Physics Letters, 288, 879 (1998)

[6] AK Sherridan, GA Turnbull, AN Safanov, IDW Samuel, *Physical Review B*, **62**, 929 (2000)

[7] Zubia, J and Arrue, J *Optical Fiber Technologies.* **7**, 101-140 (2001).

[8] Ma H, Jen, AKY. and Dalton LR, *Advanced Materials,* **14**, 1339-1365 (2002).

[9] Khoe G D, *IEEE J. Sel. Top. Quantum Electron.* **6**, 1265-1272 (2000).

[10] Monroy T I et al. *Optical Fiber Technologies.* **9**, 159-171 (2003).

[11] Eldada L, Shacklette LW, *IEEE J. Sel. Top. Quantum Electron.* **6**, 54-68 (2000).

[12] Plastic optical fibre tackles automotive requirements. *FibreSystems Europe*, May (2004), ww.mostcooperation.com

[13] OLED

[14] Sirringhaus H et al, *Science*, **290**, 2123 (2000)

[15] Lawrence JR, Turnbull GA, Samuel IDW, *Applied Physics Letters*, **82**, 4023 (2003)

[16] N. Tessler, *Advanced Materials*. **11**, 363 (1999)

[17] M. D. McGehee, A. J. Heeger. *Advanced Materials*, **12**, 1655, (2000).

[18] G. A. Turnbull, T. F. Krauss, W. L. Barnes, and I. D. W. Samuel, *Synthetic Metals*, **121**, 1759 (2001)

[19] Lawrence JR, Turnbull GA and Samuel IDW, *Applied Physics Letters*, **80**, 3036 (2002)

[20] A Tagaya, S Teramoto, E Nihei, K Sasaki, Y Koike, *Applied Optics*, **36**, 572 (1997)

[21] A Tagaya, Y Koike, E Nihei, S Teramoto, K Fujil, T Yamamoto, K Sasaki, *Applied Optics*, **34**, 988 (1995)

[22] SY Lam, MJ Damzen, *Applied Physics B*, **77**, 577 (2003)

[24] MA Reilly, C Marinelli, CN Morgan, RV Penty, IH White, M Ramon, M Ariu, R Xia, DDC Bradley, *Applied Physics Letters*, **85**,5137 (2004)

[25] MC Ramon, M Ariu, R Xia, DDC Bradley, MA Reilly, C Marinelli, CN Morgan, RV Penty, IH White, *Journal of Applied Physics*, **97**, 073517 (2005)

[26] www.ultrafast-photonics.org

[27] F. Hide, M. A. Diaz-Garcia, B. J. Schwartz, M. R. Andersson, Q. Pei, and A. J. Heeger. *Science*, 273, 1833, (1996).

[28] R. Xia, G. Heliotis, Y. B. Hou, D. D. C. Bradley, *Organic Electronics*. **4,** 165 (2003).

[29] R. Xia, G. Heliotis, and D. D. C. Bradley, *Applied Physics Letters* **82,** 3599 (2003).

[30] Koch TL, Chiu LC, and Yariv A, *Opical Communications*. **40**, 364 (1982)

[31] S. Shimada, and H. Ishio, *Optical Amplifiers and their Applications* (John Wiley & Sons Ltd.,Chichester, 1994).

[32] U. Scherf, S. Riechel, U. Lemmer, and R. F. Mahrt, *Curr. Opin. Solid State Material Science*, **5,** 143 (2001).

[33] W. Holzer, M. Pichlmaier, A. Penzkofer, D. D. C. Bradley, and W. J. Blau, *Chemical Physics* **246,** 445 (1999).

[34] Data from Dr G Heliotis, Dr Ruidong Xia, Dr Yanbin Hou, Imperial College

[35] Substrate produced by Andreas Vasdekis, University of St Andrews

Chapter 7

Conclusion

The work presented in this study was performed as part of the Ultrafast Photonics Collaboration (UPC) research into the next generation of ultrafast datacommunications. In this work the key contributions are in the fields of ultrafast polymer laser sources and solid-state amplifiers. Spectroscopic studies of a conjugated polymer and novel conjugated dendrimers have led to an improved understanding of the relationship between the photophysics of these materials and their chemical structure.

A study on the effect of the degree of conjugation in MEH-PPV has demonstrated that the conformational disorder and chemical breaks both disrupt the delocalisation of electrons in conjugated polymer chains. This causes a distribution of conjugated segments in the polymer chain , which affects the photophysical properties. By studying the photophysics as a function of temperature the breaks in conjugation caused by conformation are reduced and this flattens the chain and a red-shift is observed for both partially and fully conjugated MEH-PPV. An excitation on a partially conjugated MEH-PPV chain would encounter more breaks in conjugation, causing it to hop from one segment to another. The fully conjugated chain flattens out at lower energies and leaves only longer chains of lower energy on the chain thus shifting its emission significantly.

Time resolved measurements with a 250 fs time resolution are performed on two dendrimers previously modelled using coupled electronic oscillator calculations. The observed anisotropy of a nitrogen cored dendrimer decays within the 250 fs response of the system and this suggests an extremely fast transmission dipole reorientation upon excitation as the excitation is delocalised across the core. A similar dendrimer with a Benzene ring at its core does not exhibit this ultrafast depolarisation. This agrees with the results of the model which investigated the effect on the coherence within dendrimers with a nitrogen core and a benzene core. The different core unit made a significant difference to the dendrimer properties. In the model it was shown that for the nitrogen

cored dendrimer strong coherence is found between the stilbene units, suggesting that some sort of interaction between these segments is present after excitation. The BDSB material did not exhibit this coherence interaction in the model and the lack of fast depolarisation suggests the excited state is not delocalised cross the dendrimer but is confined to the stilbene units with no interaction between them. This study of these two dendrimers gives a clear endorsement to the model used previously and shows how dependent a dendrimers properties can be on the choice of central core unit. By changing a few atoms in two closely related structures the photophysics and electron delocalisation are altered significantly.

A highly efficient phosphorescent dendrimer was studied and the first reported singlet state emission (fluorescence) from this type of material was observed. This shows how efficient the transfer to the triplet state is in that the emission from the singlet (which is excited initially) happens within a few hundred femtoseconds. The use of femtosecond detection techniques made this possible on longer timescales the singlet emission would be a tiny part of the overall emission and impossible to separate from it.

Conjugated polymers have become very good candidates as novel gain media for laser devices. Their broad emission spectra make them ideal for tunable laser applications. Another benefit broad spectra may bring is ultrashort pulse generation as a laser needs a large range of optical energies to act together in order to shorten the pulsewidth. The temporal dynamics of a 2D –DFB laser are reported and exhibit a pulse shortening with increasing pump pulse energy to several picoseconds before the detection reaches a limit with the streak camera. Using the femtosecond up-conversion technique the laser pulses are measured with only the optical pulse width limiting the detection resolution. Laser pulses are recorded as short as 410 fs. This shows that ultrafast pulse generation is possible and this opens the path towards potential modelocking in these devices. The ultrafast pulses are also potentially useful for datacommunications networks based on Polymer Optical Fibre (POF) networks as they emit near the low loss windows of these fibres.

POF networks do not only rely on light sources but also need a device to amplify the propagating signal like SOAs and EDFAs do in modern communication networks. These devices are needed to extend the useful distance of these networks as they

compensate for transmission and splitting losses in the network. Broadband gain is initially studied in solution where a F8BT solution exhibited a peak gain of 40 dB and broadband gain of ~30 dB over a 55 nm wavelength range. Solution based devices though are inconvenient for integration into systems and so a solid-state amplifier is preferred. The difficulty in using a conjugated polymer in the solid state is that their spin coated films are always very thin (a few 100nm) and this causes very little gain if two pulses are overlapped in a small region. In order to effectively control the input and output of a probe signal through a thin waveguide, grating structures were produced on the substrate which acted as input and output couplers. In order to ensure the most gain was extracted from the amplifier a blended gain material of RedF and F8BT was provided which had been optimised for gain at the wavelengths necessary in this experiment. A solid state amplifier with a gain of 18 dB in a 300 μm long device shows the potential these devices have. Further work on MEH-PPV as a gain material has led to a 21 dB gain in a 1 mm device.

In this thesis the first sub-picosecond laser pulse from a polymer laser is reported. Solid-state conjugated polymer amplifiers were reported with a high gain of 18 dB in a 300 □m RedF/F8BT device and 21 db in a 1 mm MEH-PPV device. These are the first conjugated polymer amplifiers to be studied with control over the probe propagation into and out of the polymer film.

Future Work

There are several areas of work from this thesis which could be taken forward and they are outlined below.

- Further time-resolved studies of different phosphorescent dendrimers using the femtosecond up-conversion technique to extract more information on the singlet-triplet intersystem crossing for these materials and what effect chemical structure changes will have on the photophysical properties

- The ultrafast polymer laser work should be continued with an aim to reduce the pulsewidth further to see if there is a limit reachable by the detection and or pump lasers. A new non-colinear OPA in the laboratory should be able to provide shorter pump pulses but an auto-correlator could be used to study the output pulses. Different materials should be studied with different emission wavelengths to demonstrate whether ultrashort pulse generation is available for all materials or if there are chemical structures which inhibit this.
- The optical amplifiers need to be studied in more depth in relation to the device lengths and the use of different materials of different loss and gain properties. Ideally electrical excitation may be studied as grating couplers fabricated on ITO would allow coupling through the electrode and the effect of electrical excitation could be studied. The main obstacle is the grating fabrication on ITO which is very difficult.
- Dendrimers should be studied as gain materials as they have exhibited gain and are a promising class of materials for optoelectronic applications. Their modular structure may lead to better control over emission wavelength or output energy with further improvements in materials.

Appendix A

Publications Arising From This Work

- Goossens M, Ruseckas A, Turnbull GA and Samuel IDW, "Sub-picosecond pulses from a gain-switched polymer distributed feedback laser" *Applied Physics Letters*, **85** , 33 (2004)

- Heliotis G, Bradley DDC, Goossens M, Richardson S, Turnbull GA and Samuel IDW " Operating characteristics of travelling-wave semiconducting polymer optical amplifier", *Applied Physics Letters*, **85**, 6122 (2004).

- Amarasinghe VCD, Ruseckas A, Vasdekis AE, Goossens M, Turnbull GA and Samuel IDW "Broadband solid state optical amplifier based on a semiconducting polymer." *Applied Physics Letters*, **89** (20), 201119, 2006

- George Heliotis, Mark Goossens, Arvydas Ruseckas, Ruidong Xia, Yanbing Hou, Justin R. Lawrence, Graham A. Turnbull, Ifor D. W. Samuel and Donal D. C. Bradley "A High Gain Solid-State Semiconducting Polymer Optical Amplifier" Submitted to *Organic Electronics*, 2006